SIGNAL DESIGN AND PROCESSING TECHNIQUES FOR WSR-88D AMBIGUITY RESOLUTION

Part 9: Phase Coding and Staggered PRT

National Severe Storms Laboratory Report

prepared by: Sebastian Torres, M. Sachidananda, and Dusan Zrnić

November 2005

NOAA, National Severe Storms Laboratory
1313 Halley Circle, Norman, Oklahoma 73069

SIGNAL DESIGN AND PROCESSING TECHNIQUES FOR WSR-88D AMBIGUITY RESOLUTION

Part 9: Phase Coding and Staggered PRT

Contents

SIGNAL DESIGN AND PROCESSING TECHNIQUES FOR WSR-88D AMBIGUITY RESOLUTION

Part 9: Phase Coding and Staggered PRT

1. Introduction

The Radar Operations Center (ROC) of the National Weather Service (NWS) has funded the National Severe Storms Laboratory (NSSL) to address the mitigation of range and velocity ambiguities in the WSR-88D. This is the ninth report in the series that deals with range-velocity ambiguity resolution in the WSR-88D (all reports are listed at the end). It documents NSSL accomplishments in FY05.

We start in section 2 with a brief description of the only one data set which we have collected. In previous years we have accumulated a large number of data cases. These are listed on our website (http://cimms.ou.edu/rvamb/Mitigation_R_V_Ambiguities.htm) and some have not yet been analyzed.

Detail explanation of the spectral filter for the staggered PRT is in section 3 and the functional description is in the appendix B. Other issues of the staggered PRT are also investigated in this section. Thus the choice of PRTs and the recovery of reflectivity for different overlay scenarios are presented as well as a summary of spectral moment estimators.

The bulk of effort in testing and evolving the SZ-2 algorithm is in section 4. Significant changes were required to accommodate the case of operator defined regions for clutter

filtering. This issue was overlooked in the previously submitted algorithm and it required much investigations, simulations, and testing. An interim report was submitted to the ROC on July of 2005 addressing these changes. Testing of double processing of two overlaid echoes is also in section 4. That is, the strong and week echoes are processed twice; once by cohering the strong one, filtering it and cohering the week and the second time by cohering the week, filtering it and recohering the stronger one.

We would like to bring to your attention that the work performed in FY05 exceeded considerably the allocated budget hence a part of it had to be done on other NOAA funds.

2. Data Collection

Due to the numerous data cases collected in previous years and other projects competing for radar time, data collection during FY05 was limited to just one case. A case of a snow storm with uniform widespread reflectivity was collected on Jan 28, 2005 using VCPs 2048 and 2049. In both cases the research RDA (RRDA) recorded oversampled, dual-pol time series data. The system configuration and a detailed description of the VCPs are included in last year's report (report 8).

3. Staggered PRT

The staggered PRT technique has described in detail in previous reports of this series (e.g., see report 3) and in numerous papers in the literature. The main advantage of the Staggered PRT is that the maximum unambiguous velocity can be extended by means of a simple algorithm (see report 8); therefore, longer PRTs can be used to reduce the likelihood of overlaid echoes. In the past, this technique has been dismissed because it does not lead naturally to spectral processing and efficient ground clutter filters are difficult to design, rarely performing at par with existing filters that operate on uniform PRTs. These limitations have been overcome, and in this report, we describe an effective spectral ground clutter filter and a method to perform spectral analysis, both compatible with the staggered PRT technique. Another focus of this year's work has been in designing a suitable PRT scheme that can replace the Batch Mode in legacy volume coverage patterns (VCPs). Finally we present a scheme to recover the reflectivity for different overlay scenarios. We start with a much more detailed description of ground clutter filter than what was documented in report 3. Further, a complimentary explanation of the filter is included in the Appendix A and functional description is in Appendix B.

3.1. Clutter filtering and bias correction for staggered PRT: a re-visit.

A spectral clutter filtering procedure for staggered PRT was developed in report 3. This filter eliminates all the velocity drop-out bands observed in earlier clutter filtering methods. With this algorithm, it is practical to implement the staggered PRT scheme on operational radars to extend the maximum unambiguous velocity. While this method eliminates the velocity drop-out problem completely (although under certain conditions

which can be easily met), the bias error in the velocity around zero is more or less the same as in any uniform PRT processing. This problem is addressed in section 3.1.2, and the conclusions drawn from that study are applicable here.

The description of the ground clutter filtering algorithm in report 3 is somewhat concise, and we felt that a more detailed explanation would be useful in understanding the method and in coding the procedure on a computer. Hence, we explain the method in greater detail below before we embark on testing the algorithm on real radar data from KOUN. We start with a brief explanation of the staggered PRT transmission scheme, and the spectral signal spectrum reconstruction. Next, we explain a few mathematical concepts useful in understanding the clutter filtering method, and finally elaborate on the clutter filtering method itself in greater detail. The mathematical symbols and notations used are the same as in the report 3.

3.1.1. *The staggered PRT transmission scheme*

In the staggered PRT scheme two different pulse spacings, T_1 and T_2, ($T_1 < T_2$) are used alternately. Then, alternate pairs of samples are used to compute the autocorrelation estimates R_1 at lag T_1, and R_2 at lag T_2. In one of the methods, the velocity is estimated from the phase difference between the two using the formula,

$$v = \lambda \, arg(R_1 R_2^*)/\{4\pi(T_2 - T_1)\} \tag{3.1}$$

In an alternative method, the velocity is determined from the phase of R_1, and then the ambiguity is resolved using the phase of R_2 (see report 8 for details). The difference PRT

($T_2 - T_1$) determines the unambiguous velocity v_a, and the unambiguous range r_a is determined by T_1

$$v_a = \lambda/[4(T_2-T_1)];\ T_1 < T_2 \tag{3.2}$$

$$r_a = cT_1/2 \tag{3.3}$$

This, of course, assumes that T_1 is selected such that there are no echoes beyond r_a, hence, there are no overlaid echoes.

In the absence of the ground clutter, the spectral processing to extract the spectral moments proceeds by reconstructing the signal spectrum as if it is sampled at intervals $T_u = (T_2-T_1)$. This puts a small restriction on the selection of T_1 and T_2. They should be integer multiples of the difference T_u, so that $T_1 = n_1T_u$, and $T_2 = n_2T_u$, where n_1 and n_2 are integers. The best choice, as discussed in report 3, is $n_1 = 2$, and $n_2 = 3$, or the stagger ratio $\kappa = T_1/T_2 = 2/3$. Once this condition is satisfied, we can generate a uniform time series, v_i, $i = 1, 2, 3, \ldots, N$, (signal sampled at intervals T_u) from the staggered PRT sequence by inserting zeros in the place of missing samples. For $\kappa = 2/3$, we have only the 1st and 3rd samples available in each set of 5 samples. We call this the derived time series. Now, we can write the derived time series, v_i, $i = 1, 2, 3, \ldots, N$, as a product of sequences c and e, where e is the signal time series sampled at T_u intervals, and c_i, $i = 1, 2, 3, \ldots, N$, is a code sequence of zeros and ones given by c = [1010010100…etc.] for $\kappa = 2/3$.

$$v_i = c_i\, e_i\ ;\ i = 1, 2, 3, \ldots, N. \tag{3.4}$$

If there are M staggered PRT samples, we have $N = M\,(n_1+n_2)/2$ samples in the derived time series. The DFT spectrum of v is a convolution of the spectra of c and e

$$\mathrm{DFT}(v) = \mathrm{DFT}(c) \bigstar \mathrm{DFT}(e)\,, \tag{3.5}$$

where the symbol ★ represents the convolution operation, and the DFT( ) represents the discrete Fourier transform of the sequence in parenthesis. We use capital letters to denote DFT coefficients of the corresponding time domain quantities in lower case letters, and capital bold face letters to denote matrices or vectors. The subscript 'i' is used for time domain quantities and the subscript 'k' is used for spectral domain coefficients. For example E_k is the k^{th} spectral coefficient of DFT(e), and **E** is the column matrix of coefficients E_k , $k = 1, 2, 3, \ldots, N$. In the matrix notation, Eq. (3.5) can be written as

$$\mathbf{V} = \mathbf{C}\,\mathbf{E}. \tag{3.6}$$

V and **E** are (Nx1) column matrices and **C** is the (NxN) convolution matrix whose columns are cyclically shifted versions of the DFT(c). The convolution matrix is formed from the spectrum of the code sequence as follows: (a) Form a matrix with first row as the DFT(c), the second row is the same coefficients cyclically shifted right by one coefficient, 3rd row is same spectrum shifted right by two coefficients, and so on till the last row. This forms an NxN matrix. (b) Take the complex conjugate transpose of this matrix to get the convolution matrix, **C**. (c) Normalize the matrix. To preserve the power in the spectrum the columns of the convolution matrix are normalized such that each one is a unit vector (i.e., the norm of each column vector is unity). Note that normalizing the columns also normalizes the row vectors of **C** automatically.

The convolution matrix is singular (its rank is M), hence we cannot solve for **E**, but we can get the magnitudes without the phases under certain criterion explained below. If we discard the phases of **C**, the convolution matrix becomes non-singular and hence can be inverted. Further, we note that it is sufficient to recover the magnitude spectra of the weather signal to recover the spectral moments; the phases are not needed. Hence, we discard the phases of all the three matrices in (3.6) and write $abs\{\mathbf{V}\} = abs\{\mathbf{C}\}\ abs\{\mathbf{E}\}$ which is valid under the "narrow" spectrum condition. The spectrum is considered "narrow" if the spectral spread of the weather signal is less than $N/(n_1+n_2)$ coefficients. Because the staggered PRT scheme can be designed to have a large unambiguous velocity, v_a, this condition can be *nearly* met for most of the weather signals. In general, $abs\{\mathbf{V}\} \neq abs\{\mathbf{C}\}abs\{\mathbf{E}\}$ because of the complex addition process, however, under the "narrow" spectra condition, the complex addition does not take place, hence we can replace the inequality sign with the equality sign. Note that each row of **C** has only five non-zero coefficients spaced $M/2$ coefficients apart, and if **E** has only $M/2$ contiguous non-zero coefficients, the product of **E** and each row of **C** results in only one non-zero term, hence, no complex addition takes place in the convolution operation. Therefore, we can recover $abs\{\mathbf{E}\}$ from the inverse operation

$$abs\{\mathbf{E}\} = abs([abs\{\mathbf{C}\}]^{-1}\ abs\{\mathbf{V}\}) \tag{3.7}$$

We refer to the operation indicated in (3.7) as the "*magnitude deconvolution*". The recovery of the magnitude spectrum is exact under the "narrow" spectrum condition. If the spread of the spectral coefficients is more than $N/(n_1+n_2)$, the reconstruction is not exact; however, the velocity estimate is not biased by this non-ideal reconstruction; only

the variance is affected. The spectrum width bias is removed by eliminating the residual coefficients outside an interval $2N/(n_1+n_2)$ centered on the estimated mean velocity.

This is a brief description of the staggered PRT processing in the DFT domain without the clutter filter. Details about the spectral moment estimation and the simulation results are available in report 3. It may also be noted that this procedure gives spectral parameter estimates of more or less the same quality as the pulse pair algorithm; hence, the pulse pair algorithm is recommended whenever the ground clutter is not present in the time series. The DFT domain method is to be used in conjunction with the clutter filtering procedure.

3.1.2. *Clutter filtering procedure*

Before we explain the clutter filtering procedure, it is useful to refresh a couple of mathematical concepts from the functional analysis that are helpful in understanding the clutter filtering procedure. The concepts of interest here are the inner product, norm, and the linear independence. If $f(x)$ and $g(x)$ are two functions defined over $a \le x \le b$, then one of the ways of defining the inner product between the two functions, symbolically written as $< f, g >$, is

$$< f, g >= \int_a^b f(x) * g(x) dx , \tag{3.8}$$

and with respect to this inner product definition the norm of a function $f(x)$ is defined as

$$\|f\| = \left[\int_a^b f(x) * f(x) dx \right]^{1/2} . \tag{3.9}$$

Further, if the norm of a function is unity we call it a normalized function. A function can be normalized by dividing the function by its norm. If the inner product between two functions is zero, we call these functions orthogonal to each other. If in (3.8) $f(x)$ is a normalized function, then the inner product $< f, g >$ gives the complex amplitude of f present in g. If we subtract this part from g, what remains is orthogonal to the function f. (i.e., $[g - < f, g > f]$ is orthogonal to f).

These concepts extended to matrices take the form of matrix multiplication and summation in place of the integration. For example, if **F** and **G** are column matrices with N components each, (i.e., $\mathbf{F} = [f_1, f_2, f_3, \ldots, f_N]^T$ and $\mathbf{G} = [g_1, g_2, g_3, \ldots, g_N]^T$) then the inner product is a scalar given by the product

$$\chi = \mathbf{F}^{T^*}\mathbf{G} = \sum_{i=1}^{N} f_i^* g_i \,, \tag{3.10}$$

and the norm of the column matrix **F** is (the superscript 'T^*' represents complex conjugate transpose of the matrix, and '*' represents the complex conjugate)

$$\|\mathbf{F}\| = [\mathbf{F}^{T^*}\mathbf{F}]^{1/2} = [\sum_{i=1}^{N} f_i^* f_i]^{1/2} . \tag{3.11}$$

If the norm of a matrix is unity it is like a unit vector of the vector analysis. Two column matrices are said to be orthogonal if their inner product is zero. If **F** is a normalized matrix then the inner product χ of (3.10) is the amplitude of **F** present in **G**, or the component of **G** in the direction **F**. It is common practice to use the term vector in place of the column matrix, because there is much in common with the matrix analysis and the vector analysis. The vector analysis is developed for a 3-dimensional space, and the

matrix analysis is a generalization of these concepts to *N* dimensions. It is useful to compare the vector analysis concepts with matrix operations delineated above because we can visualize the vector operations easily.

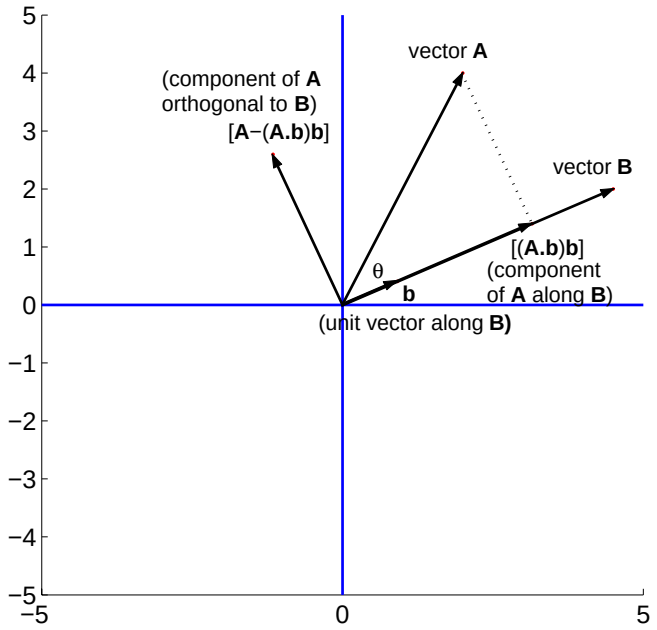

Fig. 3.1. Illustration of the vector dot product.

For simplicity of explanation, consider a 2-dimensional space, i.e., vectors having only **x** and **y** components (**x** and **y** are unit vectors along *x* and *y* directions in a Cartesian coordinate system). The inner product is the same as the dot product between two vectors. If **A** and **B** are two vectors (Fig. 3.1) given in terms of the Cartesian components as $\mathbf{A} = A_x\mathbf{x} + A_y\mathbf{y}$, and $\mathbf{B} = B_x\mathbf{x} + B_y\mathbf{y}$, then $\mathbf{A}\bullet\mathbf{B} = A_x B_x + A_y B_y = |\mathbf{A}|\,|\mathbf{B}|\,cos(\theta)$ is the dot product between the vectors (θ is the angle between the vectors **A** and **B**). The magnitude (or the norm) of the vector **B** can be obtained as $||\mathbf{B}|| = sqrt(\mathbf{B}\bullet\mathbf{B})$. If $\mathbf{b} = \mathbf{B}/||\mathbf{B}||$ is a unit vector along **B**, then the dot product, (**A•b**), gives the magnitude of the component of **A**

in the direction of **B**, or the projection of **A** onto **B**. If θ = 90º, then the vectors are orthogonal and the dot product is zero. The vector (**A**•**b**)**b** is the component of **A** along the direction **B**, and if we subtract this component from **A**, the resulting vector **C** = {**A** – (**A**•**b**)**b**} is the component of **A** orthogonal to **B**.

With the above concepts in mind, we proceed to explain the clutter filtering procedure for the staggered PRT sequence. The method is applicable to any stagger ratio provided n_1 and n_2 are integers, but here and in all the subsequent discussions we use κ =2/3. We use symbol M for the number of staggered PRT samples and $N = M\,(n_1+n_2)/2$ for the number of DFT points in the derived time series with inserted zeros. We start with (3.6) which is reproduced below for convenience.

$$\mathbf{V} = \mathbf{C}\,\mathbf{E}. \tag{3.12}$$

In this equation, **V** is the spectrum of the derived time series, and **E** is the unknown spectrum we are trying to recover. Here we assume that the weather signal and the ground clutter are present in the time series. To contain the spread of the clutter power around zero Doppler, we need to multiply the time series by the window weights. It is assumed that the window is included in the spectrum **V**. Now, if we examine the convolution matrix, we find that each row (the first column of **C** is the spectrum of the code sequence *c*, and the rest are shifted versions of the same) has only five non-zero coefficients (for κ =2/3) spaced M/2 coefficients apart. For example, with M = 64 (N = 160), of the 160 coefficients of DFT{c} = [C_1, C_2, C_3, …, C_{160}] only C_1, C_{33}, C_{65}, C_{97}, and C_{128} are non-zero. In terms of these DFT coefficients the convolution matrix will have its first row as [C_1, C_{160}, C_{159}, C_{158}, …, C_2], the second row as [C_2, C_1, C_{160}, C_{159},

C_{158}, …, C_3], which is 1st row right shifted by one element cyclically, and so on. The first row has non-zero coefficients at column numbers 1, 33, 65, 97, and 129, and the DFT coefficients of the code sequence in these positions are C_1, C_{129}, C_{97}, C_{65}, and C_{33}. In the second row these same coefficients would shift to columns 2, 34, 66, 98, 130. Thus, after the convolution operation indicated by the matrix multiplication in (3.12), the first and second elements V_1 and V_2 of the matrix **V** would be a weighted sum of the elements

$$V_1 = C_1 E_1 + C_{129} E_{33} + C_{97} E_{65} + C_{65} E_{97} + C_{33} E_{129},$$

$$V_2 = C_1 E_2 + C_{129} E_{34} + C_{97} E_{66} + C_{65} E_{98} + C_{33} E_{130}. \quad (3.13)$$

Similarly, we can write equations for all the 160 elements. Since each row of **C** is obtained by right shifting the elements of the previous row cyclically; all the coefficients are the same in the first 32 equations, and the next 32 equations the coefficients would be right shifted by one, i.e., $C_{33,}$ C_1, C_{129}, C_{97}, and C_{65}. Similarly, for every 32 equations, the coefficients right-shift by one, and there are five such sets. Therefore, we can rearrange the convolution matrix as a 5x5 matrix $\mathbf{C_r}$, and **E** and **V** are rearranged row-wise as 5x32 matrices, $\mathbf{E_r}$ and $\mathbf{V_r}$ respectively (e.g., the 1st row of $\mathbf{V_r}$ has V_1 to V_{32}, second row V_{33} to V_{64}, etc.). Equation (3.12) then becomes

$$\mathbf{V_r} = \mathbf{C_r}\, \mathbf{E_r}, \quad (3.14)$$

where the subscript 'r' represents re-arranged matrix. $\mathbf{C_r}$ can be obtained from **C** by deleting first all rows containing zero in the *first* column of **C**, and then deleting all columns containing zero in the *first* row, which reduces it to a 5x5 matrix. (Note: The five non-zero spectral coefficients of **C** can also be obtained from a code vector of length

5, [10100], taking its DFT, and normalizing the power in the spectrum.) The matrix $\mathbf{C_r}$ is also singular (its rank is 2), and its columns are normalized such that each column is a unit vector (row vectors are normalized automatically). The three matrices in (3.14) are shown below in terms of the DFT coefficients (subscript is the DFT coefficient number).

$$\mathbf{V_r} = \begin{bmatrix} V_1 & V_2 & V_3 & \cdots & V_{32} \\ V_{33} & V_{34} & V_{35} & \cdots & V_{64} \\ V_{65} & V_{66} & V_{67} & \cdots & V_{96} \\ V_{97} & V_{98} & V_{99} & \cdots & V_{128} \\ V_{129} & V_{130} & V_{131} & \cdots & V_{160} \end{bmatrix} \tag{3.15}$$

$$\mathbf{E_r} = \begin{bmatrix} E_1 & E_2 & E_3 & \cdots & E_{32} \\ E_{33} & E_{34} & E_{35} & \cdots & E_{64} \\ E_{65} & E_{66} & E_{67} & \cdots & E_{96} \\ E_{97} & E_{98} & E_{99} & \cdots & E_{128} \\ E_{129} & E_{130} & E_{131} & \cdots & E_{160} \end{bmatrix} \tag{3.16}$$

$$\mathbf{C_r} = \begin{bmatrix} C_1 & C_{129} & C_{97} & C_{65} & C_{33} \\ C_{33} & C_1 & C_{129} & C_{97} & C_{65} \\ C_{65} & C_{33} & C_1 & C_{129} & C_{97} \\ C_{97} & C_{65} & C_{33} & C_1 & C_{129} \\ C_{129} & C_{97} & C_{65} & C_{33} & C_1 \end{bmatrix} \tag{3.17}$$

Now consider a situation in which both the signal and the clutter are present in the spectrum. We select the following parameters to generate simulated spectra shown in Fig. 3.2:

- Weather signal: mean velocity 38 m s^{-1}, spectrum width = 3 m s^{-1},
- Clutter signal: clutter-to-signal ratio (CSR) = 10 dB, mean velocity = 0 m s^{-1}, spectrum width = 0.28 m s^{-1},
- The signal-to-noise ratio (SNR) is > 30 dB.

The spectra are shown in terms of the DFT coefficient magnitudes versus coefficient number along the x-axis. The radar parameters are: frequency 3 GHz (λ = 10 cm), maximum unambiguous velocity v_a = 50 m s^{-1}. Note that the velocity along the x-axis is {0 to -50; +50 to 0.625} m s^{-1} (in steps of 0.625 m s^{-1}) corresponding to the DFT coefficients numbers {1 to 80; 80 to 160}. The first spectrum (Fig. 3.2a) is that of the signal alone, and the second (Fig. 3.2b) is that of the signal plus the clutter. This is the vector **E** of (3.12) which we are trying to recover from the vector **V** shown in Fig. 3.2d. The vector **V** is the spectrum of the staggered PRT sequence obtained after converting the time series into a uniform sequence by inserting zeros in places of missing samples, or the spectrum after convolving **E** with the code spectrum. Fig. 3.2c is the spectrum of the signal alone in the staggered PRT sequence in the absence of the clutter. Note that the clutter and the weather signal have 5 weighted replicas in the spectrum because of the convolution with the code spectrum which has only five non-zero coefficients.

The next figure (Fig. 3.3) shows the two re-arranged matrices $\mathbf{V_r}$ and $\mathbf{E_r}$. The 160 coefficients of the spectra are arranged row-wise into 5x32 size matrices. In fact, (3.12) is a compact representation of the 32 independent equations, one for each column of $\mathbf{V_r}$. The first column of $\mathbf{V_r}$ is related to the first column of $\mathbf{E_r}$ via the transformation matrix $\mathbf{C_r}$, and 2nd column of $\mathbf{V_r}$ to the 2nd column of $\mathbf{E_r}$, and so on. Therefore, it is sufficient to consider one such equation to demonstrate the clutter filtering procedure. Let us take the equation corresponding to the first column of the $\mathbf{V_r}$.

$$\begin{bmatrix} V_1 \\ V_{33} \\ V_{65} \\ V_{97} \\ V_{129} \end{bmatrix} = \begin{bmatrix} C_1 & C_{129} & C_{97} & C_{65} & C_{33} \\ C_{33} & C_1 & C_{129} & C_{97} & C_{65} \\ C_{65} & C_{33} & C_1 & C_{129} & C_{97} \\ C_{97} & C_{65} & C_{33} & C_1 & C_{129} \\ C_{129} & C_{97} & C_{65} & C_{33} & C_1 \end{bmatrix} \begin{bmatrix} E_1 \\ E_{33} \\ E_{65} \\ E_{97} \\ E_{129} \end{bmatrix} \tag{3.18}$$

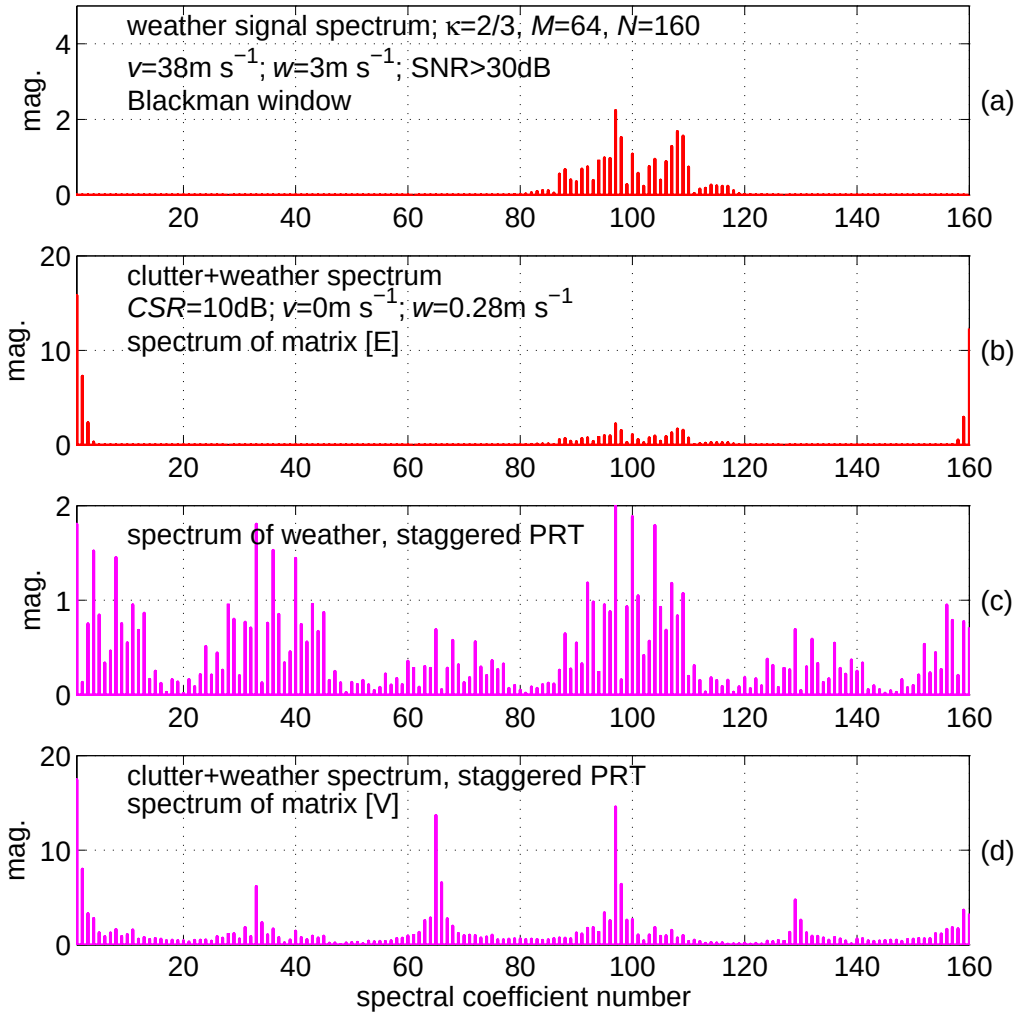

Fig. 3.2. Illustration of the staggered PRT signal spectra.

Referring to Fig. 3.2b, **E** has clutter in the first few and last few coefficients; the signal is centered on the mean velocity. When this is rearranged, the clutter is in the first few coefficients in the first row and last few coefficients in the last row. The signal coefficients are spread, at most, over two rows if the "narrow" spectrum criterion is satisfied. Therefore, in each column of $\mathbf{E_r}$, at most two elements are non-zero. In the example given in Fig. 3.3, we see that E_1 (clutter coefficient) and E_{97} (signal coefficient) are non zero in the first column. In general, we know that the clutter is in the first coefficient (ground clutter has zero velocity) in the first few columns (last coefficients in the last few columns), and the signal can be in any one of the five coefficients. After the transformation via the matrix $\mathbf{C_r}$, powers in these two coefficients spread to all the elements of the first column of $\mathbf{V_r}$ on the left hand side of the equation. For simplicity, let us write the transformation matrix $\mathbf{C_r}$ in terms of its column vectors and number them as $\mathbf{C_1}$ to $\mathbf{C_5}$. With this modification the (3.18) would be rewritten as

$$\begin{bmatrix} V_1 \\ V_{33} \\ V_{65} \\ V_{97} \\ V_{129} \end{bmatrix} = \begin{bmatrix} \mathbf{C_1} & \mathbf{C_2} & \mathbf{C_3} & \mathbf{C_4} & \mathbf{C_5} \end{bmatrix} \begin{bmatrix} E_1 \\ E_{33} \\ E_{65} \\ E_{97} \\ E_{129} \end{bmatrix} \tag{3.19}$$

where vectors $\mathbf{C_1}$ to $\mathbf{C_5}$ are the columns of the matrix $\mathbf{C_r}$. Note that the vectors $\mathbf{C_1}$ to $\mathbf{C_5}$ are pair-wise linearly independent, i.e., the magnitude of the inner product between any two vectors is less than unity. With E_{33}, E_{65}, and E_{129} being zero, we can reduce the equation to

$$\mathbf{V_1} = \mathbf{C_1}\, E_1 + \mathbf{C_4}\, E_{97}, \tag{3.20}$$

where vector $\mathbf{V_1}$ on the left hand side is the first column of $\mathbf{V_r}$. This is an over determined system with two unknowns and 5 equations. Only two of these equations are sufficient to solve for the unknowns E_1 and E_{97}, other three equations happen to be dependent equations (rank of $\mathbf{C_r}$ is 2). However, in practice we know only the position of the clutter coefficient, but not that of the signal.

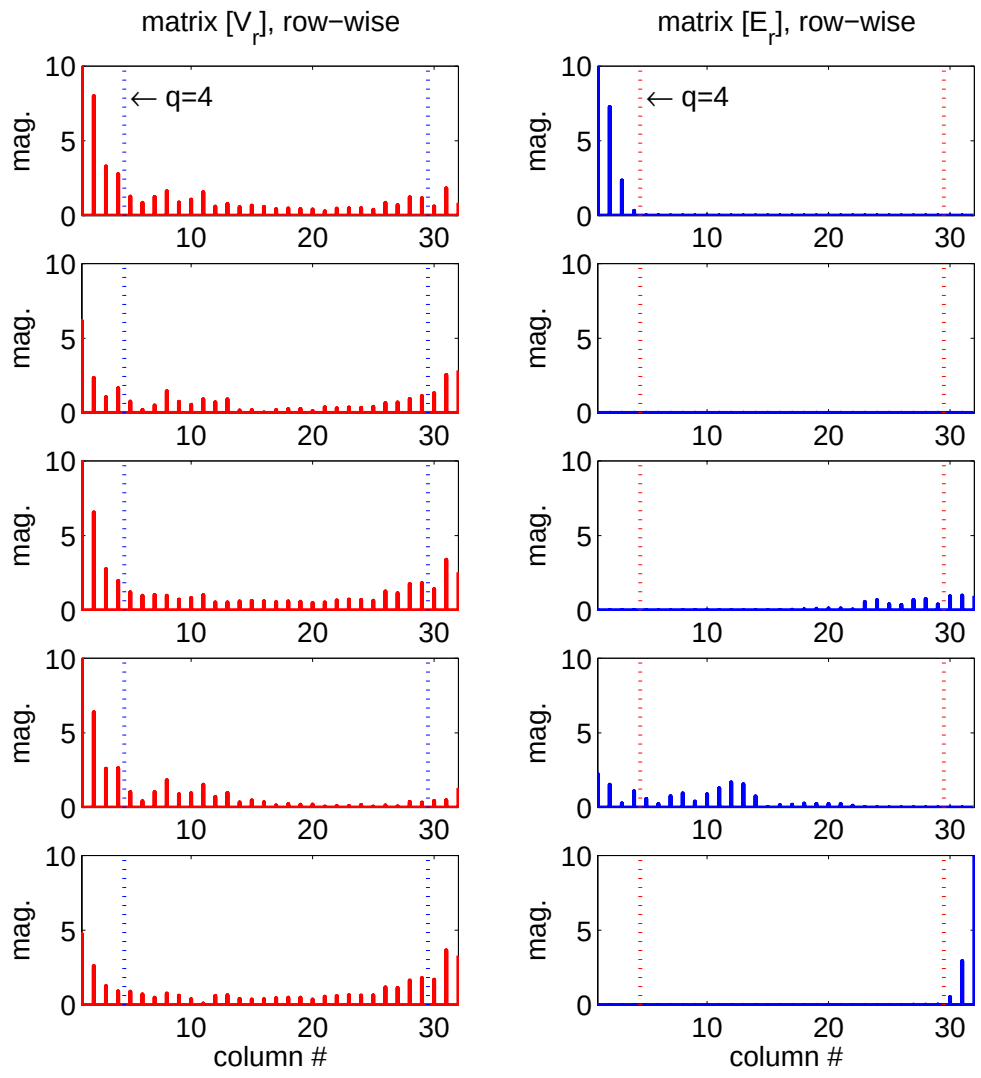

Fig. 3.3. Illustration of the staggered PRT clutter filtering procedure.

Now, the vector $\mathbf{V_1}$ is a sum of the clutter coefficient, E_1 times the vector $\mathbf{C_1}$, plus the signal coefficient E_{97} times the vector $\mathbf{C_4}$. Therefore, to filter the clutter we take the component of $\mathbf{V_1}$ along the direction $\mathbf{C_1}$ and subtract it from $\mathbf{V_1}$. This is accomplished by taking the inner product between $\mathbf{C_1}$ and $\mathbf{V_1}$ to get the amplitude of the component, multiply this by $\mathbf{C_1}$, and then subtract it from $\mathbf{V_1}$.

$$\mathbf{V_{f1}} = \mathbf{V_1} - (\mathbf{C_1}^{\mathbf{T}} * \mathbf{V_1})\, \mathbf{C_1}\,, \tag{3.21}$$

where $\mathbf{V_{f1}}$ is the residual vector after clutter is filtered. Substituting for $\mathbf{V_1}$ from (3.20) we get

$$\mathbf{V_{f1}} = \{\mathbf{C_1}\, E_1 + \mathbf{C_4}\, E_{97}\} - \{\mathbf{C_1}^{\mathbf{T}} * (\mathbf{C_1}\, E_1 + \mathbf{C_4}\, E_{97})\}\mathbf{C_1}\,.$$

$$= \mathbf{C_4}\, E_{97} - \{\mathbf{C_1}^{\mathbf{T}} * \mathbf{C_4}\, E_{97}\}\mathbf{C_1}$$

$$= \mathbf{C_4}\, E_{97} - (\mathbf{C_1}^{\mathbf{T}} * \mathbf{C_4})\mathbf{C_1}\}E_{97}$$

$$= \{\mathbf{C_4} - (\mathbf{C_1}^{\mathbf{T}} * \mathbf{C_4})\mathbf{C_1}\}E_{97.} \tag{3.23}$$

Note that the first term of (3.20) (the clutter vector present in $\mathbf{V_1}$) is completely removed, and the $\mathbf{C_1}$ component of the signal vector is also filtered. Since the vectors $\mathbf{C_1}$ and $\mathbf{C_4}$ are not collinear (the vectors $\mathbf{C_1}$ to $\mathbf{C_5}$ are pair-wise linearly independent) the complex multiplier, $\{\mathbf{C_4} - (\mathbf{C_1}^{\mathbf{T}} * \mathbf{C_4})\mathbf{C_1}\} \neq \{0\}$, except when the signal also happens to be in the first coefficient (i.e., the clutter and signal are in E_1). In such a case (3.20) would have only the first term, and all the vectors in the R.H.S. of (3.23) are $\mathbf{C_1}$.

It is easy to see that we can recover the original complex amplitude of the signal coefficient, E_{97} in (3.20) by dividing the 4^{th} element of $\mathbf{V_{f1}}$ by the 4^{th} element of $\{\mathbf{C_4}$ -

$(\mathbf{C_1}^{\mathbf{T}}\mathbf{*}\ \mathbf{C_4})\mathbf{C_1}\}$, but again, only if we know the position of the signal in the spectrum. Hence, the signal cannot be restored at this stage. This lost part of the signal produces a small bias in the spectral moment estimates. We shall come back to this shortly while explaining the bias removal. Note that the clutter is completely removed, but the signal is partially removed by the clutter filter as long as the signal and clutter are not in the same coefficient.

Since the clutter is present in the first few and the last few columns of $\mathbf{E_r}$, we apply this procedure only to those columns in which the clutter is present (the extent shown in dotted lines in Fig. 3.3). Depending on the clutter filter width, n_c, in terms of the DFT coefficients, the ground clutter filtering procedure described above is applied to the first q columns and the last (q-1) columns ($n_c = 2q$-1). In the last columns the clutter coefficient is in the last row, hence, in (3.23) we need to replace the vector $\mathbf{C_1}$ by the vector $\mathbf{C_5}$ while applying the clutter filter to these columns. For example, the clutter filtering equation corresponding to the last column (32nd column) would be

$$\mathbf{V_{f32}} = \mathbf{V_{32}} - (\mathbf{C_5}^{\mathbf{T}}\mathbf{*}\ \mathbf{V_{32}})\ \mathbf{C_5}. \tag{3.24}$$

After the clutter is filtered using this process, we apply the *magnitude deconvolution*, which also can be carried out using the rearranged matrices. First, take only the magnitude matrices by discarding the phases, and then pre-multiply both sides by the inverse of $abs\{\mathbf{C_r}\}$. Again let us take one column, $\mathbf{V_{f1}}$ of (3.23). After the magnitude deconvolution we get

$$abs(\mathbf{E_{r1}}) = abs([abs\{\mathbf{C_r}\}]^{-1}\ abs\{\mathbf{V_{f1}}\})$$

$$= abs(\ [abs\{\mathbf{C_r}\}]^{-1}\ abs[\{\mathbf{C_4} - (\mathbf{C_1}^{t*}\ \mathbf{C_4})\mathbf{C_1}\}E_{97}\ ]\ ), \tag{3.25}$$

Interestingly, all the coefficients of the resulting vector, $abs(\mathbf{E_{r1}})$, have same amplitude, because the vector

$$\mathbf{D_4} = [abs\{\mathbf{C_r}\}]^{-1}\ abs\{\mathbf{C_4} - (\mathbf{C_1}^{T*}\ \mathbf{C_4})\mathbf{C_1}\} \tag{3.26}$$

has all the elements the same (except for sign), and this result is true for any combination of vectors $\mathbf{C_1}$ to $\mathbf{C_5}$; only the values are different. Hence, we can make all the elements of $abs(\mathbf{E_{r1}})$ the same as $abs\{E_{97}\}$ by multiplying by the inverse of any one of the elements of $abs\{\mathbf{D_4}\}$, $\xi = 1/\ D_{4,1}$ ($D_{4,1}$ is the first element of $abs\{\mathbf{D_4}\}$). Now, of the five elements of the vector $abs(\mathbf{E_{r1}})$, only one is the signal (i.e., in this example the 4th element), the rest are to be discarded. To determine which element to retain, we use the *initial* velocity estimate (this is an approximate velocity and it has bias due to the clutter filter). The initial mean velocity of the weather signal is obtained from the spectrum after the magnitude deconvolution but before the multiplication by this constant (ξ) to restore the amplitude. There will be five identical replicas of the signal components, although with reduced amplitudes, in the five locations from which the clutter is removed. Since they are symmetrically distributed about the zero Doppler, their contribution to the mean velocity is zero. The small bias in the mean velocity is because one of these five replicas is actually the signal, whose contribution to the mean velocity is neutralized by the other four replicas. Once we know the approximate mean velocity we can determine which one replica is the signal and discard the other four. This is accomplished by retaining the one replica that falls within the $M/2$ coefficients centered on the *initial* velocity estimate. The amplitude of this correct replica is restored by multiplying by the factor ξ. It may be

noted that we can multiply all the replicas by the factor before estimating the initial velocity with no effect on the velocity, because as mentioned earlier, its contribution to the mean velocity is zero because of the symmetry.

It is important to note that the initial velocity comes from only those coefficients which are not contaminated by the clutter. Hence, if the clutter filter is very wide then the approximate velocity may be too poor to correctly determine the original position of the signal coefficients, although we know the exact amplitude. This sometimes causes erroneous velocity for very wide clutter filter, but in general, the clutter spectrum width is narrow, requiring a fairly narrow clutter filter which leaves enough coefficients for a reasonably accurate initial mean velocity estimate. For example, a test on an actual staggered PRT radar data with a CNR = 90 dB, the clutter filter parameter q = 4 was sufficient to filter the clutter. q = 4 corresponds to 2*q-1 columns from which clutter is filtered; i.e., in this case {160 - (2*4-1)*5} = 115 coefficients out of 160 are available for the initial velocity estimation. The Blackman window was used for this analysis.

Now, we put together the whole clutter filtering and the bias correction process in a compact matrix operation form. If the clutter filter width in terms of the number of DFT coefficients is n_c, we place these symmetrically about the 1st coefficient (zero Doppler). For this, it is necessary to make n_c an odd number. Therefore, we select first q columns and last q-1 columns for filtering the clutter, so that n_c = 2*q-1. The clutter from the first q columns of $\mathbf{V_r}$ is removed by subtracting the projection of each column onto $\mathbf{C_1}$ multiplied by $\mathbf{C_1}$. Similarly, the clutter from the last q-1 columns is removed by subtracting the projection of each column onto $\mathbf{C_5}$ multiplied by $\mathbf{C_5}$. The rest of the columns are left unchanged. This complete operation can be written in matrix notation as

$$\mathbf{V_f} = \mathbf{V_r} - \mathbf{C_{f1}}\,\mathbf{V_r}\,\mathbf{I_{f1}} - \mathbf{C_{f2}}\,\mathbf{V_r}\,\mathbf{I_{f2}}, \tag{3.27}$$

where $\mathbf{C_{f1}}$ and $\mathbf{C_{f2}}$ are the clutter filter matrices, and $\mathbf{I_{f1}}$ and $\mathbf{I_{f2}}$ are matrices that select the columns to be filtered. These are given by

$$\mathbf{C_{f1}} = \mathbf{C_1}\,\mathbf{C_1}^{\mathbf{T}}\mathbf{*}, \tag{3.28a}$$

$$\mathbf{C_{f2}} = \mathbf{C_5}\,\mathbf{C_5}^{\mathbf{T}}\mathbf{*}. \tag{3.28b}$$

The matrix $\mathbf{I_{f1}}$ is a M/2xM/2 diagonal matrix with diagonal elements equal to 1 for the first q elements and 0 for the rest. Similarly, the matrix $\mathbf{I_{f2}}$ is a M/2xM/2 diagonal matrix with last (q-1) elements unity and the rest zeros. For example, the diagonals of the matrices for q = 4 are

$$diag\ \{\mathbf{I_{f1}}\} = [11110000\ ....\ 000], \tag{3.29a}$$

and

$$diag\ \{\mathbf{I_{f2}}\} = [0000\ ....\ 000111]. \tag{3.29b}$$

Note that (2q-1) = n_c is the clutter filter width in terms of the number of spectral coefficients. Hence, the first four 1's in (3.29a) correspond to 0^{th} to 3^{rd} spectral coefficients and the last three 1's in (3.29b) are the three coefficients close to 0^{th} coefficient on the negative side. These matrices ensure that all the rest of the columns of $\mathbf{V_r}$ are not filtered. $\mathbf{V_f}$ is the matrix of the signal spectrum after clutter filtering. This filtering procedure does not delete all the signal power present in the coefficients from which clutter is filtered. Of course, if the signal velocity is also near zero, it cannot be distinguished from the clutter, and hence, will be deleted completely. For signals with mean velocity other than near zero, a part of the signal power is retained, but is reshuffled

in amplitude and phase in the clutter filtering process. This produces a bias in the velocity estimate, which can be eliminated if we can reconstruct the original signal from the residual signal power. The original signal coefficients can be restored completely in the complex domain, or alternately, we can recover only the magnitudes, which is sufficient to estimate the spectral moments. The second procedure involves fewer computations. Both procedures require the approximate mean velocity of the signal. In the next section we explain both procedures for restoring the lost signal. To obtain the approximate mean velocity estimate we use magnitude deconvolution after filtering the ground clutter. Magnitude deconvolution is applied to the rearranged matrix directly, and is given by the equation

$$abs\{\mathbf{E_r}\} = abs([abs\{\mathbf{C_r}\}]^{-1}\ abs\{\mathbf{V_f}\}). \tag{3.30}$$

The magnitude spectrum $abs\{\mathbf{E_r}\}$ is rearranged in a column matrix $\mathbf{E_s}$. The autocorrelation $R(T_u)$ is calculated from the magnitude coefficients of $\mathbf{E_s}$, and the *initial* approximate velocity estimate is obtained from the phase of $R(T_u)$.

In (3.26) vector $\mathbf{D_4}$ is calculated from the columns of the re-arranged convolution matrix. The inverse of any one of the elements of this vector gave the correction factor needed to restore the signal component partially lost in the clutter filtering process. Since the signal could be in any one of the rows, we introduce a subscript '*k*' in place of '4', and generate five different vectors, one for each row; i.e., if the signal is in the first row we use $\mathbf{D_1}$, for the second row $\mathbf{D_2}$, etc. Thus, for the first *q* columns the correction factors are obtained from the 1st elements of $\mathbf{D_k}$, given by

$$\mathbf{D_k} = [abs\{\mathbf{C_r}\}]^{-1}\ abs\{\mathbf{C_k} - (\mathbf{C_1}^{\mathbf{t}} * \mathbf{C_k})\mathbf{C_1}\};\ k = 1,2,3,4, \text{ and } 5. \tag{3.31}$$

For the last q-1 columns the corrections factors are derived from

$$\mathbf{D_k} = [abs\{\mathbf{C_r}\}]^{-1}\, abs\{\mathbf{C_k} - (\mathbf{C_5}^{\mathbf{t}} * \mathbf{C_k})\mathbf{C_5}\};\ k = 1,2,3,4, \text{ and } 5. \tag{3.32}$$

For M = 64, the element values (all element values are the same) of $abs(\mathbf{D_k})$ are 0, 0.9045, 0.5590, 0.5590, and 0.9045 respectively for k = 1, 2, 3, 4, and 5, from (3.31). These values are the fraction of the original signal amplitude retained after the clutter is filtered. We get the same values for $abs(\mathbf{D_k})$ from (3.32) also but in the reverse order, i.e., 0.9045, 0.5590, 0.5590, 0.9045, and 0 for k = 1, 2, 3, 4, and 5. One of the elements is zero because no signal is left in the spectrum after clutter filtering. This happens when the clutter and signal are in the same coefficients around zero velocity. We notice that the coefficients are in reverse order in the second equation, and there are only three distinct values, of which one is zero, hence not usable. We have to devise some other mechanism of restoring the signal for this case; hence, we set this number to unity in the processing algorithm to avoid multiplication by infinity. If we set (1/0.9045) = 1.1056 = ξ_2, and (1/0.5590) = 1.789 = ξ_3, the correction factors for different positions of the signal components in the rearranged matrix $\mathbf{E_r}$ are as follows:

$$\mathbf{Z}_r = \begin{bmatrix} \infty & \infty & \cdots & \infty & \xi_2 & \xi_2 & \cdots & \xi_2 \\ \xi_2 & \xi_2 & \cdots & \xi_2 & \xi_3 & \xi_3 & \cdots & \xi_3 \\ \xi_3 & \xi_3 & \cdots & \xi_3 & \xi_3 & \xi_3 & \cdots & \xi_3 \\ \xi_3 & \xi_3 & \cdots & \xi_3 & \xi_2 & \xi_2 & \cdots & \xi_2 \\ \xi_2 & \xi_2 & \cdots & \xi_2 & \infty & \infty & \cdots & \infty \end{bmatrix} \tag{3.33}$$

In the 5x32 matrix of correction factors above, the first 16 columns are identical and the next 16 columns are upside down flipped version of the first 16. The values in the first 16 columns are obtained from (3.31), and the next 16 from the (3.32). If we row-wise unfold

this into a single column matrix, **Z**, we get the 160 values in a column corresponding to the 160 coefficients of the spectrum. Values going to infinity are changed to 1 in the algorithm, and this region is dealt with separately. We can divide the entire $-v_a$ to v_a interval into three regions according to the correction factor to be applied: *velocity region* (1): $\{|v| < v_a/5\}$, *velocity region* (2): $\{v_a/5 < |v| < 3v_a/5\}$, and *velocity region* (3): $\{3v_a/5 < |v| < v_a\}$. The correction factors are ξ_2 for *velocity region* (2) and ξ_3 for *velocity region* (3).

To restore the true signal amplitude in the filtered columns of $\mathbf{V_f}$, we first identify the row in which signal component is to be restored based on the *initial* velocity estimate, and multiply that coefficient by ξ_k, corresponding to the *velocity region* (2) or (3). The rest of the elements of that column are set to zero. For *velocity region* (1) we can use linear interpolation (in the power domain). The coefficients are filled with interpolated values between the $(q+1)^{th}$ and the $(M/2-q+1)^{th}$ value. With this interpolation method, the bias removal is not exact for *velocity region* (1), but is reasonably good for most applications (see simulation results in section 2 on linear interpolation). This procedure is carried out for the all columns from which clutter is filtered. In matrix notation this operation is represented by

$$\mathbf{E_s^c} = \mathbf{E_s^m} \bullet \mathbf{I_1} + \mathbf{E_s^m} \bullet \mathbf{I_2} \bullet \mathbf{I_v} \bullet \mathbf{Z}, \tag{3.34}$$

where $\mathbf{E_s^c}$ is the corrected spectrum, and $\mathbf{E_s^m}$ is the modified spectrum in which the *velocity region* (1) (the first q and the last $(q-1)$ elements) is filled with interpolated values. This modification takes care of the bias correction in *velocity region* (1). The dot (•) symbolizes an element by element multiplication operation of the two columns, like

the (•*) operation in MATLAB. The other column matrices used in (3.34), $\mathbf{I_1}$, $\mathbf{I_2}$, $\mathbf{I_v}$, and $\mathbf{Z}$ are defined by

$$\mathbf{I_2} = [(diag\{\mathbf{I_{f1}}\} + diag\{\mathbf{I_{f2}}\}),\ldots \text{ repeat } (n_1+n_2) \text{ times}]^t, \tag{3.35}$$

$$\mathbf{I_1} = \text{complement of } \mathbf{I_2}, \text{ (interchange 0s and 1s)}, \tag{3.36}$$

$$\mathbf{I_v} = [000\ldots\ 001111\ldots1110000\ldots]^t, \tag{3.37}$$

($\mathbf{I_v}$ is a (Nx1) element vector with $N/(n_1+n_2)$ ones placed such that the 1s are centered on the mean velocity coefficient, the rest are all zeros), and

$$\mathbf{Z} = [1111\ldots,\xi_2,\xi_2,\xi_2\ldots,\xi_3,\xi_3,\xi_3,\ldots\ ,\xi_2,\xi_2,\xi_2\ldots,111\ldots]^T. \tag{3.38}$$

The spectral parameters are then estimated from the corrected spectrum $\mathbf{E_s^c}$. The mean power and the mean velocity are estimated in the usual manner, except for the width estimation.

In practice, the "narrow" spectrum criterion, based on which the magnitude deconvolution procedure works, is not satisfied exactly for weather signals. Although the power outside the $M/2$ extent centered on the mean velocity is small, the spectral components are never exactly zero elsewhere in the spectrum. Further, noise is always present across the spectrum, if not the signal. Hence, the magnitude deconvolution is never exact, and the reconstructed spectrum has some residual spectral power spread over the rest of the spectrum which affects the width estimate. The other two parameters are not affected by it (see Fig. 3.1d of report 3). Simulation studies indicated that if we estimate the spectrum width from M coefficients centered on the mean velocity, we get

an unbiased width estimate. A very interesting observation from the simulation studies is that the reconstructed spectrum using the magnitude deconvolution procedure gives correct spectral moments even when the weather signal spectral power spread is as much as M coefficients, which is twice that specified by the "narrow" spectrum criterion. Note that in this case the reconstructed spectrum is not exact, but the mean power and mean velocity are not affected. The change in the width can be offset by selecting M coefficients centered on the mean velocity for the width estimation. The other two parameters are estimated with the complete spectrum.

Report 7 gives a detailed description of the pulse pair algorithm as applied to staggered PRT sequences. It also includes a part which censors the velocity data whenever there is overlaid signal. In appendix B, we list only the clutter filtering part of the algorithm. In the algorithm given in report 7, the clutter filtering removes only the D.C. component from the I and Q samples; this does not filter the clutter adequately.

3.2. Choice of PRTs

The staggered PRT algorithm described in previous reports works, in principle, for any given pair of PRTs. Performance, however, strongly depends on the choice of these PRTs, and choosing the optimum pair of T_1 and T_2 for the operational environment is critical. The PRTs are constrained by (1) system limits, (2) range coverage requirements, (3) design considerations, and (4) desired errors of estimates. We elaborate on these constraints next.

System limits include the transmitter's maximum RF duty cycle and the memory allocated for time series data in the signal processor. The former imposes a lower limit on the PRTs; i.e., the duty cycle τ/T_s cannot exceed 0.2%; hence, the shortest PRT possible with the WSR-88D's short pulse (1.57 μs) is 780 μs. The latter imposes an upper limit on the PRTs; for example, on the RVP-8 processor, the maximum number of range bins is set to 3072, with a typical sample spacing of 1.67 μs (250 m), the longest PRT possible is 5.12 ms, which exceeds our needs.

Range coverage requirements are specified in terms of the maximum unambiguous range $r_a = cT_s/2$; thus, the longer the PRT the better. For the WSR-88D, reflectivity has to be retrieved up to a range of 460 km and Doppler velocity (and spectrum width) up to a range of 230 km. Recalling that in the staggered PRT technique the short PRT determines the maximum unambiguous range for velocity and spectrum width (r_{a1}) and the long PRT the one for reflectivity (r_{a2}), we have that $T_1 \geq 1.53$ ms and $T_2 \geq 3.07$ ms. However, actual requirements for intermediate to higher elevations can be relaxed if we assume that storm tops are below 18 km (~59000 ft). For example, for a height of 18 km, the slant range is

~300 km at an elevation of 2.4 deg and ~150 km at an elevation of 6 deg. Therefore, actual requirements for range coverage at intermediate elevations (> 2 deg) are 300 km or less, and the requirements on T_1 and T_2 stated above can be relaxed. At 2.4 deg, $r \leq 300$ km, so the maximum unambiguous range for reflectivity can be relaxed to $r_{a2} \geq 300$ km, but the one for velocity and spectrum width remains as $r_{a1} \geq 230$ km. This leads to $T_1 \geq$ 1.53 ms and $T_2 \geq 2$ ms. On the other hand, at 6.0 deg $r \leq 150$ km; thus, $r_{a1} \geq 150$ km and $r_{a2} \geq 150$ km, leading to T_1, $T_2 \geq 1$ ms.

Design constraints are inherent to the particular staggered PRT algorithm. For example, the recommended algorithm assumes that T_1 is the short PRT and T_2 the long one, so $T_1 < T_2$. In addition, the preferred PRT ratio is $\kappa = T_1/T_2 = 2/3$. This leads to the fewest number of rules for the velocity dealiasing algorithm and to optimum performance of the spectral ground clutter filter. The reader should note that none of the currently existing PRTs in the WSR-88D satisfy this condition. Although the signal processor and the transmitter are not limited to the 5 legacy sets of 8 PRTs each, adding new PRTs into the system would most likely impact the ORPG since, for example, all VCP definitions use PRI numbers (not the actual PRT in microseconds). A more thorough analysis of the impacts to the rest of the system is beyond the scope of this work. We recommend that this analysis is carried out before a decision is made regarding the implementation of the staggered PRT technique.

Errors of estimates add another constraint to the PRTs. For example, echo coherency is required for precise Doppler measurements. Echo coherency is achieved if the spectrum width (σ_v) is much smaller than the Nyquist interval. For a spectrum width of 4 m/s (the

median value in severe storms) $T_1 < 2.2$ ms; in general, larger values of σ_v require shorter PRTs. Note that this requirement competes with the one for range coverage.

Combining all these constraints, it is possible to arrive at a set of "acceptable" PRTs. Figure 3.2.1 shows the area of valid PRTs obtained by combining system limits, range coverage, design constraints, and signal coherency requirements. Further, by limiting the PRT ratio to 2/3, the set of possible PRTs lies on the highlighted line. Of these PRTs, the shortest ones would lead to more pairs in the given dwell time and better statistical performance. These are also indicated in the figure.

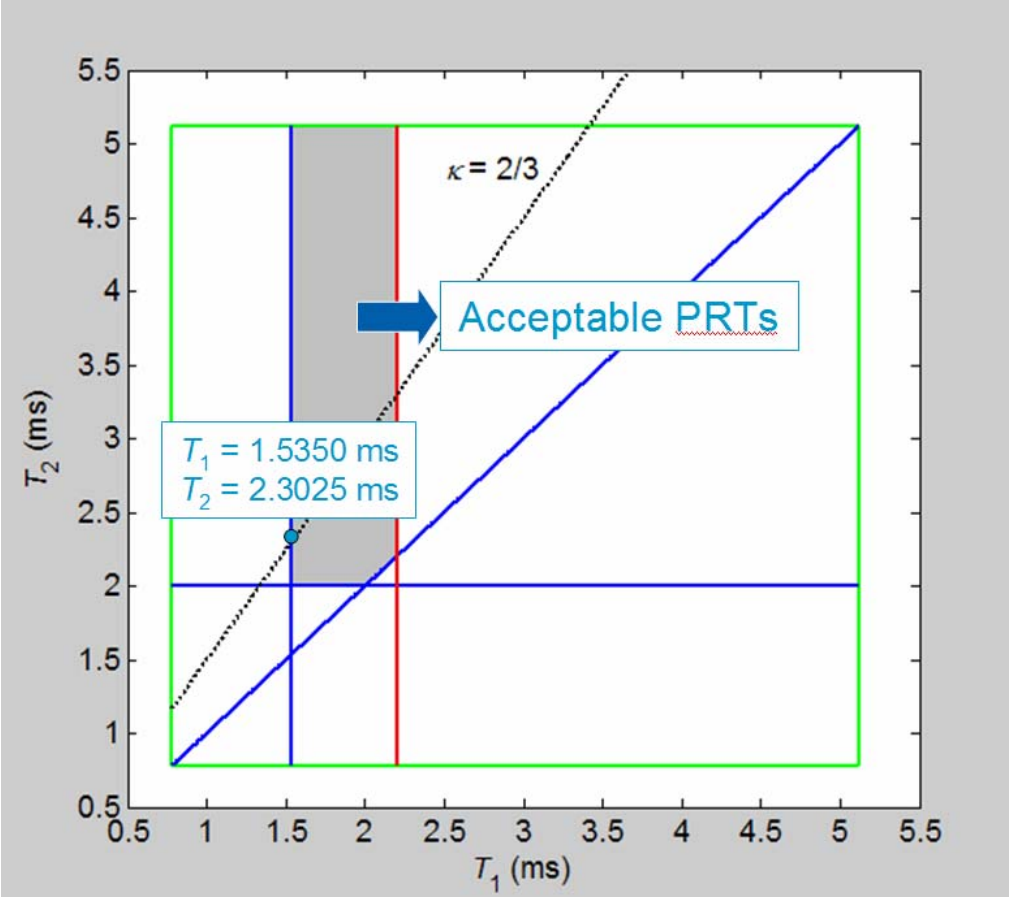

Fig. 3.2.1. Acceptable PRTs for the staggered PRT technique considering system limits, range coverage, design constraints, and signal coherency requirements.

3.3. Errors of Estimates

From the analysis in the previous section, we have the values of PRTs that can potentially fulfill all the constraints imposed by an operational system. However, do these values of T_1 and T_2 lead to acceptable errors of estimates? The answer to this question is not trivial because the staggered PRT technique uses different sets of spaced pairs to estimate each of the spectral moments, so the usual formulas for the standard error of estimates have to be modified. This is because the estimation of reflectivity in the staggered PRT algorithm depends on the location of the range gate with respect to three zones, as depicted in Fig. 3.3.1.

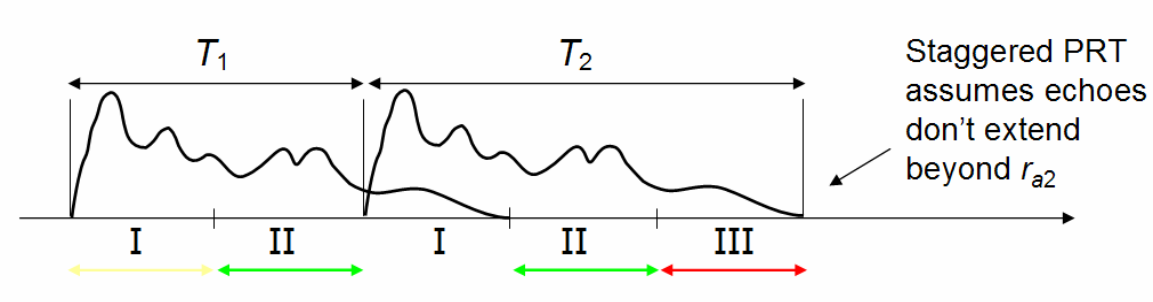

Fig. 3.3.1. Depiction of the three zones used for reflectivity estimation in the staggered PRT algorithm

Because the algorithm assumes that echoes do not extend beyond r_{a2}, only overlay of the short PRT into the long PRT is allowed, and the three zones depicted in Fig. 3.3.1 are determined accordingly. Zone I has clean returns in the short PRT, but may not in the long PRT; hence, only short PRT pulses are used in the estimation of reflectivity for all the range gates within zone I. Range gates in Zone II exhibit uncontaminated returns in both short and long PRTs; hence, all pulses can be used in the estimation process, leading to more accurate estimates of reflectivity, especially for large spectrum widths. Finally,

zone III is only available from the long PRT returns, and these are used for reflectivity estimates within this zone. Fig. 3.3.2 summarizes the performance of the three reflectivity estimators corresponding to each of the zones (performance shown here does not include averaging in range). Note that all estimators exhibit equivalent performance for narrow spectrum widths. This is because, for heavily correlated samples, the number of equivalent independent samples depends on the dwell time more than on the number of samples. For large spectrum widths, estimators that use all pulses perform better than those using just one set of pulses (either short or long PRT pulses). Also, performance improves for shorter PRTs as there are more samples in the dwell time.

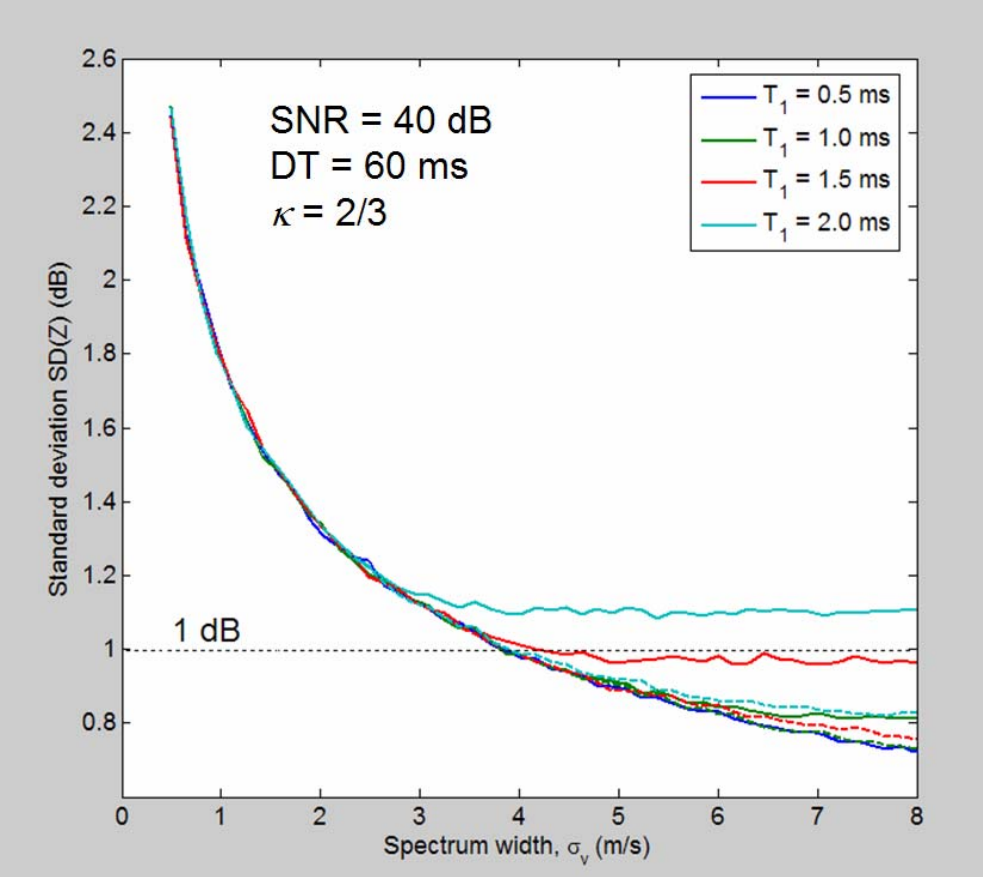

Fig. 3.3.2. Standard deviation of 250-m reflectivity estimates vs. spectrum width for different staggered PRT sets and constant PRT ratio (2/3), dwell time (60 ms), and signal-to-noise ratio (40 dB). Solid curves correspond to the estimators using short (or long) PRT pulses only; dashed curves correspond to estimators that use all pulses.

Doppler velocities in the staggered PRT algorithm are obtained by dealiasing v_1 (estimated from short PRT pairs) using v_2 (estimated from long PRT pairs); hence, errors of velocity estimates are those of v_1. Figure 3.3.3 shows the errors of velocities for this case and also for the case in which v_2 is dealiased using v_1. It is evident that the former is always better, and that shorter PRTs lead to better performance as there are more samples in the dwell time.

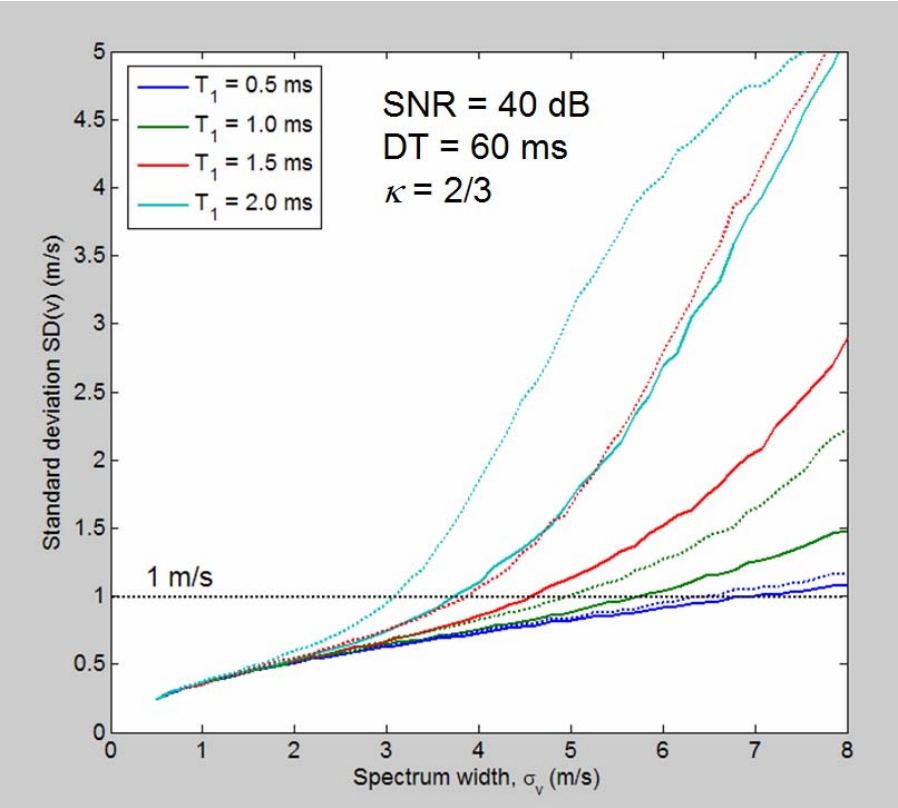

Fig. 3.3.4. Standard deviation of mean velocity estimates vs. spectrum width for different staggered PRT sets and constant PRT ratio (2/3), dwell time (60 ms), and signal-to-noise ratio (40 dB). Solid curves correspond to the estimators using short PRT pairs; dashed curves correspond to estimators that use long PRT pairs.

Spectrum width estimation in the staggered PRT algorithm uses the power estimate as described before and the lag-1 autocorrelation estimate that can be derived either from the short or the long PRT pairs. As shown in Fig. 3.3.3, decision of which set of pairs to use for the spectrum width estimation is not obvious. On one hand, estimation of spectrum widths from long PRTs is impaired by the saturation phenomenon described in our previous report (report 8). However, there is a crossover point for all curve pairs below which, estimates using long PRT pairs perform better than those using short PRT pairs. If we assume that most of the time the measured spectrum widths will be less than about 4 m/s, then, especially for the shorter PRTs, it is better to use the lag-1 autocorrelation estimates from the short PRT pairs. This contradicts what we recommended in our previous report and what was suggested by Zrnić and Mahapatra (1985). However, the decision depends on the actual PRTs being used and the true spectrum width of the signal (which is what we are trying to measure!).

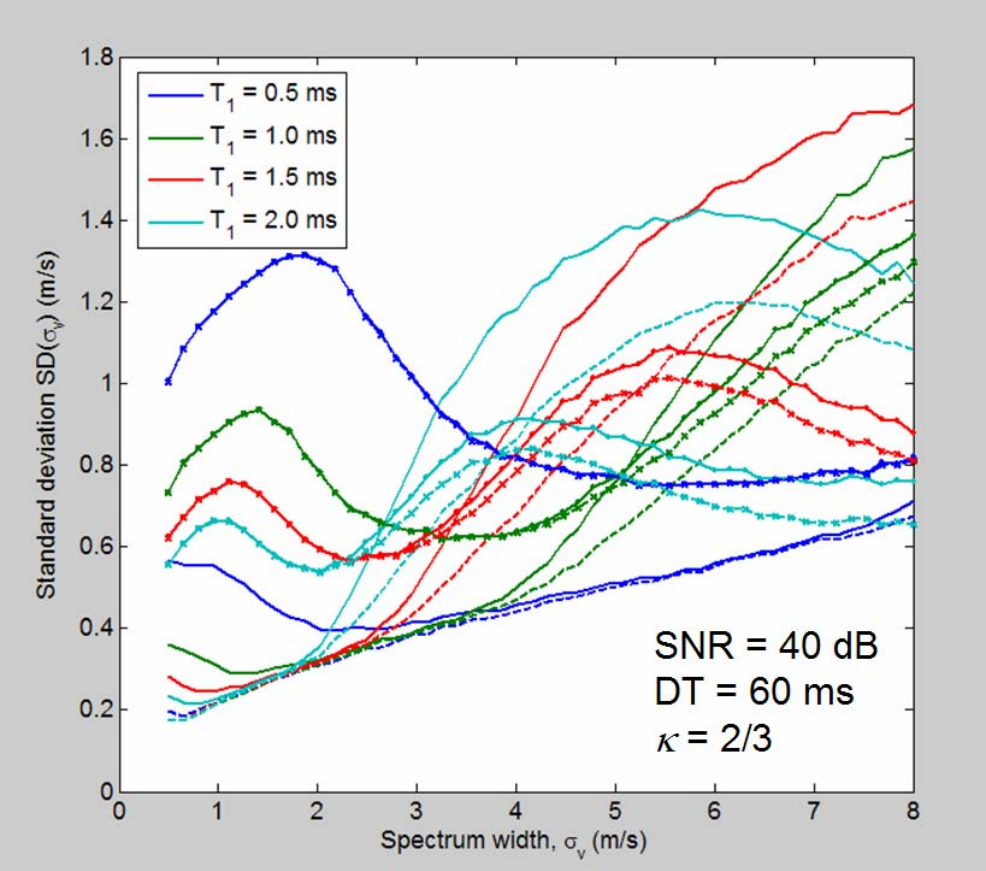

Fig. 3.3.4. Standard deviation of spectrum width estimates vs. spectrum width for different staggered PRT sets and constant PRT ratio (2/3), dwell time (60 ms), and signal-to-noise ratio (40 dB). Solid curves correspond to estimators using power estimates from short PRT pairs only; dashed curves correspond to estimators that use power estimates from all pairs. Curves with no markers correspond to estimators using lag-1 autocorrelation estimates from short PRT pairs; curves with markers correspond to estimators that use lag-1 autocorrelation estimates from long PRT pairs.

3.4. Replacing the Batch Mode

Because requirements for range coverage can be relaxed at intermediate to high elevations, staggered PRT appears as an excellent candidate to mitigate range and velocity ambiguities in the WSR-88D at these elevations, significantly improving the performance over the current batch mode. The staggered PRT technique can perform better than the batch mode both in terms of improving range coverage and reducing velocity aliasing.

Replacement scans for those using batch waveforms should have the same or larger range coverage. The range coverage should meet NEXRAD requirements but can be adjusted (relaxed) using maximum height of storm tops as discussed before. Note that requirements for range coverage in the WSR-88D are larger for reflectivity than those for velocity and spectrum width. This perfectly matches the performance of the staggered PRT technique, since r_{a2} (the maximum unambiguous range for reflectivity which is derived from the long PRT) is always larger than r_{a1} (the maximum unambiguous range for velocity and spectrum width which is derived from the short PRT). In addition to matching or exceeding range coverage requirements, a replacement of the batch mode should maintain the current update times (dictated by the antenna rotation rate). Hence, a replacement staggered PRT scan should operate with the same dwell times as the batch scan that is trying to replace. Finally, after a suitable set of PRTs is determined based on the previous conditions, we must make sure that the resulting errors of estimates meet or exceed NEXRAD requirements.

The process of selecting staggered PRTs is as follows:

(1) T_1 is selected based on range coverage requirements for Doppler velocity assuming that storm tops are not higher than 18 km (see Fig. 3.4.1),

(2) T_2 is selected based on T_1 and the PRT ratio ($\kappa = 2/3$ is preferred)

(3) The number of pairs in a radial is determined by the batch mode dwell time and the selected staggered PRTs.

(4) Finally, T_1, T_2, and M_p determine the errors of estimates.

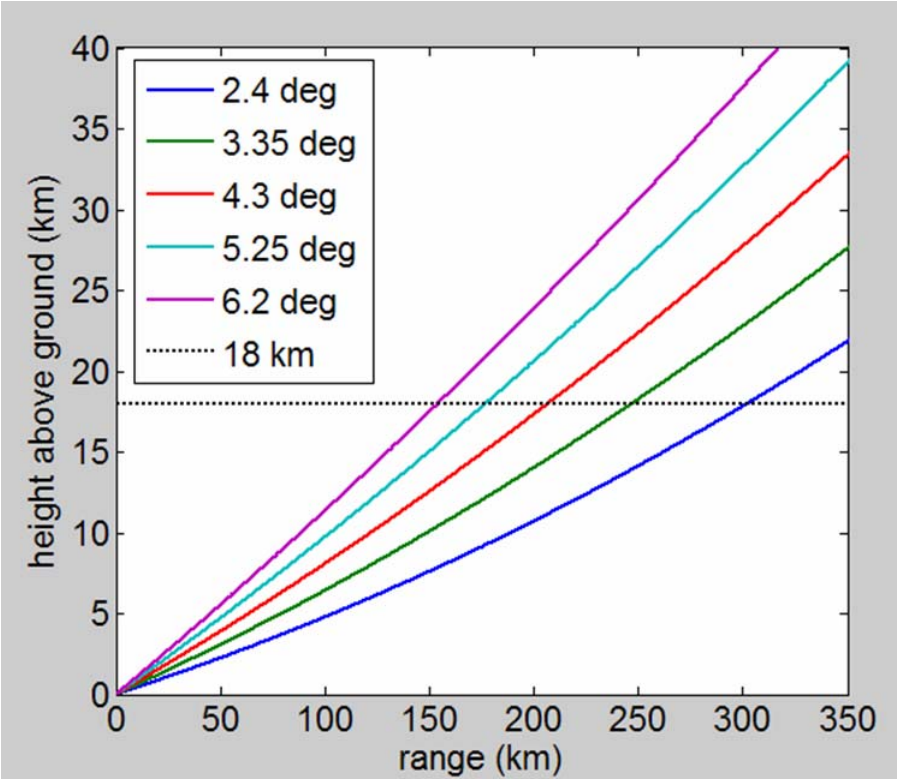

Fig. 3.4.1. Antenna beam height above the ground vs. slant range for different elevation angles. Required maximum range coverage can be derived by assuming that storm tops do not extend higher than 18 km above the ground (dotted line).

In what follows, the staggered PRTs for batch mode replacement are selected, and the performance of staggered-PRT-based estimates is compared to that of the batch mode for the standard WSR-88D VCPs (note that VCP 31 does not employ the batch mode, and the VCP 121 employs MPDA to achieve improved velocity dealiasing in the ORPG). Errors are computed using theoretical formulas (Doviak and Zrnić, 1993) and the following parameters:

	SNR (dB)	σ_v (m/s)
Reflectivity	10	4
Mean velocity	8	4

Errors for reflectivity in the batch mode are given for the long and short PRT estimates (the algorithm uses short PRT estimates in places with no overlaid echoes, and reverts to the long PRT estimates otherwise). In all cases, reflectivity errors do not include range averaging.

a) VCP 11: 5 scans (out of 16) employ batch waveforms

EL (deg)	**Batch Mode DT (ms)**	T_1 **(ms)**	T_2 **(ms)**	M_p
2.4	59.09	1.535	2.3025	**15**
3.35	53.89	1.535	2.3025	**14**
4.3	53.89	1.381	2.0715	**16**
5.25	55.99	1.181	1.7715	**19**
6.2	55.99	1.028	1.542	**22**

	Batch Mode		**Staggered PRT**	
EL (deg)	SD(Z) (dB)	SD(v) (m/s)	**SD(Z) (dB)**	**SD(v) (m/s)**
2.4	1.73 / 1.19	0.995	**1.12**	**1.17**
3.35	1.91 / 1.19	0.995	**1.16**	**1.21**
4.3	1.91 / 1.19	0.995	**1.18**	**1.17**
5.25	1.77 / 1.19	0.995	**1.08**	**1.15**
6.2	1.77 / 1.19	0.995	**1.07**	**1.15**

b) VCP 12: 5 scans (out of 17) employ batch waveforms

EL (deg)	**Batch Mode DT (ms)**	T_1 **(ms)**	T_2 **(ms)**	M_p
1.8	35.33	1.535	2.3025	**9**
2.4	36.23	1.535	2.3025	**9**
3.2	36.23	1.535	2.3025	**9**
4	36.23	1.455	2.182	**10**
5.1	34.26	1.208	1.8116	**11**

	Batch Mode		**Staggered PRT**	
EL (deg)	SD(*Z*) (dB)	SD(*v*) (m/s)	**SD(*Z*) (dB)**	**SD(*v*) (m/s)**
1.8	2.44 / 1.37	1.18	**1.40**	**1.5**
2.4	2.65 / 1.32	1.12	**1.40**	**1.5**
3.2	2.65 / 1.32	1.12	**1.40**	**1.5**
4	2.65 / 1.32	1.12	**1.35**	**1.45**
5.1	2.65 / 1.35	1.16	**1.36**	**1.49**

c) VCP 21: 4 scans (out of 11) employ batch waveforms

EL (deg)	**Batch Mode DT (ms)**	T_1 **(ms)**	T_2 **(ms)**	M_p
2.4	86.99	1.535	2.3025	**23**
3.35	86.99	1.535	2.3025	**23**
4.3	86.99	1.381	2.0715	**25**
6.0	87.71	1.054	1.5814	**33**

	Batch Mode		**Staggered PRT**	
EL (deg)	SD(*Z*) (dB)	SD(*v*) (m/s)	**SD(*Z*) (dB)**	**SD(*v*) (m/s)**
2.4	1.71 / 0.94	0.765	**0.93**	**0.94**
3.35	1.71 / 0.94	0.765	**0.93**	**0.94**
4.3	1.71 / 0.94	0.765	**0.92**	**0.93**
6.0	1.65 / 0.94	0.765	**0.88**	**0.93**

d) VCP 32: 3 scans (out of 7) employ batch waveforms

EL (deg)	**Batch Mode DT (ms)**	T_1 **(ms)**	T_2 **(ms)**	M_p
2.5	241.71	1.535	2.3025	**63**
3.5	241.71	1.535	2.3025	**63**
4.5	241.71	1.335	2.002	**72**

	Batch Mode		**Staggered PRT**	
EL (deg)	SD(*Z*) (dB)	SD(*v*) (m/s)	**SD(*Z*) (dB)**	**SD(*v*) (m/s)**
2.5	1.5 / 0.56	0.43	**0.58**	**0.57**
3.5	1.5 / 0.56	0.43	**0.58**	**0.57**
4.5	1.5 / 0.56	0.43	**0.57**	**0.56**

From the previous tables, it is evident that reflectivity estimates are always better with staggered PRT (for example, VCP 32 and VCP 21 would not require range averaging to produce acceptable reflectivity estimates). However, errors in velocity estimates are always the same or higher than with the batch mode. Whereas staggered PRT based estimates using VCP 32 and VCP 21 are within 1 m/s, those from VCP 11 and VCP 12 are above 1 m/s by as much as 50% (see VCP 12). However, note that velocity errors from the batch mode in VCP 12 are also larger than 1 m/s.

To reduce the errors of estimates, one might attempt to use shorter PRTs and sacrifice range coverage (and increase the likelihood of overlaid echoes). Figure 3.4.2 shows the errors of reflectivity, velocity, and spectrum width for different PRT values. In all cases, the dwell time is about 60 ms and the true spectrum width is 4 m/s. For reflectivity and spectrum width estimates, the SNR is 10 dB; for velocity, the SNR is 8 dB. The bottom right panel of this figure shows the decreasing number of pairs as the PRT increases for a

fixed dwell time. As expected, reflectivity errors increase for larger PRTs as the number of pairs is reduced. However, NEXRAD requirements can be met with any PRT set in the allowable range. Alternatively, spectrum width estimates are only acceptable for the range 0.85 ms < T_1 < 1.8 ms. However, errors of velocity estimates achieve a minimum value of 1.125 m/s at T_1 = 1.3 ms. Therefore, it is not possible to reduce the errors of velocities estimates by reducing the PRTs and maintaining the same dwell times.

A solution to this problem consists in adding staggered PRT pairs to each radial (i.e., increasing the dwell time). To reduce the errors of velocity estimates to less than 1 m/s, we would need to increase the scan time by about 7 sec; effectively adding approximately 30 sec to the entire volume coverage pattern. If this is deemed unacceptable, the requirements could be relaxed to allow slightly higher errors of estimates (as currently done with VCP 12). Still, if this were also unacceptable, we could use range oversampling techniques to reduce the errors of estimates without increasing the acquisition time. The staggered PRT technique is fully compatible with range oversampling techniques, and these are already scheduled to be incorporated in future ORDA upgrades.

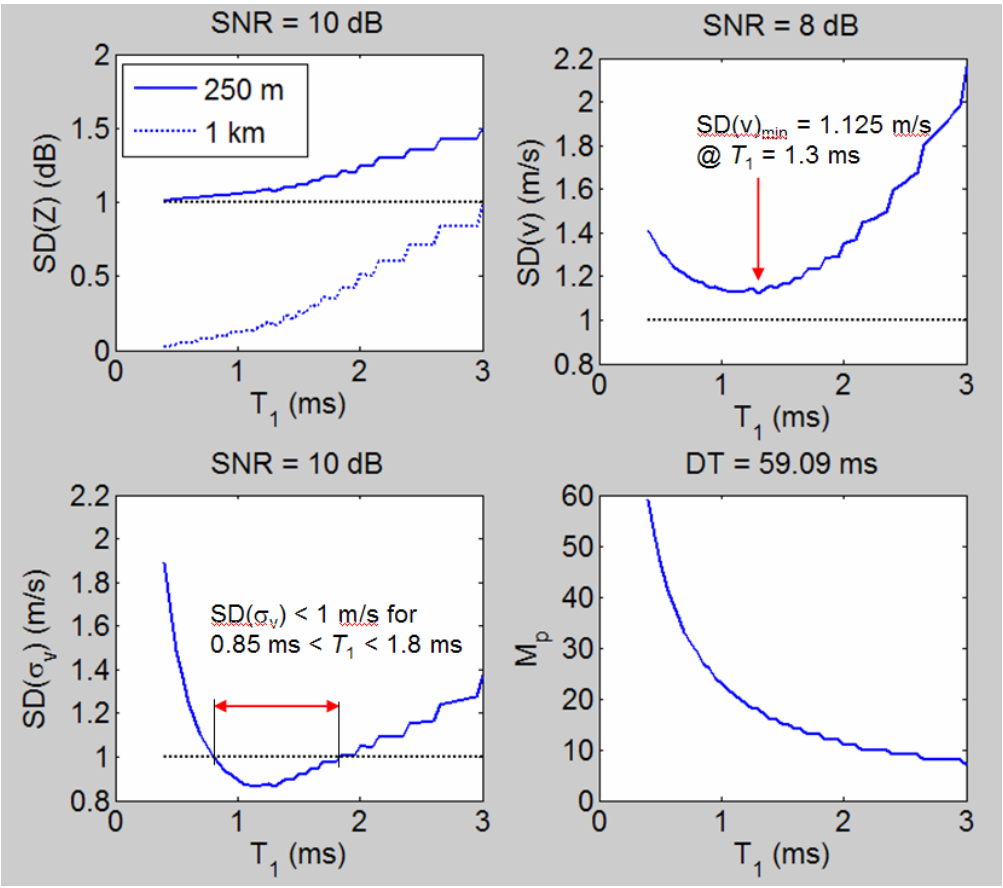

Fig. 3.4.2. (a, b, c) Errors of reflectivity, velocity, and spectrum width for different staggered PRT sets using $\kappa = 2/3$ and a constant dwell time of 59.09 ms. In all cases the true spectrum width is 4 m/s and the SNR is indicated in the figure. (d) Number of staggered PRT pairs for different staggered PRT sets using $\kappa = 2/3$ and a constant dwell time of 59.09 ms.

Figure 3.4.3 shows an example of the improvement realized by replacing the batch mode with a suitable staggered PRT scheme. Time series data was collected with the KOUN radar in Norman, OK using the experimental VCP 2049 (see report 8) in which a batch mode scan is immediately followed by a staggered PRT scan employing the same dwell times (i.e., achieving the same update times). A side-by-side comparison of reflectivity and Doppler velocity fields confirms that the staggered PRT can unambiguously recover reflectivities with the required range coverage and at the same time produce velocity

fields free of aliasing and/or obscuration (purple haze). In addition, the predicted increase of velocity errors is almost unnoticeable, at least for the conditions of SNR and spectrum width existing in this case.

In summary, compared to the batch mode, the staggered PRT technique allows for an extension of both the maximum unambiguous range and maximum unambiguous velocity by means of a relatively simple algorithm. In addition, reflectivity estimates are more accurate, and there exist effective ways to mitigate clutter contamination and perform spectral analysis. However, velocity estimates exhibit slightly larger errors (about 15 to 30% larger than the batch mode at SNR = 8 dB and σ_v = 4 m/s). Despite of this, the staggered PRT technique is an excellent candidate to replace the batch mode (and possibly the continuous Doppler mode at higher elevation angles) in standard WSR-88D VCPs. In this regard, replacement of the batch mode in VCPs 32 and 21, as indicated in the previous section, could proceed while meeting NEXRAD requirements; however, VCPs 11 and 12 exhibit velocity errors that are larger than 1 m/s. This could be handled by adding time to the VCPs, or by employing range oversampling techniques. In any case, the impact of adding new PRTs to other components of the system should be evaluated.

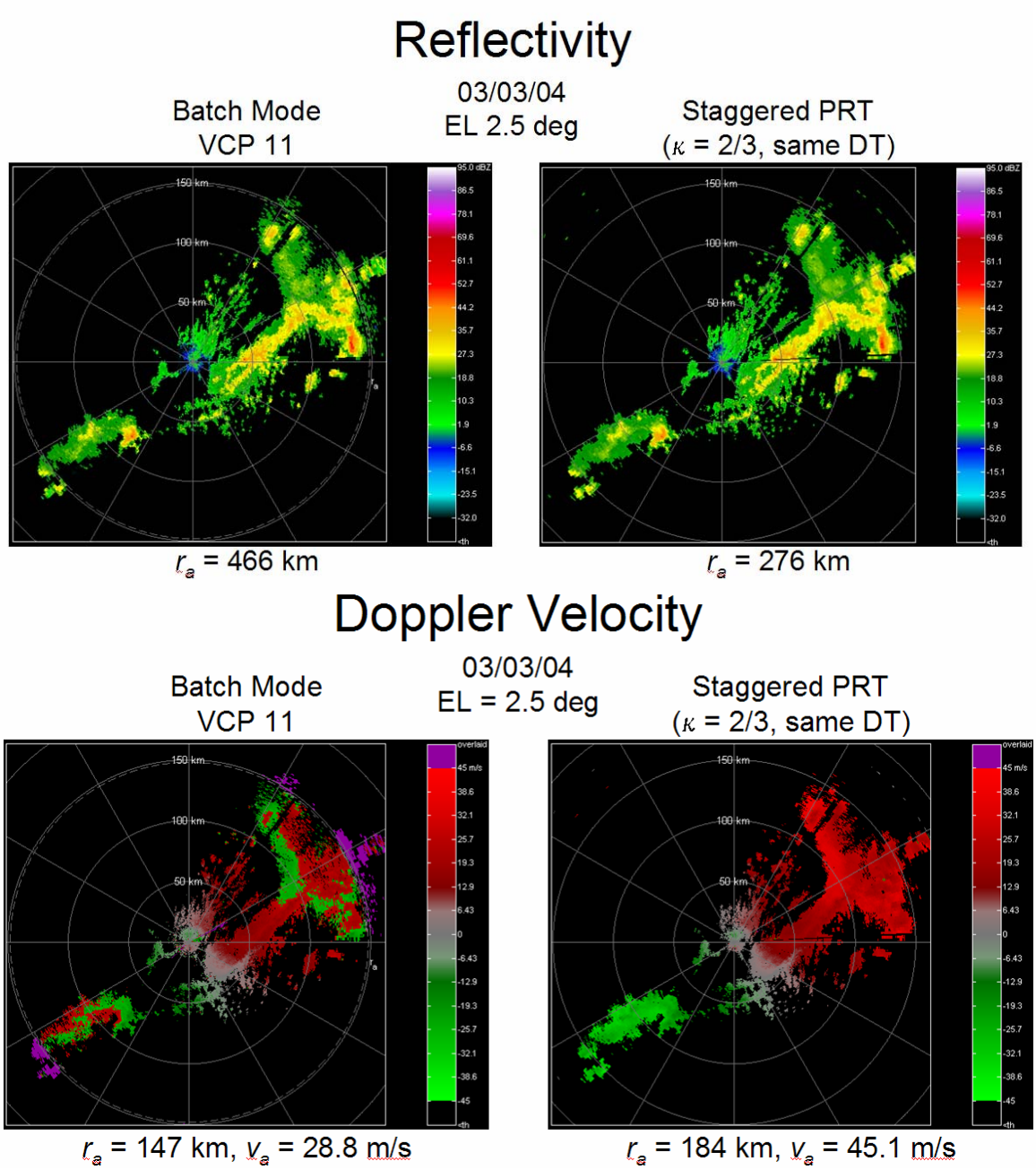

Fig. 3.4.3. Reflectivity and Doppler velocity fields obtained with batch mode and staggered PRT processing of time series data collected on March 3, 2004 with the KOUN radar in Norman, OK. The antenna elevation angle is 2.5 deg, the dwell time is the same in both cases, and the staggered PRTs have a ratio $\kappa = 2/3$.

3.5. Recovery of Reflectivity to $5T_u$ in Staggered PRT

3.5.1. *Introduction.*

The staggered PRT scheme designed for obtaining a larger unambiguous velocity using the difference PRT, (T_2-T_1), can also give a larger unambiguous range. Without any kind of overlay resolution method the staggered PRT technique has an unambiguous range of $r_{a1} = cT_1/2$, and with one-overlay resolution (report 4) it is possible to extend the range to $r_{a2} = cT_2/2$ corresponding to the longer of the two PRTs. By overlay resolution it is implied that all three spectral moments (the reflectivity, the mean Doppler velocity, and the spectrum width) of both the overlaid signals are estimated to within acceptable accuracy. However, the one-overlay resolution is effective only for overlay power ratios less than about 20 dB for median spectrum widths. If the overlay is too strong, then it is not possible to accurately estimate the spectral parameters of the weaker of the two overlaid signals. The maximum range requirement can be met using the staggered PRT transmission in elevations 2.42° and higher (Table A.3. report 8) with an unambiguous velocity, $v_a \geq 45$ m s^{-1}. In the WSR-88D VCP11 scan using the contiguous Doppler (CD) scan, the unambiguous velocity is 25 m s^{-1}. Thus the staggered PRT improves v_a by 1.8 times while retaining the maximum r_a. In the lowest two elevations the long PRT scan is retained to get the reflectivity over 460 km. Only the short PRT Doppler scan is replaced by the SZ phase coded transmission to double the range over which the velocity is recovered. In this section we explore the possibility of using the staggered PRT transmission for the lowest two elevations as well without compromising the present capability of WSR-88D.

3.5.2. *Reflectivity estimation with overlaid signals*

In the one-overlay resolution algorithm an assumption is made that there is no weather beyond the range r_{a2}. With that assumption, the overlay occurs only for certain ranges and in alternate samples; hence, it is possible to separate the two overlaid echoes. If this criterion is not met, the overlay can occur in all the samples from certain ranges which cannot be resolved easily. However, it may be possible to estimate the mean powers if not all the spectral moments. Because the overlaid echoes from two different ranges are uncorrelated, the mean power estimate from the sample sequence is a sum of the mean powers of the two overlaid echoes.

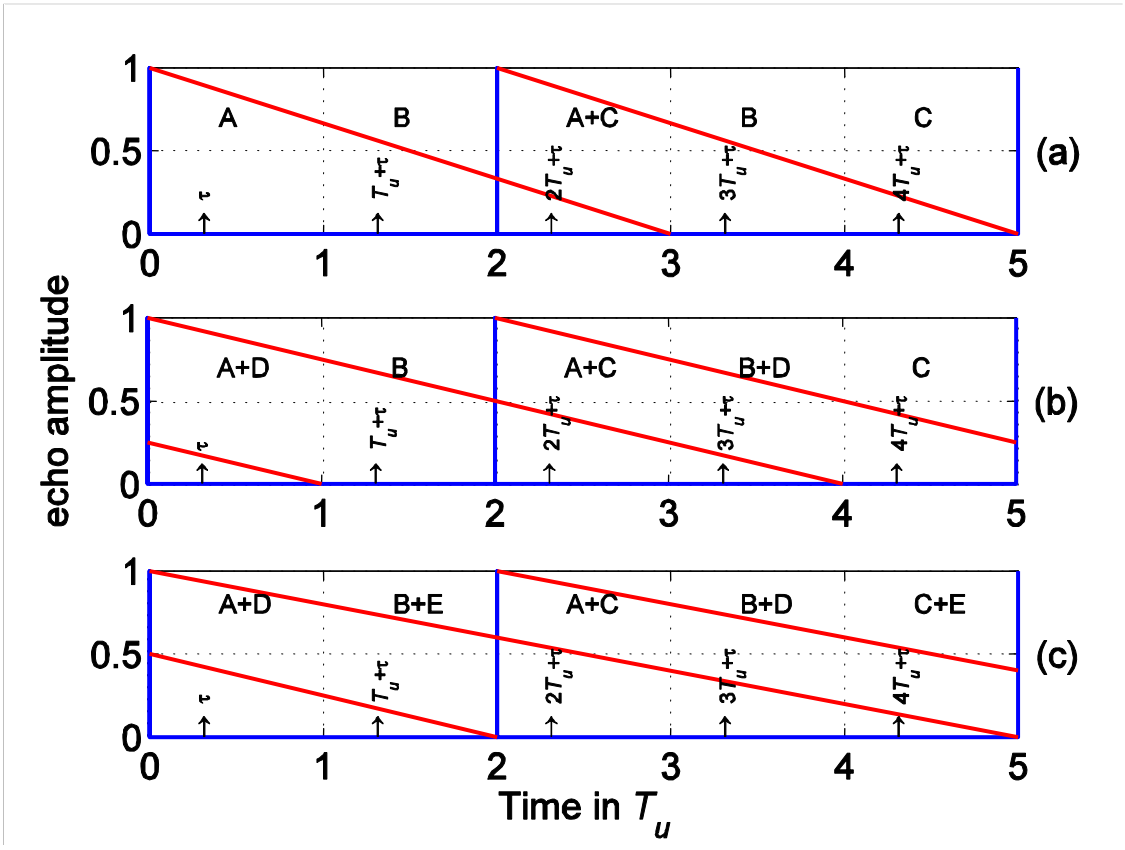

Fig. 3.5.2.1. Illustration of different overlay situations in staggered PRT scheme.

Fig. 3.5.2.1 shows the staggered PRT transmission scheme for $\kappa = T_1/T_2 = 2/3$ for one cycle (T_1+T_2). The transmitted pulses are at 0 and $2T_u$. The sloping lines represent the echo amplitude as a function of time. The three figures 3.5.2.1 (a), (b) and (c) depict the echoes extending to $3T_u$, $4T_u$, and $5T_u$ intervals after the pulse transmission. No overlay occurs if the echoes extend to only $2T_u$. We label the ranges in the delay time interval $(n\text{-}1)T_u$ to nT_u, n = 1, 2, 3, 4, and 5, as A, B, C, D, and E regions, respectively. We take a set of 5 echo samples at delay times τ ($\tau < T_u$), ($\tau + T_u$), ($\tau + 2T_u$), ($\tau + 3T_u$), and ($\tau + 4T_u$), after the T_1 pulse is transmitted, and label them as v_1 to v_5. From the figure, it is clear that for one-overlay situation (Fig. 3.5.2.1a) only the 3rd sample has overlay from A and C regions. For the second case (Fig. 3.5.2.1b) we have overlay in three of the five samples. The samples v_1, v_3, and v_4 have returns from regions A&D, A&C, and B&D, respectively. We label this situation as 3-overlay situation. Similarly, the last case (Fig. 3.5.2.1c) has overlay in all the 5 samples (5-overlay case).

If this were a deterministic problem, it would be easy to solve the system of equations and determine the echo powers from each of the five ranges involved. For example, consider the 5-overlay situation and let the power returns from samples 1 through 5 be p_1 through p_5. If the power returns from ranges A though E are p_a, p_b, p_c, p_d, and p_e, respectively, then we can write a matrix equation which relate these powers as

$$\begin{bmatrix} 1 & 0 & 0 & 1 & 0 \\ 0 & 1 & 0 & 0 & 1 \\ 1 & 0 & 1 & 0 & 0 \\ 0 & 1 & 0 & 1 & 0 \\ 0 & 0 & 1 & 0 & 1 \end{bmatrix} \begin{bmatrix} p_a \\ p_b \\ p_c \\ p_d \\ p_e \end{bmatrix} = \begin{bmatrix} p_1 \\ p_2 \\ p_3 \\ p_4 \\ p_5 \end{bmatrix}. \tag{3.39}$$

The matrix is non-singular and hence can be inverted to get the individual powers p_a to p_e.

$$\begin{bmatrix} p_a \\ p_b \\ p_c \\ p_d \\ p_e \end{bmatrix} = \frac{1}{2} \begin{bmatrix} 1 & 1 & 1 & -1 & -1 \\ -1 & 1 & 1 & 1 & -1 \\ -1 & -1 & 1 & 1 & 1 \\ 1 & -1 & -1 & 1 & 1 \\ 1 & 1 & -1 & -1 & 1 \end{bmatrix} \begin{bmatrix} p_1 \\ p_2 \\ p_3 \\ p_4 \\ p_5 \end{bmatrix} \tag{3.40}$$

However, this does not work perfectly in extracting the individual range powers when the powers involved are estimates available from the overlaid echo samples. Therefore, we can expect (3.39) to work only if the weaker of the two overlaid powers is more than the estimate error in the stronger power. It can be argued that if the standard error of the stronger power estimate is ±1dB (~25.8%), the weaker overlaid power must be larger than 0.25 (1dB) of the stronger power, i.e., the overlay power ratio must be within ±6 dB, for (3.39) to resolve the powers. Since each sample has overlay from two ranges, all the five ranges must have echo powers within ±6 dB of each other. This is generally not satisfied in actual weather situations. Most often, the overlay power ratio has a large dynamic range.

3.5.3. *Simulation study*

To test this scheme of resolving the overlay powers, time series is simulated with five-overlays and velocities (for each range) were chosen randomly within the interval ± v_a (v_a = 41.66 m s^{-1}). The PRTs are T_1 = 1.2 ms, and T_2 = 1.8 ms, so that the maximum range corresponding to (T_1+T_2) is 450 km at 3 GHz transmission frequency. The spectrum width is set to 4 m s^{-1} for all the five ranges. Individual time series are generated for each of the five ranges and then are combined appropriately to form a staggered PRT overlaid sample sequence.

Mean powers are estimated using a time series length of 32 pairs of staggered PRT pulse transmissions. The total number of samples is 5x32 = 160, and each power estimate, p_1 through p_5, is computed from 32 samples. For example, p_k , k = 1 to 5, is given by

$$p_k = \frac{1}{32}\sum_{i=0}^{31} | v_{5i+k} |^2 \tag{3.41}$$

Individual powers are resolved (assigned a correct range) using these five estimates in (3.40). The resolved power estimates are compared with the actual power estimates from the complete time series for individual ranges to compute the errors. If the resolved power is within 3 dB of the actual power, it is assumed to be correct and if the error is more than 3 dB, it is discarded as unresolved. A large number of simulations were carried out to generate the statistics of reflectivity resolution using this procedure.

Because five different ranges are involved, there are different combinations of overlay power ratios possible. Fig. 3.5.3.1 shows one such plot of success in resolving the mean powers of individual ranges. In this plot, the percentage success in recovering the weaker

signal p_c is a function of overlay power ratio p_o/p_c, where p_o is the total sum of all five powers. The stronger signal p_a is always recovered, but the weaker signal recovery depends on the overlay power ratio. Further, the presence of other range overlays also affects the recovery. The four traces in Fig. 3.5.3.2 indicate the extent of degradation in the recovery of the weaker signal when more than one overlay is present. The first two traces are for one-overlay situation; without and with p_b present. Note that in a one-overlay situation all three powers can be estimated directly, because $p_a = p_1$, $p_b = p_2$, and $p_c = p_5$ (Fig. 3.5.2.1a). We do not have to use the overlaid samples at $3T_u$. Similarly for the situation in Fig. 3.5.2.1b, we have $p_b = p_2$ and $p_c = p_5$ available directly, and the other two can be obtained from $p_a = (p_3 - p_5)$ and $p_d = (p_4 - p_2)$. The recovery of p_a will be affected if $p_a < p_c$, and p_d will be affected if $p_d < p_b$. However, we must have an a priori knowledge of the overlay extent to exercise this option. In the absence of any prior information from a long PRT scan, we have to assume the presence of all the five echoes and apply (3.40). On the other hand, it is possible to choose the PRTs and an elevation angle such that the situation depicted in Fig. 3.5.2.1b is satisfied.

Figure 3.5.3.1 is generated using (3.40) for resolving the overlaid powers with no a priori knowledge of the weather extent. In case that the overlay extends only up to $4T_u$ (Fig. 3.5.2.1b) the powers p_a and p_d need to be resolved. The percentage of success for this case is plotted in Fig. 3.5.3.2. It is clear that the weaker signal cannot be reliably recovered if the overlay power ratio is more than about ±6 dB when only two signals are involved, and this extent is further reduced if more than two signals are involved. Thus, the long PRT transmission appears to be indispensable to get a clear range up to 460 km.

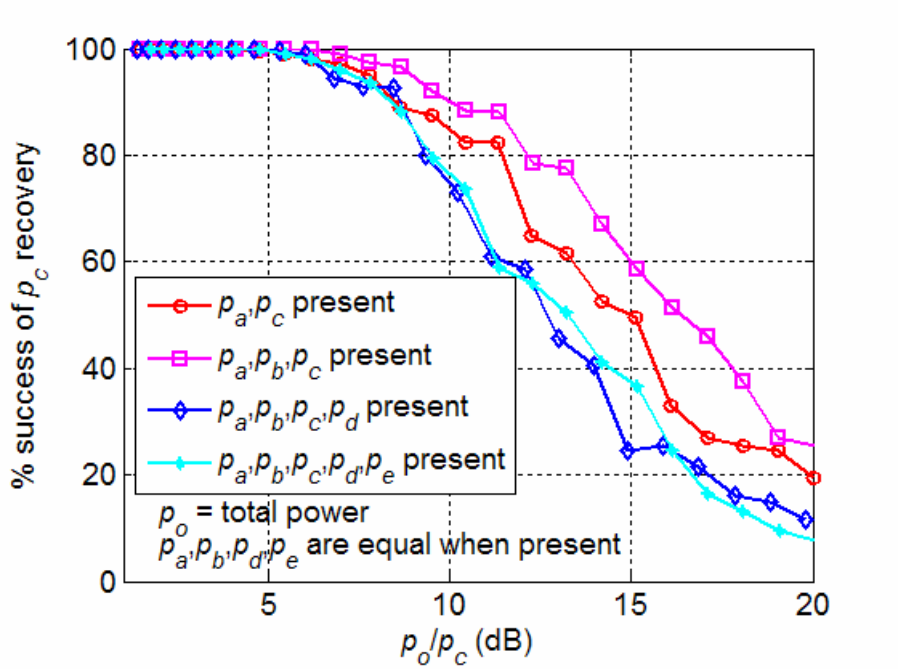

Fig. 3.5.3.1. The percentage success rate of weaker signal power recovery for echo extent up to $5T_u$. Note that the red curve is offset from the pink because we plot the logarithm of $1 + (p_a/p_c)$ and $1 + (p_a + p_b)/p_c$, but $p_a = p_b$ so it is $1 + 2p_a/p_c$. Hence, for the same p_c the curve shifts to the right.

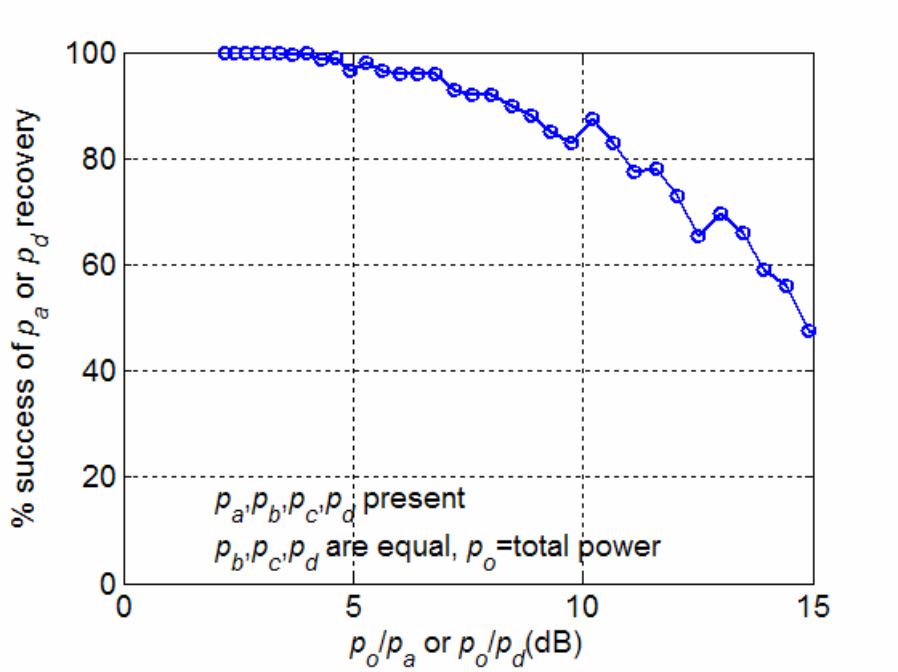

Fig. 3.5.3.2. Percentage of success rate of weaker signal power recovery for echo extent up to $4T_u$.

3.6. Summary of spectral moment estimators

Spectral moment estimates from staggered pulse sequences have been studied in several reports (reports 3, 4, and 5). Herein, a summary of the results is presented. In the spectral domain clutter filtering scheme (section 3.1), the staggered PRT time series is converted to a uniform time series with signal sampled at T_u intervals by inserting zeros in places where samples are not available. The spectral processing can be carried out on the derived time series to filter the clutter. The reconstruction of the spectrum after the clutter is filtered is accomplished by the "magnitude deconvolution" procedure. This reconstructs the magnitude spectrum well if the condition of "narrow" criterion (width less than 1/5 the of the extended unambiguous velocity interval) is satisfied.

The spectrum width is computed from 2/5 (for $\kappa = 2/3$) of the spectral coefficients centered on the mean velocity. Now, from this spectrum, we can compute autocorrelations $R(T_u)$ and $R(2T_u)$, and the mean power S. From these three quantities, we can calculate the spectrum width in three different ways.

It is also possible to reconstruct the complex spectrum over the 2/5 of the Nyquist interval using spectral restoration procedure-2 (Sachidananda and Zrnić, 2005). This procedure is derived especially for estimating dual polarized parameter Φ_{DP} and ρ_{hv} because Φ_{DP} requires the phases of the spectral coefficients. For all other parameters magnitude spectra are sufficient. However, if the computational time is not a great constraint we can apply this procedure to reconstruct the complex spectra in the case of single polarized radar. From these spectra we can obtain the moments; we compare the

quality of these moments with moments obtained by other means (as previously reported) herein.

In the absence of ground clutter, the ground clutter filter (GCF) is not required, and pulse pair processing can be used for computing the autocorrelations in the time domain. It is also possible to reconstruct 2/5 of the complex spectrum centered on the mean velocity and estimate the spectrum width from the spectrum. However, this involves additional computations. Thus, we have several alternatives for width estimation.

Extensive simulation is carried out with each of the estimators to determine the accuracy of the width estimates with respect to the various parameters that affect its accuracy. The mean and standard deviation of the error in the width estimate width respect to the width input to the time series simulation program is calculated to determine the performance of each estimator.

3.6.1. *Spectrum width estimators for staggered PRT data without GCF*

The performance of the width estimators based on the autocorrelation estimates have been studied for the uniform PRT sequences, and formulae are available for the mean and standard errors of these estimators (Doviak and Zrnić, 1993). However, first we shall include the results of simulations on uniform PRT sequences as a reference for comparison with the staggered PRT estimators. Here, we use the notation T_u for the uniform PRT as well as the derived uniform PRT from the staggered PRT sequence. We consider $\kappa = T_1/T_2 = 2/3$ for the staggered PRT, where T_1 and T_2 are the two PRTs, with $T_1 = 2T_u$ and $T_2 = 3\ T_u$. We use the notation S for the mean power, and $R(T_u)$, the autocorrelation at lag T_u, etc., with lag time in brackets.

For the uniform PRT, we can compute S, $R(T_u)$, and $R(2T_u)$. Thus, for uniform PRT we consider three estimators: est#1 using S/$R(T_u)$, est#2 using S/$R(2T_u)$, and est#3 using $R(T_u)/R(2T_u)$. The est#1 and est#2 are given by equation 6.27 of Doviak and Zrnić (1993), and the est#3 is by equation 6.32 in the same book. The same holds for estimates from spectra which are reconstructed out of staggered sequences; the only computations are from sinusoidal weighting of spectra which is exactly equivalent to the est#3. These give us some reference values to evaluate the "staggered PRT" width estimators.

The staggered PRT has less information (2 samples out of 5) than available in a uniform PRT sequence. For the staggered PRT, we number the estimators in the same way but using T_1 and T_2 in places of T_u and $2T_u$. Thus, the estimators for the staggered PRT are: est#1 using S/$R(T_1)$, est#2 using S/$R(T_2)$, and est#3 using $R(T_1)/R(T_2)$.

In the absence of the ground clutter filter, it appears best to use the time domain pulse pair method of computing the autocorrelations $R(T_1)$ and $R(T_2)$. Hence for the staggered PRT we have three estimators for the spectrum width, σ_v, given by

Est#1:
$$\hat{\sigma}_v = \frac{\sqrt{2}v_{a1}}{\pi}\sqrt{|\ln(|\hat{S}/\hat{R}(T_1)|)|} \tag{3.42}$$

Est#2:
$$\hat{\sigma}_v = \frac{\sqrt{2}v_{a2}}{\pi}\sqrt{|\ln(|\hat{S}/\hat{R}(T_2)|)|} \tag{3.43}$$

Est#3:
$$\hat{\sigma}_v = \frac{2v_a}{\sqrt{6}\pi}\sqrt{|\ln(|\hat{R}(T_1)/\hat{R}(T_2)|)|} \tag{3.44}$$

where S is the mean power, $v_a = \lambda/(4T_u)$, $v_{a1} = \lambda/(4T_1)$ and $v_{a2} = \lambda/(4T_2)$. The hat over the parameter indicates an estimate. The staggered PRT time series is simulated with input

widths varying from 0.5 m/s to 8 m/s, samples at intervals of 0.5 m/s, and the input velocity is spread uniformly over the extended Nyquist interval. The extreme 10 percent of the Nyquist is not included to avoid velocity aliasing. The mean power is made sufficiently large to provide a SNR > 30 dB. The width estimates are obtained using the above three expressions for each realization of the time series. The error in the width is defined as the difference between the input spectrum width to the simulation program and the estimated width. One hundred simulations are carried out at each of the input parameter sets, and mean bias and the standard error is computed with respect to the simulation input parameters.

If the clutter is to be filtered from a staggered PRT sequence, a spectral domain filtering and bias correction procedure (report 3) should be applied. This spectrum reconstruction procedure can also be applied in the absence of the clutter filter to generate the spectrum of the signal samples at T_u intervals. The spectrum can be reconstructed either in the magnitude domain or, with a more elaborate procedure, the complex spectrum can also be reconstructed over 2/5 of the extended Nyquist interval. The magnitude domain spectrum reconstruction is exact only if the "narrow" criterion is satisfied by the weather signal. However, if the weather signal coefficients are spread over 2/5 (or less) of the extended Nyquist interval, accurate velocity estimates can be obtained even though the reconstructed spectrum is not exact. In the absence of the clutter, the complex spectral reconstruction procedure restores 2/5 of the spectrum accurately. Hence for the complex spectrum reconstruction procedure, the signal spectrum can have significant coefficients spread over 2/5 of the extended Nyquist which is twice that defined by the "narrow" criterion.

The velocity and the spectrum width can also be estimated from the reconstructed spectra using the spectral reconstruction procedure. In an effort to compare all these estimation procedures, the bias and standard deviation of the error in the spectrum width as well as the reflectivity and velocity are computed using simulated time series, and are presented in the following figures.

Fig. 3.6.1.1 compares the bias error in the width estimates using estimator #1, i.e., $w\{S/R(T_u)\}$ for the uniform PRT and for the reconstructed spectra, and $w\{S/R(T_1)\}$ for the staggered PRT pulse pair processing as indicated in the figure. The blue curve is the standard error in the width estimate using the uniform time series, and serves as a reference. It is seen from the figure that the magnitude deconvolution procedure without the window performs as good as the uniform PRT for widths up to 5 m s^{-1}. This is about the "narrow spectrum" limit of the PRT in the simulation. With the von Hann window, the magnitude deconvolution procedure performs much better for widths less than 5 m s^{-1} in terms of the width estimate standard error. The staggered PRT pulse pair, magnitude deconvolution with window, and the complex spectral reconstruction with window perform almost the same. It is interesting to note that the complex spectral reconstruction method without the window performs better than the uniform PRT reference. From the simulations, we concluded that this is because the spectral skirts are removed from the 3/5 of the extended Nyquist interval. It is also seen that the cross over point between this curve (cyan) and the uniform PRT curve (blue) is about 7.5 m/s, which is approximately where the signal spectra exceeds the 2/5 of the extended Nyquist interval.

Figure 3.6.1.2 is a similar plot for the estimator #2 (i.e., $w\{S/R(T_{2u})\}$; $w\{S/R(T_2)\}$). Except for the staggered PRT pulse pair processing, all other curves using $w\{S/R(2T_u)\}$

for width estimation, show improvements in the standard error. The performance of the complex spectral reconstruction method (cyan) is almost comparable to the uniform PRT method (blue). In fact, the uniform PRT performance has improved to make it comparable to the other one. Only the performance of the staggered PRT pulse pair method has deteriorated with respect to the estimator #1.

Figure 3.6.1.3. is for estimator #3. This clearly is not the best choice except for the last three (black, cyan, and yellow). The performance with window (black and yellow) seems to be immune to the estimator type! Another interesting observation is that the complex spectral reconstruction method performs almost equally well with all three estimators.

Next, we examine the bias errors in the width estimates. Figures 3.6.1.3, 3.6.1.4, 3.6.1.5, and 3.6.1.6 depict the bias errors in the estimators #1,#2 and #3, respectively, for all the cases discussed in the previous three figures. The est#1 has a small bias when used with uniform PRT, magnitude deconvolution, and the complex spectrum reconstruction. All the rest have almost zero bias. With the est#2 the bias in the uniform PRT case is reduced to nearly zero, but the other two cases the reduction is marginal. Figure 3.6.1.6 indicates the performance of the est#3 is worst of the three. Only the two cases with von Hann window appear to give zero bias with all three estimators. The application of a window (von Hann or Blackmann) becomes imperative if ground clutter is to be filtered. This set of 6 figures can be used to select an appropriate estimator depending on the type of processing utilized. With clutter filtering, there is additional loss of the signal and some residual clutter remains in the spectrum. Both these factors affect the estimates in different ways. This needs to be looked at while selecting the width estimators. However, a major part of the PPI is without the clutter, hence these figures are sufficient.

Next we present the bias and standard errors in the mean velocity and mean power estimates. Figure 3.6.1.7 shows the standard error in the velocity estimate as a function of the spectrum width. Here again the uniform PRT case (blue curve) is used as a reference for comparison. The best velocity estimator for the staggered PRT is the complex spectral reconstruction method, followed by the velocity estimation from the phase of $R(T_1)$ and de-alias using the phase of $R(T_2)$. Figure 3.6.1.8 shows the bias error in the velocity which is negligible in all the cases considered. These results are without the clutter filter.

The mean power estimates are obtained in the time domain or frequency domain. In either case these estimates are averages of a number of samples (in time or frequency). For a fixed number of samples the standard error of estimates is smallest if no window is applied (Fig. 3.6.1.9) because then the information contained in the samples is utilized to the fullest extent possible. Although the power estimates have no bias, the estimates of reflectivity factor in dBZ units do have a bias which is caused by the logarithmic transformation (into dBZ units) of the sample power estimates (Fig. 3.6.1.10).

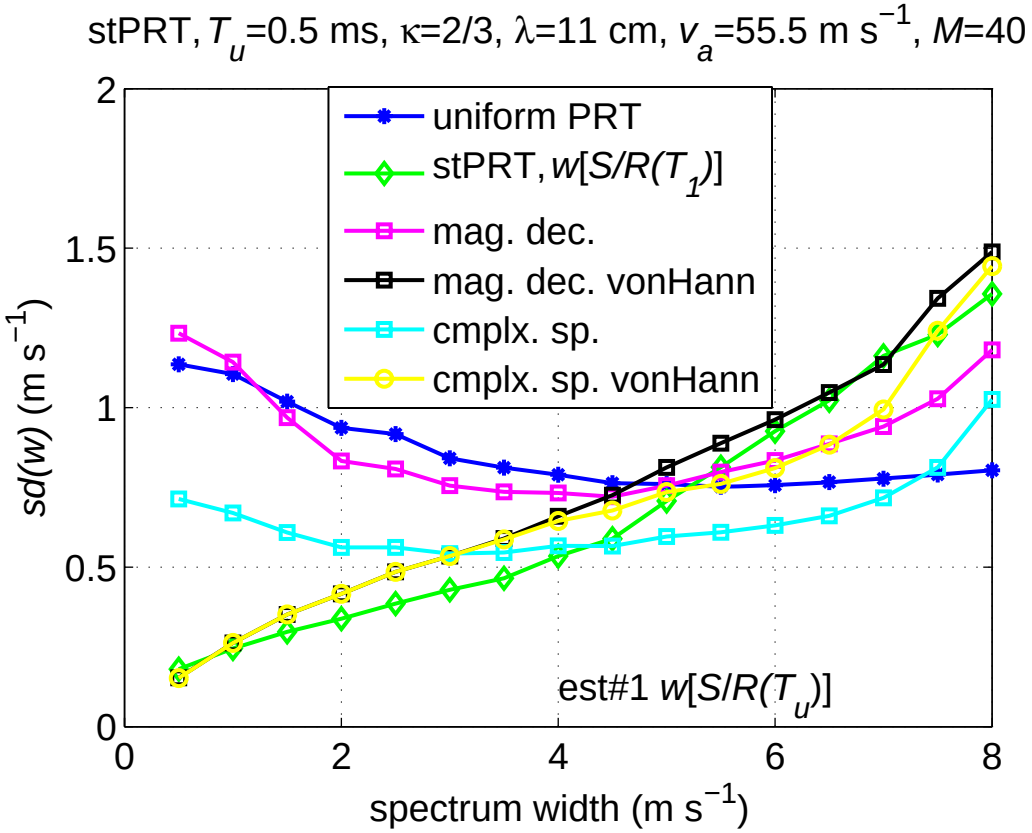

Fig. 3.6.1.1. Standard error in the width estimates using estimator #1. All the estimators except the stPRT use $S/R(T_u)$. T_u is the spacing of samples in the uniform PRT, hence the number of these samples is 100. M is the number of samples in the staggered sequence (here 40). The stPRT uses $S/R(T_1)$ where T_1 is the short PRT ($T_1 = 2T_u = 1$ ms). In the magnitude deconvolution and complex spectrum estimators, the spectra are reconstructed and then the autocovariance processing is applied; this computation is done in the spectral domain; that is, the moments are obtained from sinusoidal weighting of the spectra (i.e., 6.17 in Doviak and Zrnić, 1993). The von Hann window indicates that this was applied to staggered sequence before spectral reconstruction.

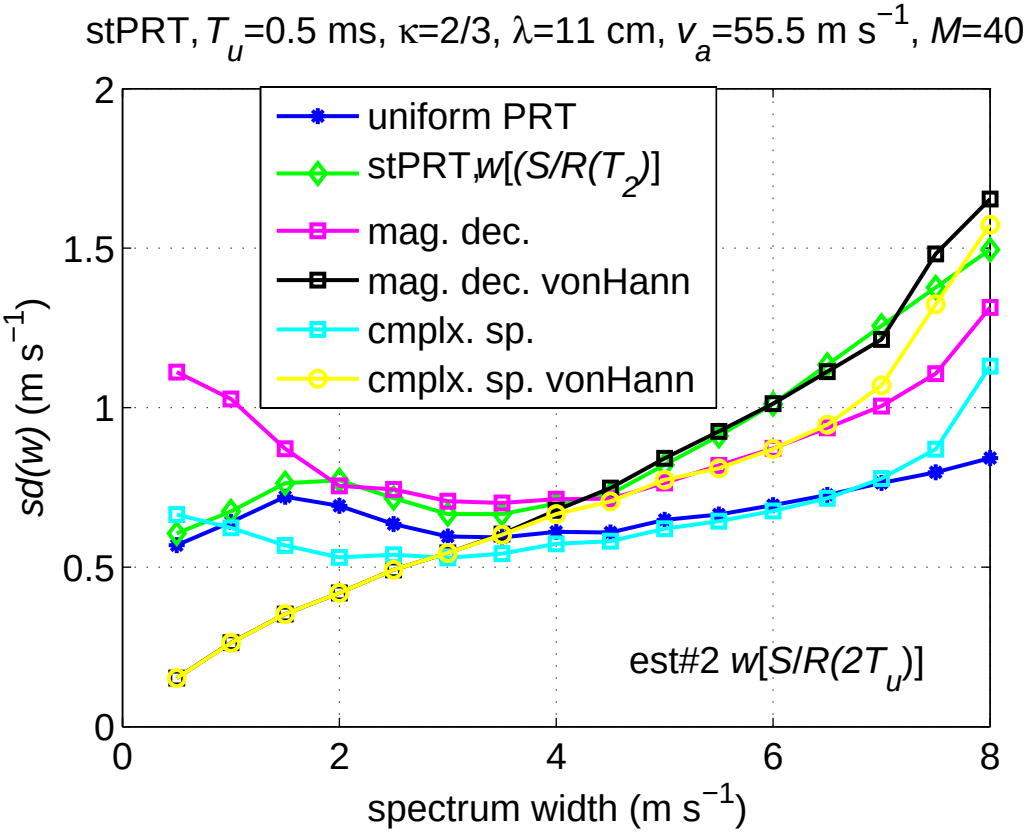

Fig. 3.6.1.2. Standard error in the width estimates using estimator #2. Here the staggered pulse pair estimator uses lag $T_2 = 3T_u$, the other estimators use lag $2T_u$ as indicated in the figure.

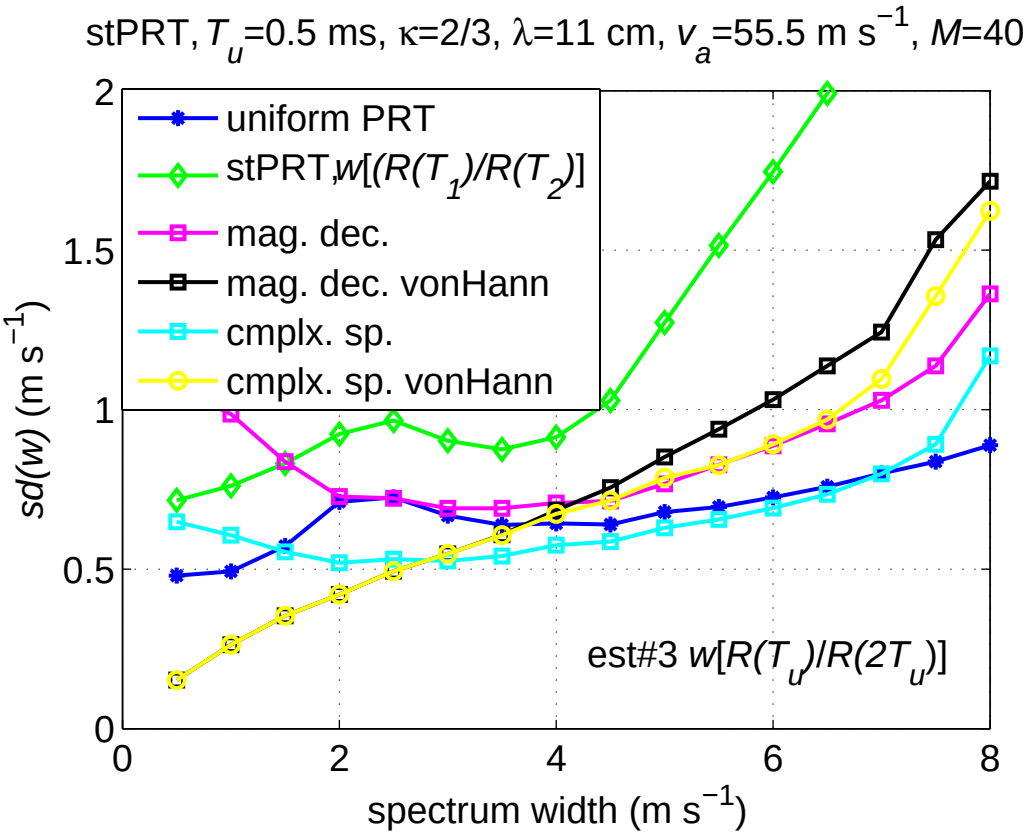

Fig. 3.6.1.3. Standard error in the width estimates using estimator #3. The staggered PTR estimator uses the autocovariances at lags T_1 and T_2 as indicated. The other estimators use autocovariances at lags T_u and $2T_u$.

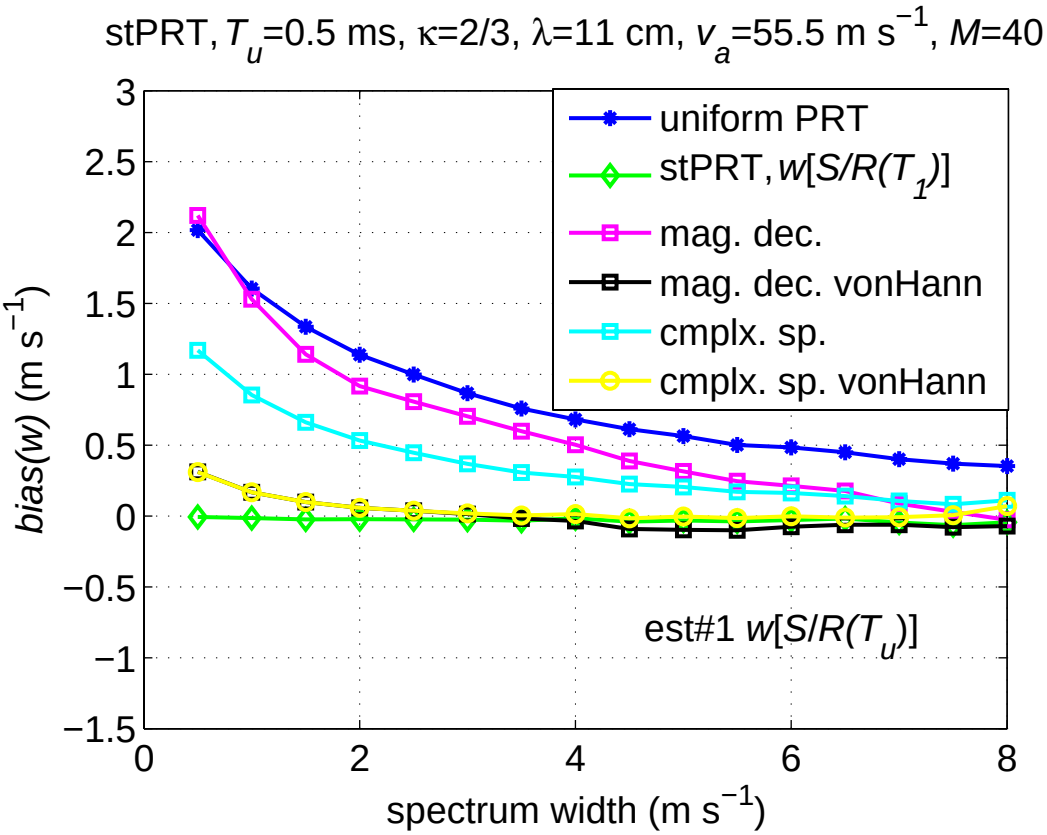

Fig. 3.6.1.4. Bias error in the width estimates using estimator #1. Other parameters are as in Fig. 3.6.1.1

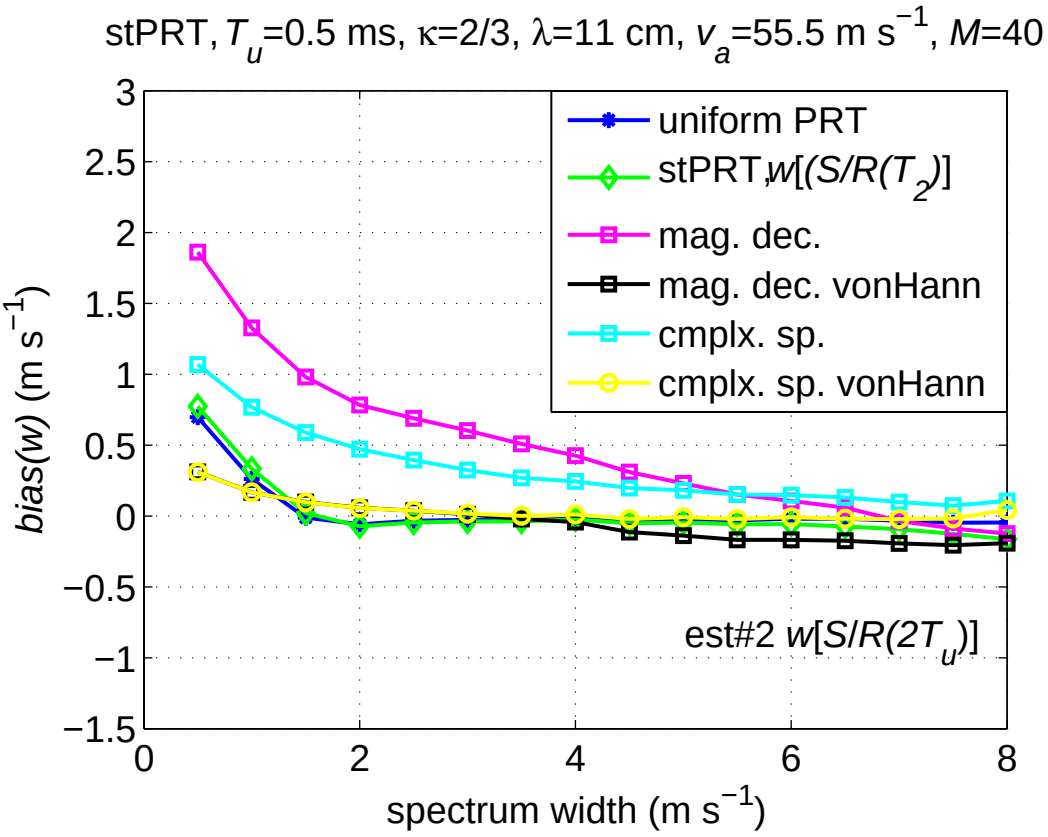

Fig. 3.6.1.5. Bias error in the width estimates using estimator #2. Other parameters are as in Fig. 3.6.1.2.

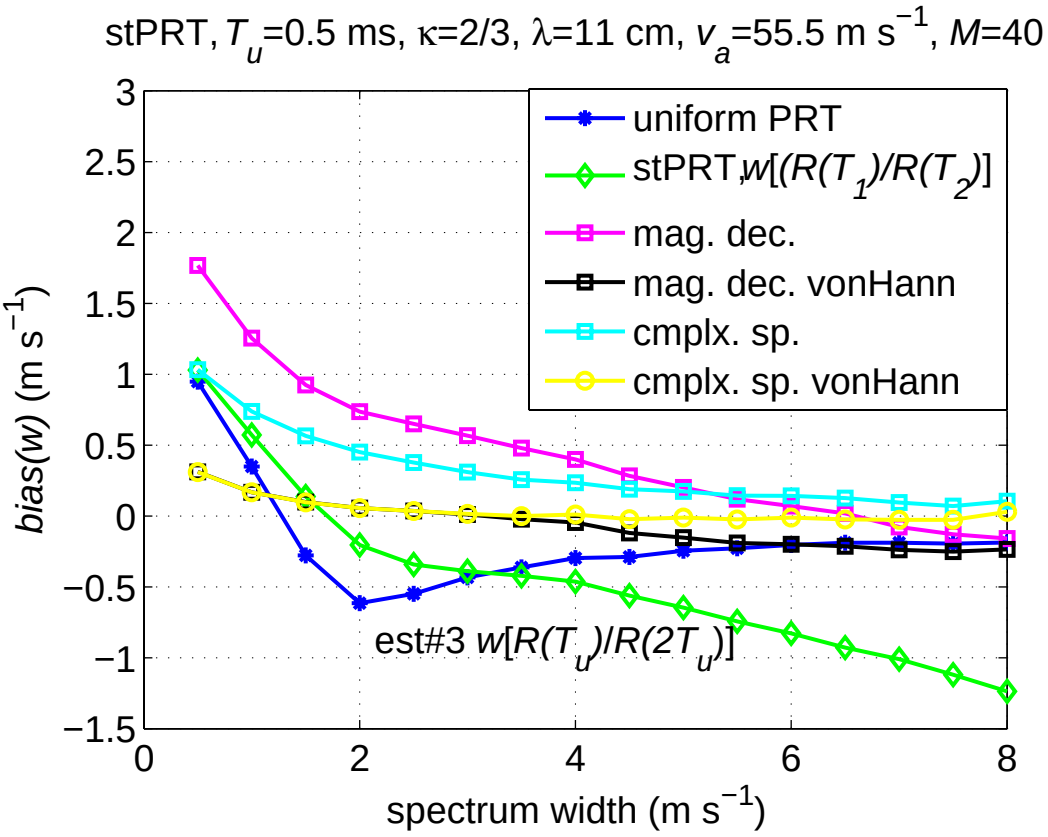

Fig. 3.6.1.6. Bias error in the width estimates using estimator #3. Other parameters are as in Fig. 3.6.1.3.

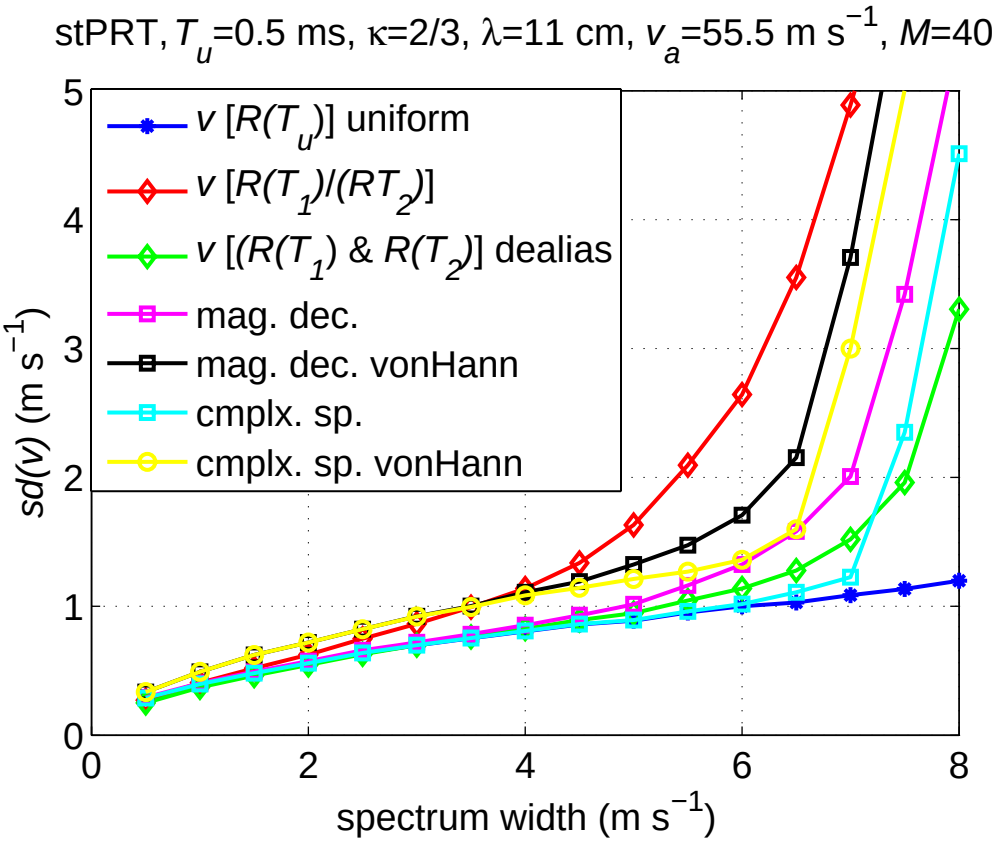

Fig. 3.6.1.7. Standard error in the velocity estimate using different methods. The methods use autocovariances at indicated lags and divide these with the powers, except in $v[R(T_1)/R(T_2)]$. The dealiasing method obtains the velocity from lag T_1 but uses both lags T_1 and T_2 for dealiasing. The magnitude deconvolution and complex spectral processing obtain the spectra from the staggered PRT sequence and then use sinusoidal weighting of the spectra to obtain the mean velocity (equation 6.17 of Doviak and Zrnić, 1993); this is mathematically identical to pulse pair processing.

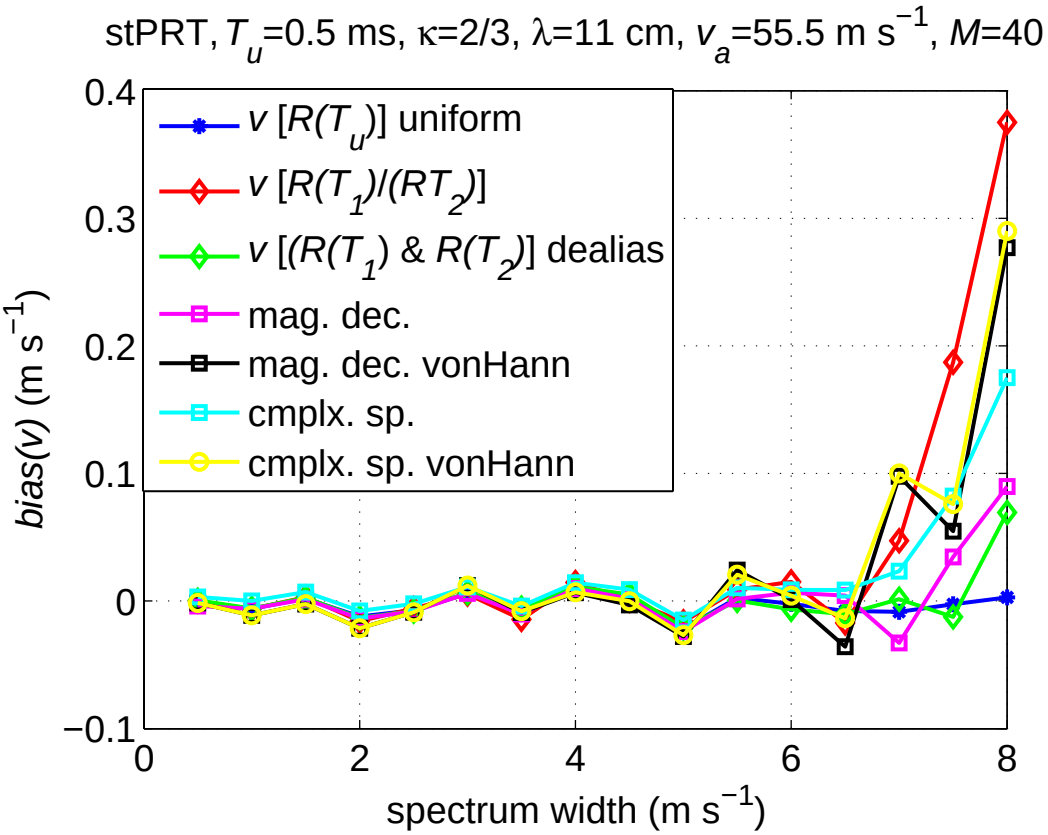

Fig. 3.6.1.8. Bias error in the velocity estimate using different methods. The corresponding standard deviations are in Fig. 3.6.1.7.

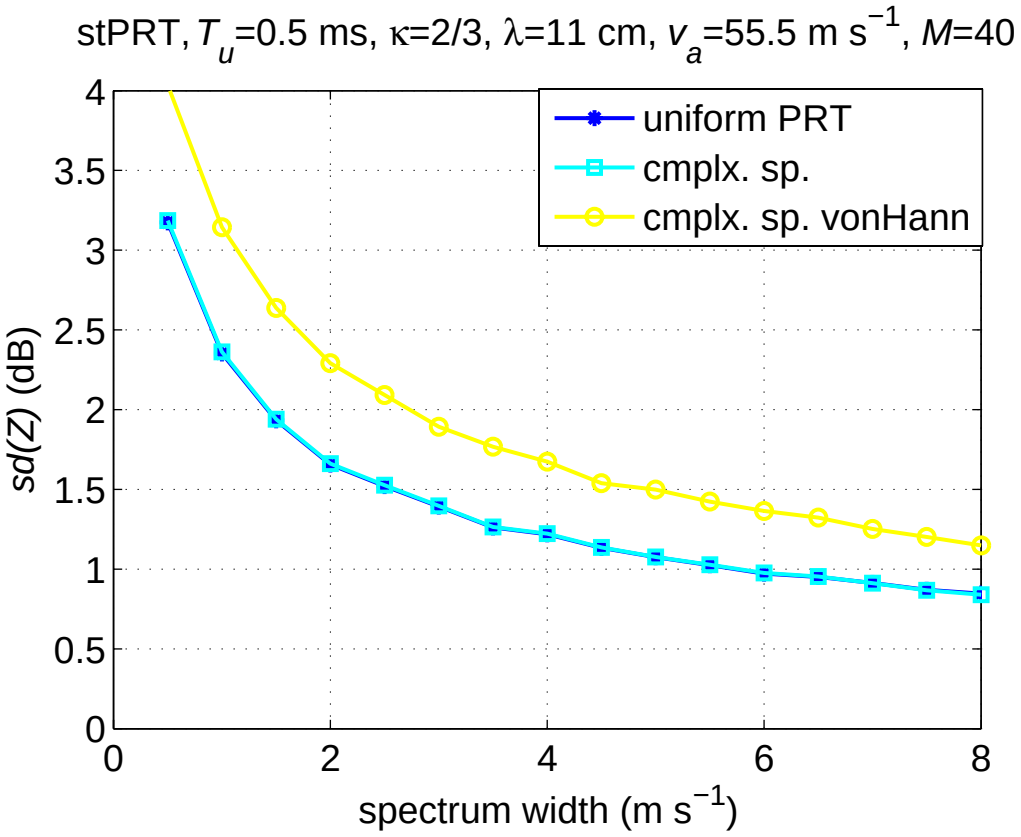

Fig. 3.6.1.9. Standard error in the mean power estimate using different methods.

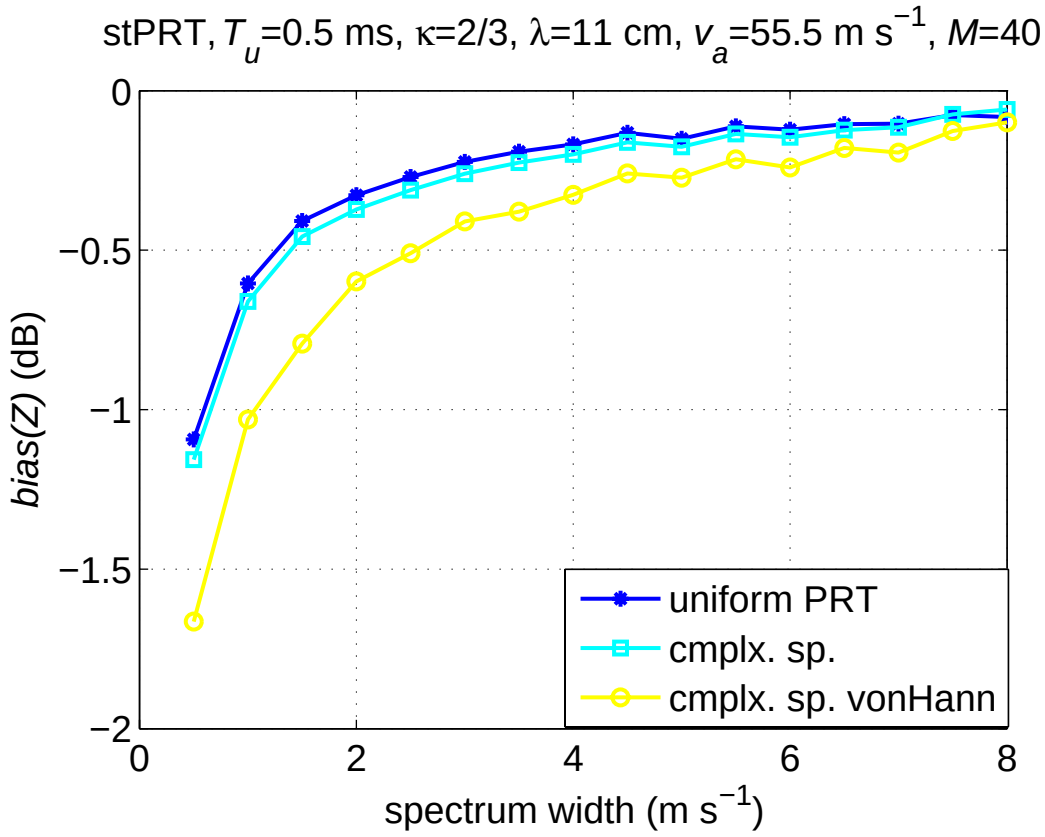

Fig. 3.6.1.10. Bias error in the mean power estimate using different methods.

4. Phase Coding

Last year NSSL and NCAR provided an algorithm recommendation for the first stage of range and velocity ambiguity mitigation on the WSR-88D. The algorithm is termed SZ-2 and will replace the "split cuts" in legacy VCPs. This algorithm is scheduled for implementation on the ORDA, and is expected to provide significant reduction of obscuration (purple haze) at the lower elevation angles. Although the provided algorithm recommendation was extensively tested in a research environment, a number of enhancements were investigated in the past year. First, we introduce a few enhancements that are critical for the implementation of the SZ-2 algorithm in an operational environment. These relate to handling clutter in multiple trips and the use of windows. Last, we cover an evolutionary enhancement referred to as double processing. Although not critical, this enhancement could significantly improve the algorithm's performance.

A functional description of the critical enhancements to the SZ-2 algorithm and errata to the June 2004 SZ-2 algorithm recommendation are included in Appendix C.

4.1. Critical Enhancements to the SZ-2 Algorithm

4.1.1. *Handling clutter in multiple trips*

The June 2004 SZ-2 algorithm included modifications to handle clutter in multiple trips. However, those modifications dealt mostly with censoring and not recovering signals in those range gates with overlaid clutter (i.e., with clutter in more than one trip). In fact, it is the phase coding technique itself that does not work well with clutter in multiple overlaid trips because the manipulation of the spectrum to remove clutter from multiple

trips destroys the coherence of overlaid signals and precludes their recovery. The June 2004 SZ-2 algorithm handled this situation by giving up on recovering of data with overlaid clutter. In addition, if clutter was with the weak trip, only recovery of the strong trip was possible. Therefore, in a situation where most of the gates are presumed to have clutter, the June 2004 SZ-2 algorithm could potentially perform worse than legacy algorithms since the presence of clutter is solely determined from the clutter filter map.

It has been reported that at some radar sites the operators incorrectly define clutter censor zones that cover all the range gates in a given scan. The effect of this abuse on legacy algorithms is noticeable but only in the first trip, since the clutter maps are effectively ignored for higher order trips (this is the reported behavior of the legacy RDA and the ORDA). Conversely, the June 2004 SZ-2 algorithm implements a "clutter location determination" function by looking at all the trips within the clutter map. If there is more than one trip with clutter, the weak trip is immediately deemed as unrecoverable; the strong trip might be recoverable only if it is much stronger than the sum of the out-of-trip powers. With this in mind, let's look at an example (Figures 4.1.1.1 to 4.1.1.3) in which the June 2004 SZ-2 algorithm is run with the "filter everywhere" option. Comparing the results from the legacy "split cut" processing and the ones from the June 2004 SZ-2 algorithm, it is obvious that the performance of the latter is negatively affected by an incorrectly-defined clutter map. Looking at the cause for censoring, the plot in Fig. 4.1.1.4 indicates that most of the censoring occurred due to the location of clutter (i.e., due to the presence of clutter in multiple overlaid trips), which confirms the need for a "smarter" decision as to the presence of clutter in multiple trips.

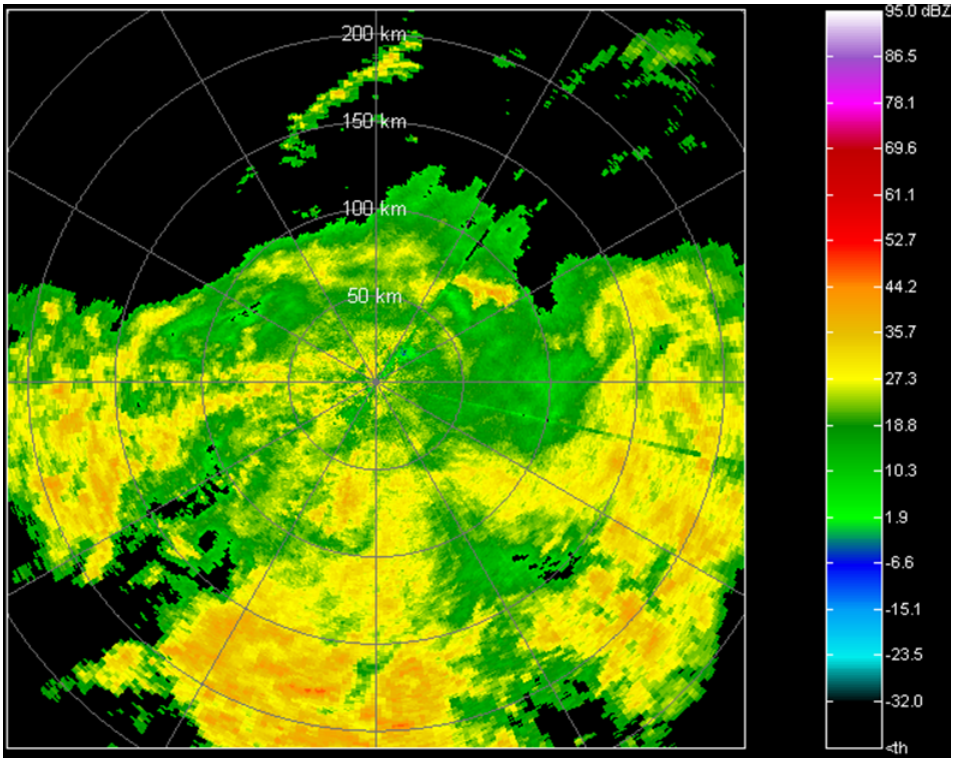

Fig. 4.1.1.1. Reflectivity field of data collected on the KOUN radar on Oct 08, 2002. Widespread echoes extend beyond 250 km.

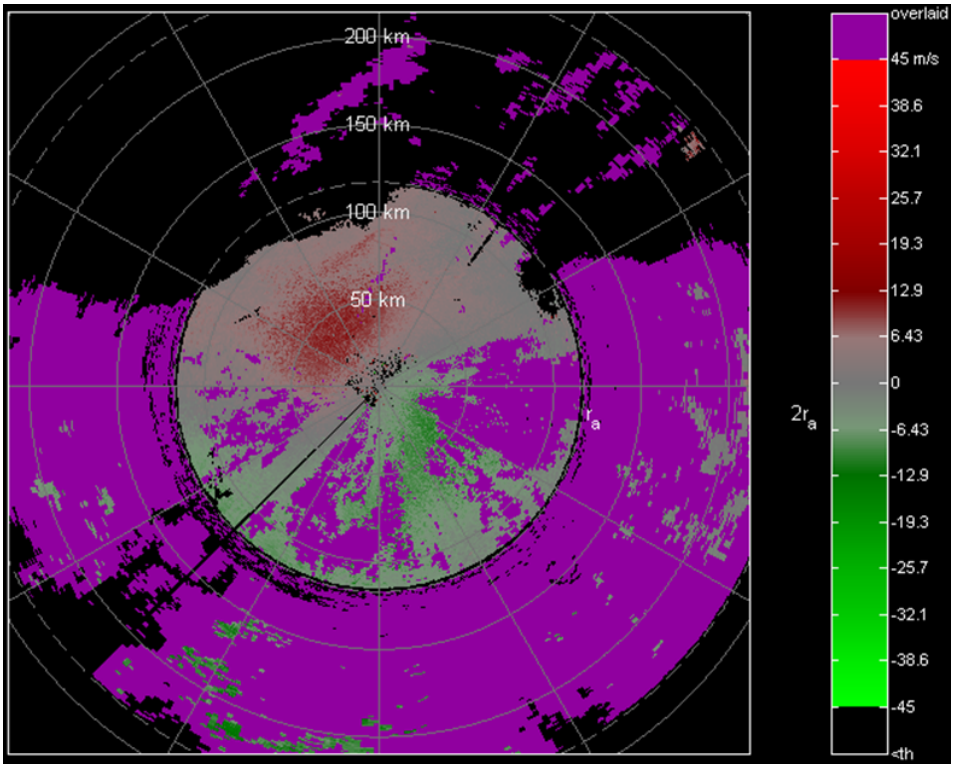

Fig. 4.1.1.2. Doppler velocity field corresponding to the reflectivity in Fig. 4.1.1.1 obtained through the legacy algorithm (split cut processing).

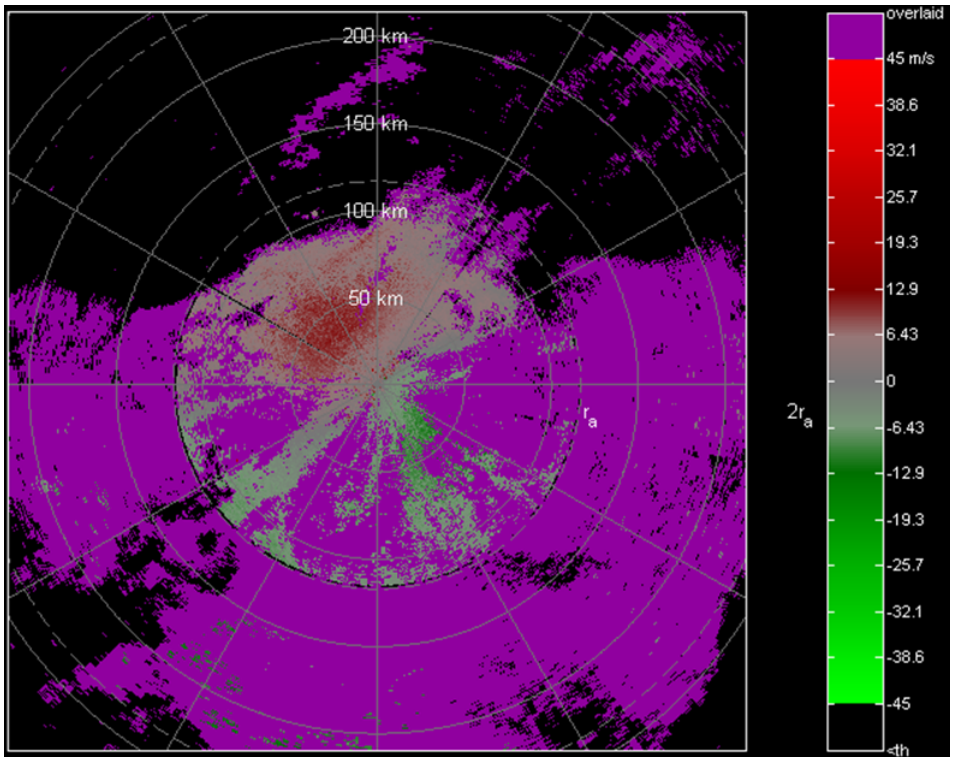

Fig. 4.1.1.3. Doppler velocity field corresponding to the reflectivity in Fig. 4.1.1.1 obtained with the June 2004 SZ-2 algorithm.

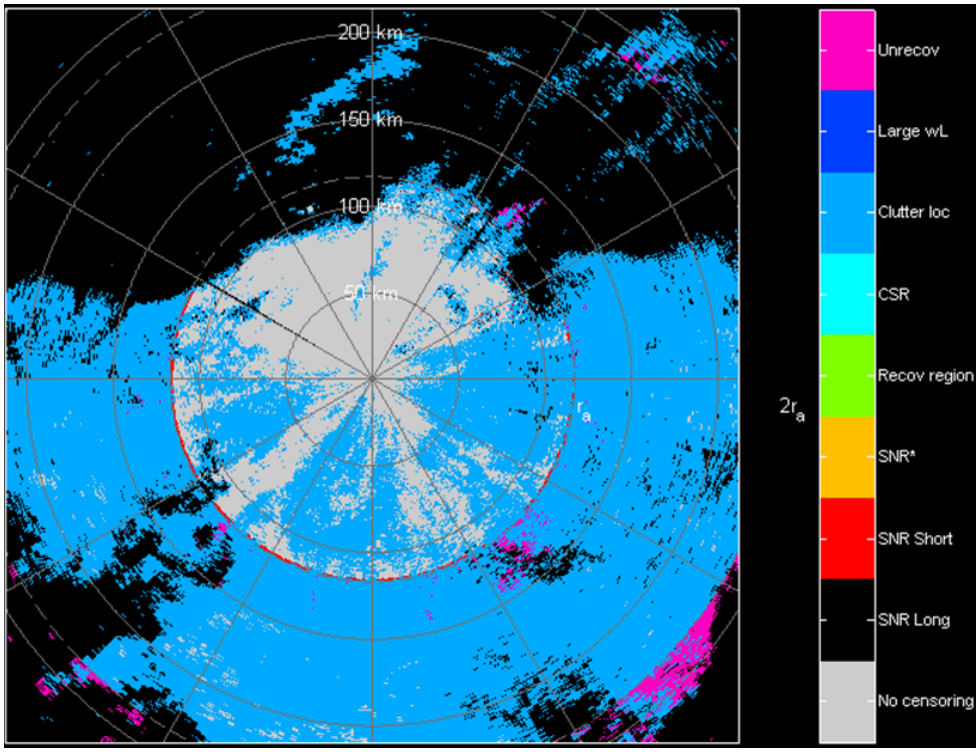

Fig. 4.1.1.4. Censoring field corresponding to the Doppler velocity field in Fig. 4.1.1.3. Reasons for censoring are referenced in the color bar.

The proposed solution involves a re-determination of clutter contamination only if the clutter map indicates the presence of clutter in multiple trips (i.e., only when the June 2004 SZ-2 algorithm would fail). The long-PRT powers removed by the GMAP clutter filter are used for this.

The enhanced "clutter location determination" function is given below, where `Nc` is the number of trips with clutter, `N` is the number of bins in the short PRT, `n` is the current short-PRT bin, and `i` is the long-PRT bin corresponding to trip `l`. The clutter map corresponding to the current radial is denoted by `B`; this map can indicate either `FILTER` or `BYPASS`. Arrays `PL` and `CL` correspond to the long-PRT filtered powers and powers removed by GMAP, respectively. The threshold `KCSR3` is an adaptable parameter with a recommended value between 10 and 15 dB. This algorithm starts by performing a determination of clutter location based solely on the clutter map; exactly the same that was recommended in the June 2004 version. What is different here is that if the number of trips with clutter after the preliminary determination is larger than one, the algorithm performs a re-determination based on both the clutter map and the clutter-to-signal ratio (as determined by GMAP during the long PRT scan).

```
Nc = 0
For l = 1 to 4
     i = n + (l – 1)N
     If B(i) = FILTER
           There is clutter in trip l
           Nc = Nc + 1
     Else
          There is no clutter in trip l
     End
End
If Nc > 1
     Nc = 0
     For l = 1 to 4
          i = n + (l – 1)N
          If B(i) = FILTER and CL(i) > PL(i) KCSR3
               There is clutter in trip l
          Nc = Nc + 1
          Else
               There is no clutter in trip l
          End
      End
End
```

As shown in Fig. 4.1.1.5, with this enhancement, the new SZ-2 algorithm performs much better with a clutter map that aggressively indicates “filter everywhere”. This improvement is realized by effectively “second guessing” the operator-defined clutter censor zones if they indicate the presence of clutter in multiple overlaid trips.

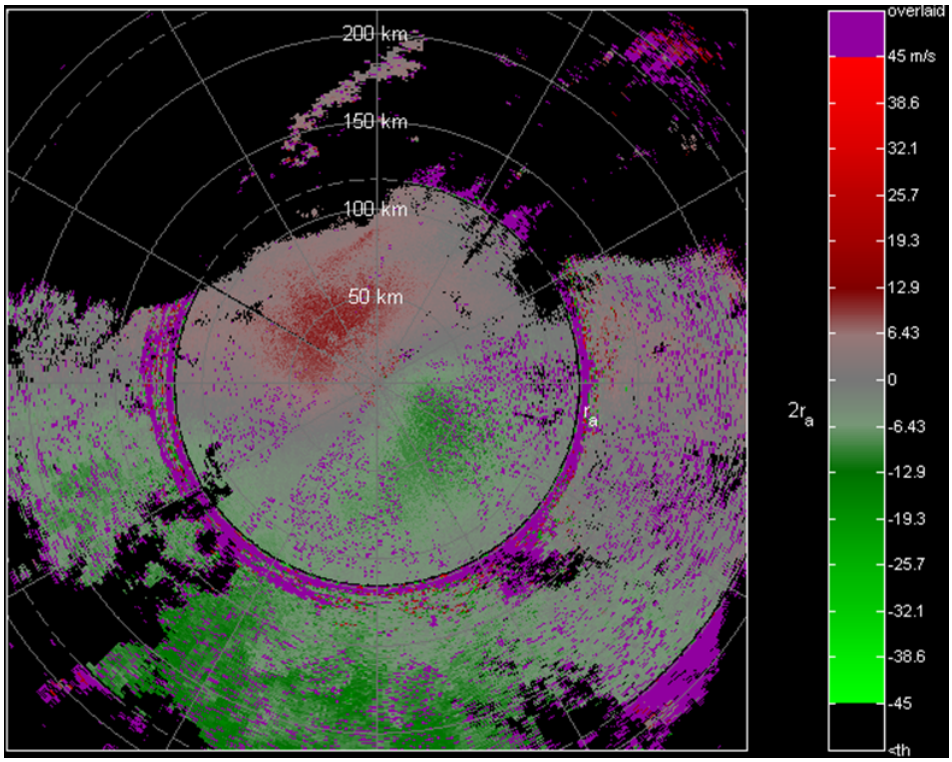

Fig. 4.1.1.5. Doppler velocity field corresponding to the reflectivity in Fig. 4.1.1.1. obtained with the enhanced SZ-2 algorithm.

Another enhancement is recommended to handle several special cases more efficiently in the algorithm. This is, once clutter location is determined, a decision must be made regarding how to proceed with the recovery of the two strongest overlaid trips. In the June 2004 SZ-2 algorithm recommendation, only a few special cases like this were considered. This scheme was revisited this year, and we extended the list of cases that require special handling to 12 cases. Note that only obvious cases are considered; those that require precise knowledge of the clutter-to-signal ratio for each trip cannot be easily identified, since the power removed by GMAP is only a good estimator of clutter power for large CSRs (see report 8). The list of cases is presented in the table below. Although this list is exhaustive, these represent a very small addition to the algorithm's computational complexity since the detection rules can be implemented with `if-then-else` statements and some of the cases listed are very unlikely to occur.

In the following table, S, W, and U stand for 'strong', 'weak', and 'unrecoverable' trips; P_i (i=0, 1, 2, 3) are the long-PRT filtered powers sorted in descending order; and Q_i are the long-PRT total powers sorted according to the P's.

Number of trips with clutter	Case no.	Clutter location*			Condition	GCF trip	Recoverable trips based on clutter location**	
		S	W	U			S	W
0	1						x	x
1	2	x				S	x	?
	3		x		if $P_0 >> Q_1$		x	
					else	W	x	?
	4			x	if $P_0 >> Q_{2(3)}$		x	x
					else	U	x	o
2	5	x	x		if $P_0 >> Q_1$	S	x	
					else			
	6	x		x	if $P_0 >> Q_{2(3)}$	S	x	?
					else			
	7		x	x	if $P_0 >> Q_1 + Q_{2(3)}$		x	
					elseif $P_0 >> Q_{2(3)}$	W	x	?
					elseif $P_0 >> Q_1$	U	x	
					else			
	8			xx	if $P_0 >> Q_2 + Q_3$		x	x
					elseif $P_0 >> Q_2$	U2	x	o
					elseif $P_0 >> Q_3$	U1	x	o
					else			
3	9	x	x	x	if $P_0 >> Q_1 + Q_{2(3)}$	S	x	
					else			
	10	x		xx	if $P_0 >> Q_2 + Q_3$	S	x	?
					else			
	11		x	xx	if $P_0 >> Q_1 + Q_2 + Q_3$		x	
					elseif $P_0 >> Q_2 + Q_3$	W	x	?
					elseif $P_0 >> Q_1 + Q_2$	U2	x	
					elseif $P_0 >> Q_1 + Q_3$	U1	x	
					else			
4	12	x	x	xx	if $P_0 >> Q_1 + Q_2 + Q_3$	S	x	
					else			

* Strong (S), weak (W), and unrecoverable (U) trips are determined according to the long PRT powers. Note that S and W may get swapped according to the short PRT data.

** These are potentially recoverable trips. Censoring based on other considerations is performed at the end of the algorithm. 'x' stands for "recoverable trip", '?' stands for "unable to determine due to possible switching between strong and weak", and 'o' stands for "should not prematurely censor weak trip due to potential switch between strong and weak trips"

Note 1: '>>' should involve a threshold that is large enough to obtain acceptable estimates of the spectrum width (recall that $Th_v < Th_{\sigma v}$). A value of 10 dB may work.

Note 2: This table is also valid if only one ($t_B = -1$) or no trips ($t_A = t_B = -1$) are recoverable.

4.1.2. *Windowing in SZ-2*

It is well known that spectral processing has many advantages over time-domain processing. However, the cost to pay is an increase in computational complexity from the computation of the spectrum and an increase in errors of estimates due to the use of non-rectangular windows. In general, the more aggressive the window, the smaller the equivalent number of independent samples (Doviak and Zrnić, 1993) and the larger the errors of estimates. In earlier reports, we documented that the best window for the SZ-2 algorithm is the Von Hann window, yielding the best performance in terms of resolution for spectral processing and errors of estimates. However, with the introduction of spectral ground clutter filters (i.e., GMAP) it was determined (Ice et al., 2004) that a more aggressive window such as the Blackman window was needed to achieve the required clutter suppression. Therefore, in the June 2004 SZ-2 algorithm recommendation we proposed using the Blackman window for all range gates.

After familiarizing ourselves with the inner workings of the ORDA signal processor (the RVP-8), we realized that it is relatively easy for the RVP-8 processor to use different windows at different range locations. Thus, we are revising our initial recommendation and proposing to use different windows depending on the presence of clutter. That is, use the Von Hann window if there is no clutter to achieve better accuracy of estimates, and use the Blackman window in the presence of clutter to achieve the required clutter suppression. Without increasing the computational complexity, the gain from this change should be noticeable as indicated by figures 4.1.2.1 and 4.1.2.2.

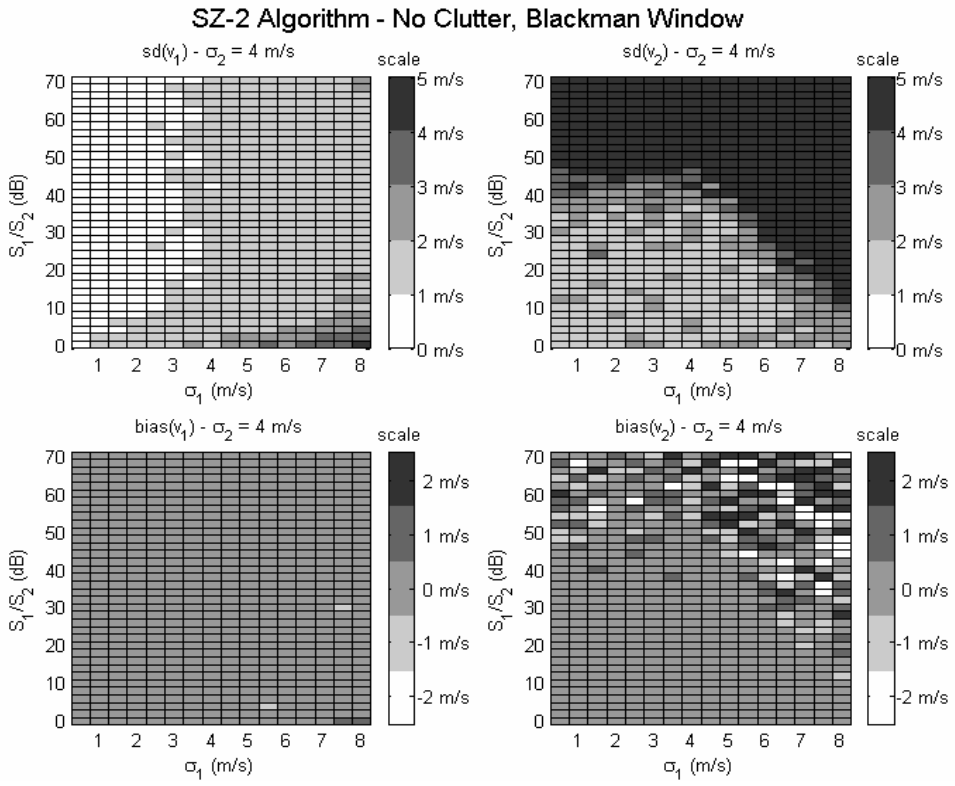

Fig. 4.1.2.1. Standard error and bias of strong and weak trip velocities in the SZ-2 algorithm using the Blackman window as a function of strong-to-weak trip power ratio and strong trip spectrum width for a weak-trip spectrum width of 4 m/s.

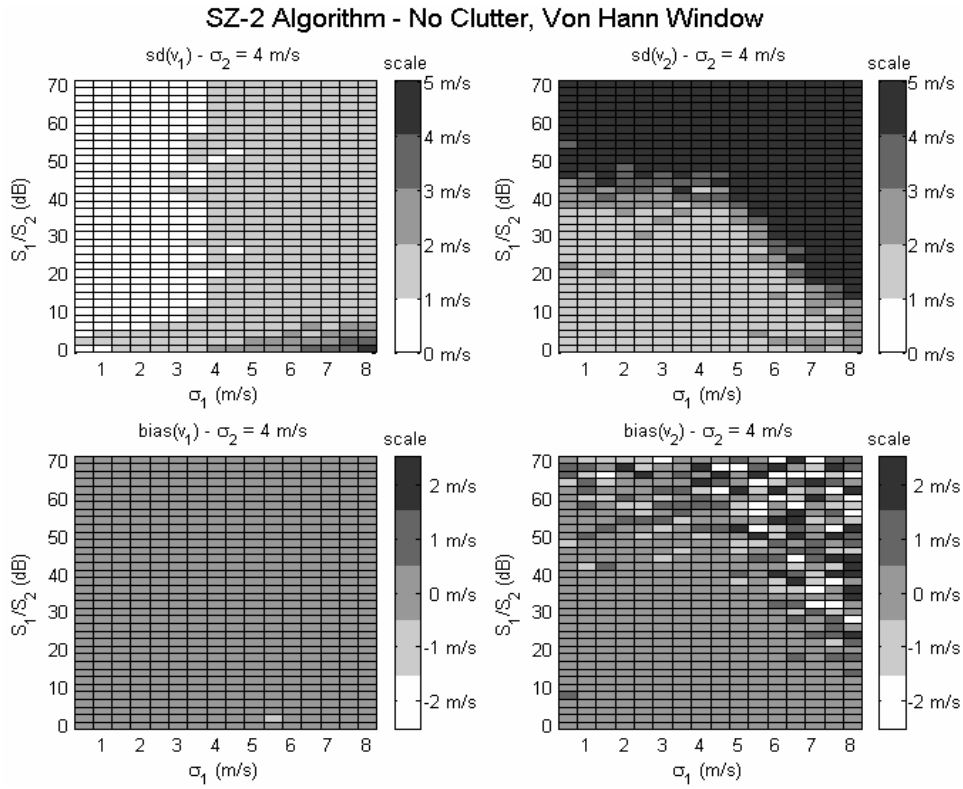

Fig. 4.1.2.2. Standard error and bias of strong and weak trip velocities in the SZ-2 algorithm using the Von Hann window as a function of strong-to-weak trip power ratio and strong trip spectrum width for a weak-trip spectrum width of 4 m/s.

4.2. Double processing for phase coding algorithms

It has been observed that recovery of the strong-trip velocity is more difficult if the strong and weak trip powers are about the same. This is because the strong trip velocity is recovered directly, without attempting to remove contamination from the out-of-trip echoes. This is evident by the larger errors of estimates observed when the strong-to-weak trip power ratio is less than 3 dB (Fig. 4.2.1).

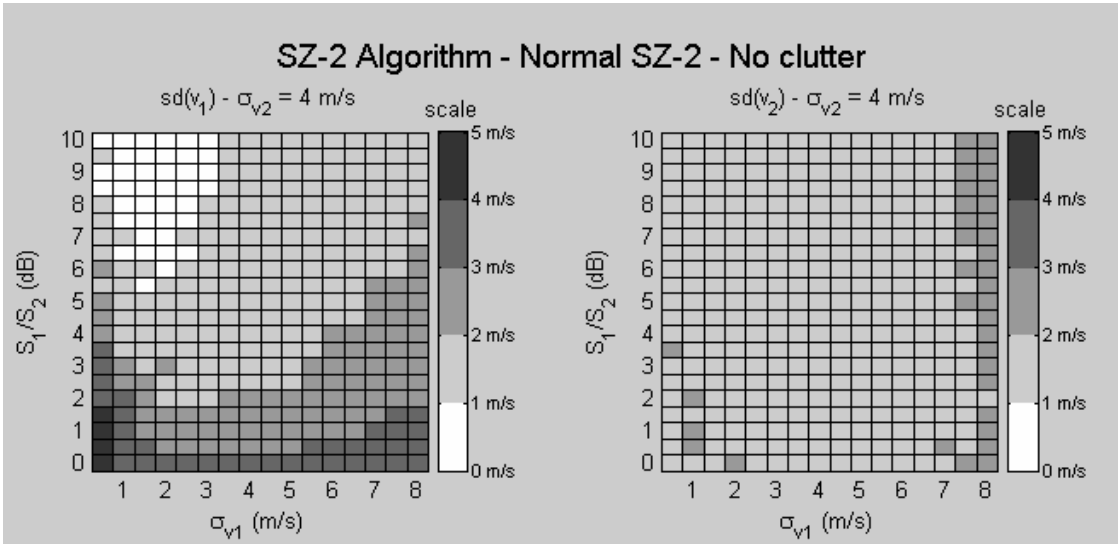

Fig. 4.2.1. Standard error of strong and weak trip velocities in the normal SZ-2 algorithm as a function of strong-to-weak trip power ratio and strong trip spectrum width for a weak-trip spectrum width of 4 m/s. Range of strong-to-weak trip powers is 0 to 10 dB.

Recovery of the weak-trip velocity is not affected by this because the weak-trip velocity is always recovered after notching most of the strong-trip echo with the "processing notch filter" (PNF). Thus, if the strong and weak trip powers are about the same, we could recover the strong trip velocity in a similar way as we do the weak trip velocity; i.e., by means of a PNF. This is termed as double processing, and the processing sequence is depicted in the block diagram of Fig. 4.2.2. The upper branch in that figure

corresponds to the normal SZ-2 processing; the lower branch proceeds in a similar fashion with the strong and weak trips swapped so that both the strong and weak trip velocities are estimated after a PNF.

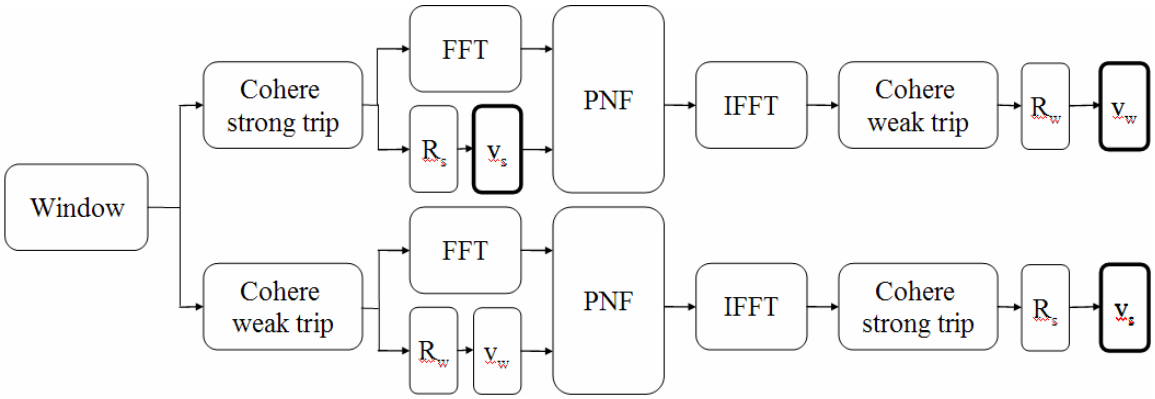

Fig. 4.2.2. Block diagram of double processing for the SZ-2 algorithm.

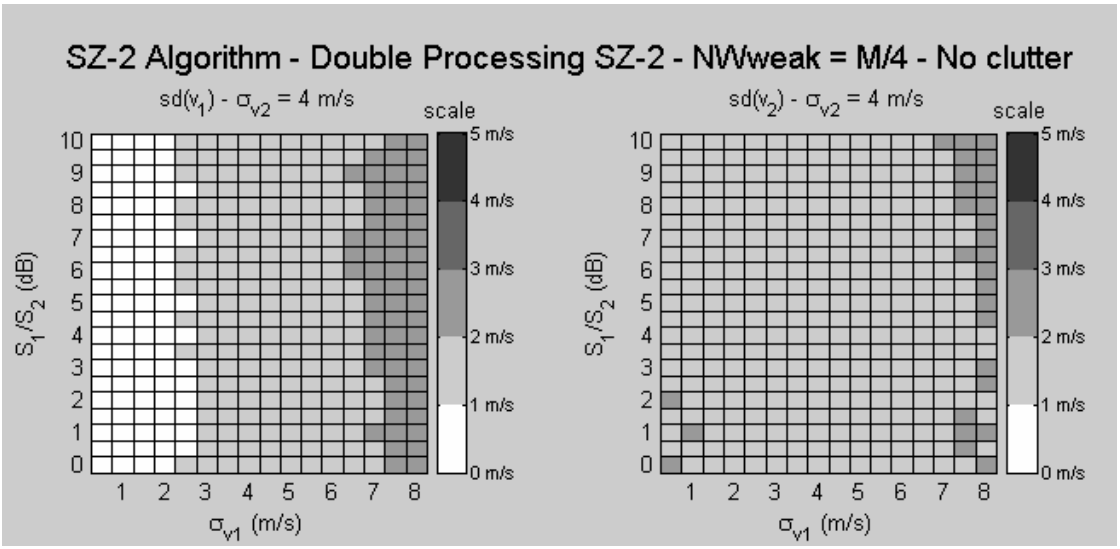

Fig. 4.2.3. Standard error of strong and weak trip velocities in the double-processing SZ-2 algorithm as a function of strong-to-weak trip power ratio and strong trip spectrum width for a weak-trip spectrum width of 4 m/s and a weak-trip PNF notch width of *M*/4. The range of strong-to-weak trip powers is 0 to 10 dB.

Performance of double processing is shown in fig. 4.2.3. As stated before, the improvement is in the recovery of the strong-trip velocity (compare the left panels of

figures 4.2.1 and 4.2.3), the recovery of the weak-trip velocity is the same in both algorithms. Performance of double processing depends on the strong-to-weak trip power ratio and on the weak-trip PNF notch width. For large power ratios, normal processing is preferred over double processing (there is no need to disturb the spectrum if we do not have to!). Hence, double processing is to be applied selectively depending on the parameters of the overlaid signals. On one hand, the strong-trip PNF notch width is traditionally either $3M/4$ or $M/2$ depending on the strong and weak trip numbers. However, the weak-trip PNF notch width does not need to be as aggressive. Actually, the more replicas that are left after the PNF process, the better the recohering of the out-of-trip signals. To demonstrate this, performance of double processing was compared to normal processing for different values of weak-trip PNF notch width (figures 4.2.4 through 4.2.7). In these figures a white color indicates that normal processing performs better than double processing, a dark color indicates the opposite, and a light gray color indicates that both algorithms perform about the same (no significant improvement is gained from double processing). It is evident that the smaller the notch width, the larger the region in which double processing performs significantly better than normal processing. However, we cannot make the weak-trip PNF notch width as small as we want, since the goal is to remove at least some contamination from the weak trip. This becomes clearer after comparing figures 4.2.6 and 4.2.7, where double processing ran with weak-trip PNF notch widths of $M/4$ and $M/8$, respectively. The improvement from using the latter over the former is negligible. Therefore, from this preliminary analysis we recommend a weak-trip PNF notch width of $M/4$.

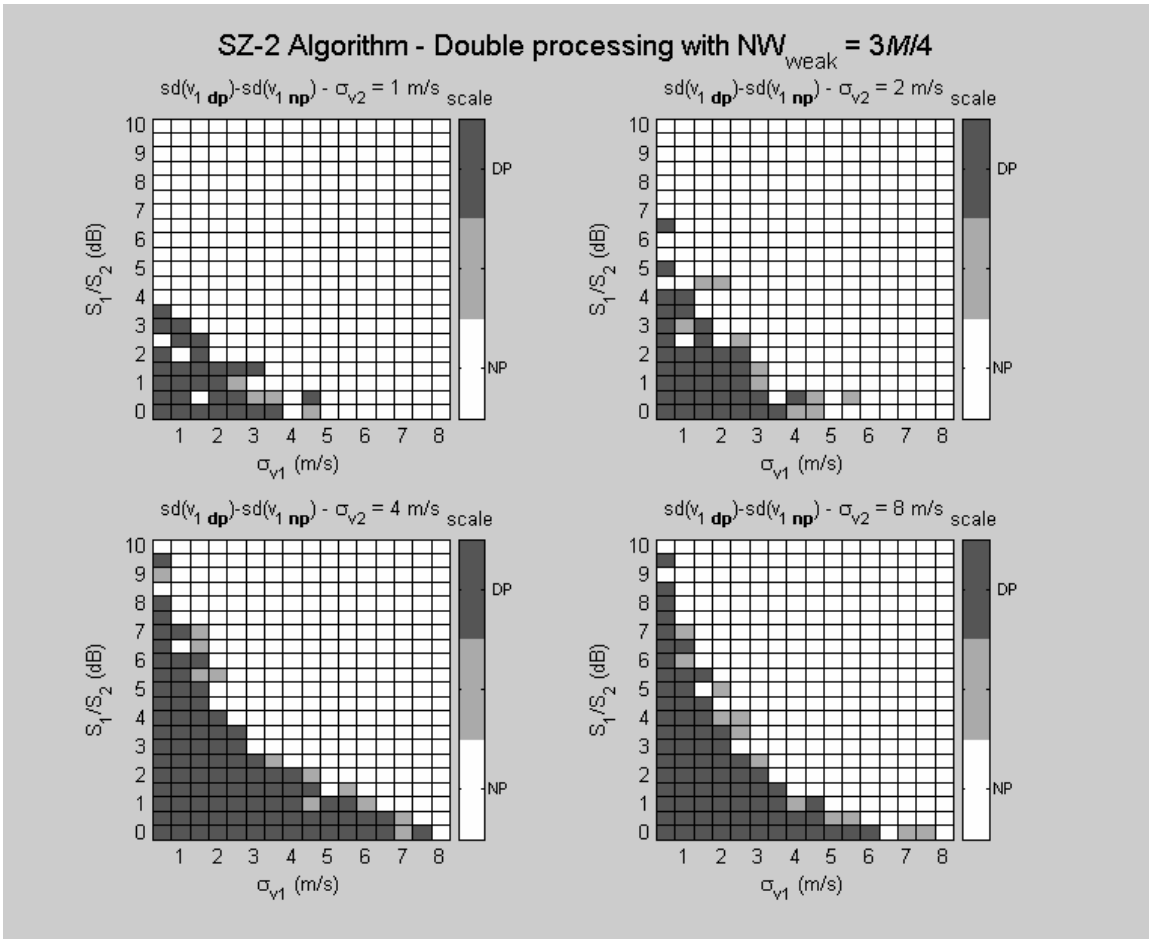

Fig. 4.2.4. Comparative performance of double processing and normal processing for the SZ-2 algorithm as a function of the strong-to-weak trip power ratio and the strong and weak trip spectrum widths for a weak-trip PNF notch width of 3*M*/4. A Dark color indicate the double processing performs better than normal processing, a light gray color indicates that both techniques perform about the same, and a white color indicates that there is no improvement from using double processing (normal processing performs better).

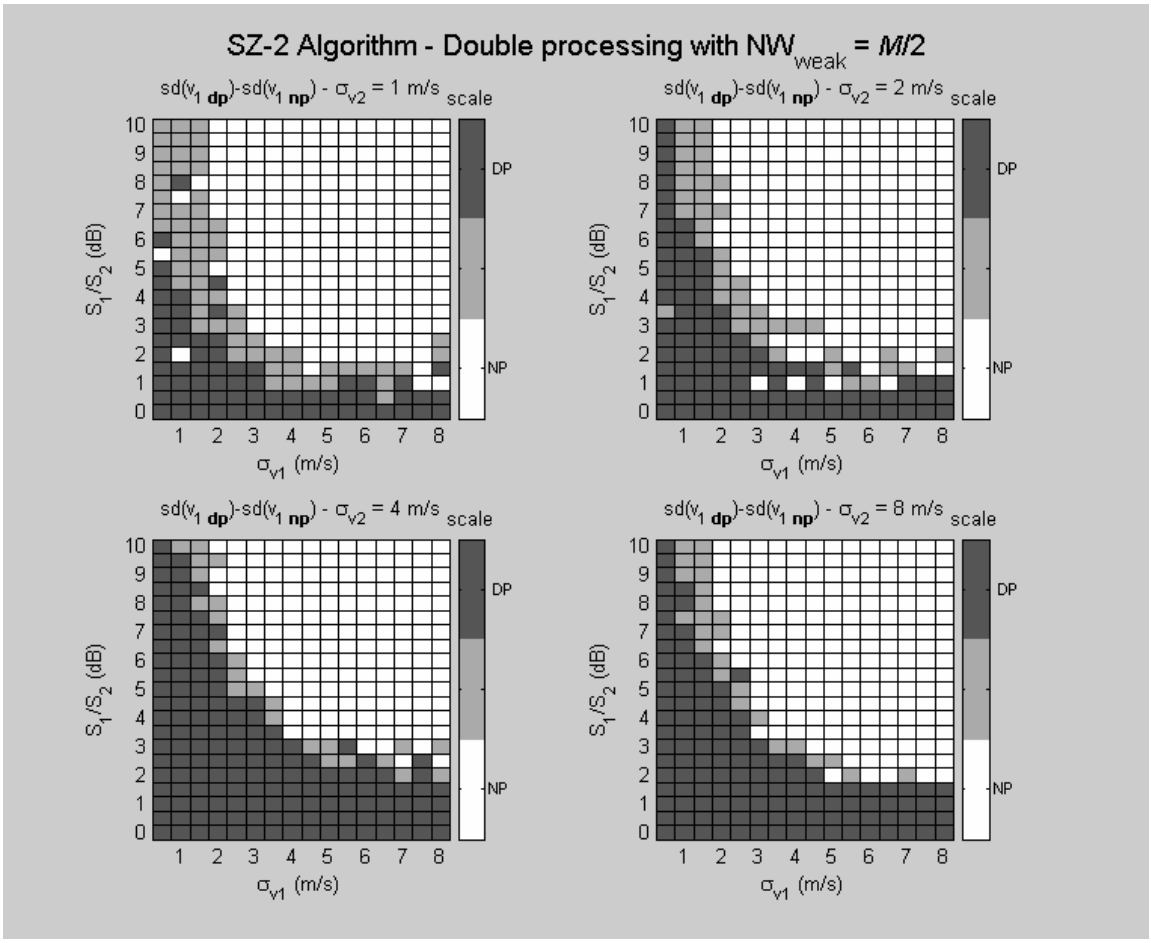

Fig. 4.2.5. Comparative performance of double processing and normal processing for the SZ-2 algorithm as a function of the strong-to-weak trip power ratio and the strong and weak trip spectrum widths for a weak-trip PNF notch width of *M*/2.

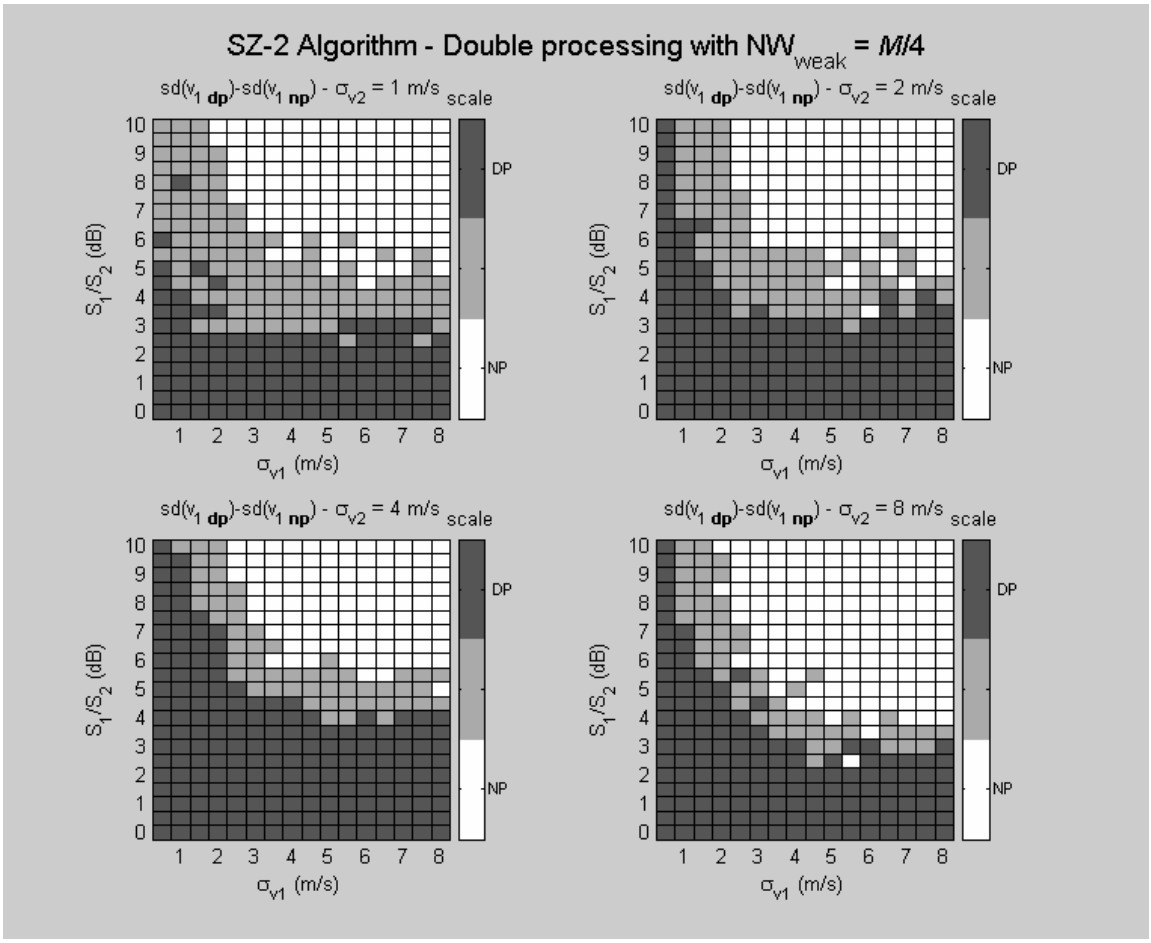

Fig. 4.2.6. Comparative performance of double processing and normal processing for the SZ-2 algorithm as a function of the strong-to-weak trip power ratio and the strong and weak trip spectrum widths for a weak-trip PNF notch width of *M*/4.

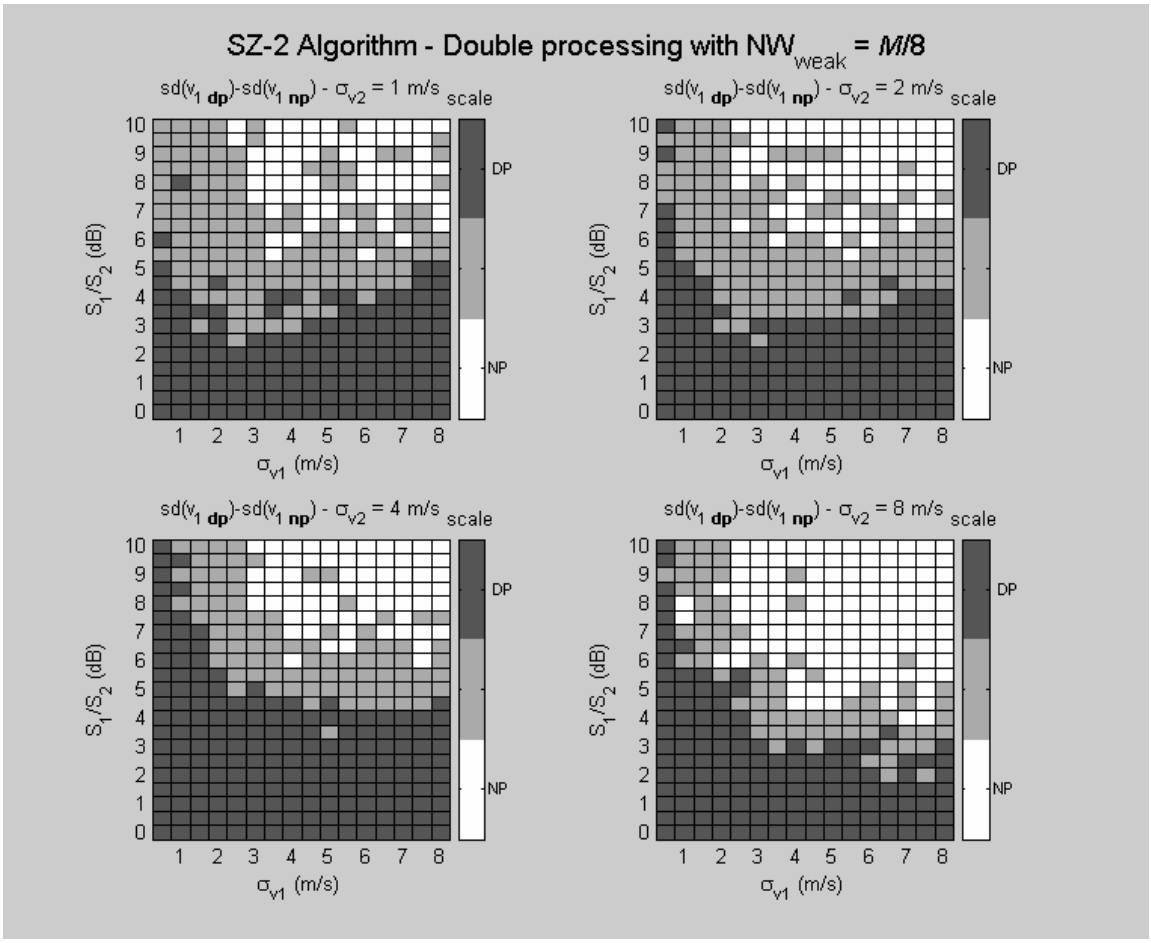

Fig. 4.2.7. Comparative performance of double processing and normal processing for the SZ-2 algorithm as a function of the strong-to-weak trip power ratio and the strong and weak trip spectrum widths for a weak-trip PNF notch width of *M*/8.

To summarize, double processing for SZ-2 improves the recovery of the strong-trip velocity for strong-to-weak power ratios less than at least 3 dB for the usual range of spectrum width values. A simple rule to invoke double processing could be based on this power ratio regardless of other parameters. This would be preferred over more complex rules involving such parameters as the spectrum widths of strong and weak trip echoes. It is obvious that double processing, as its name implies, would almost double the computational complexity of the SZ-2 algorithm. Hence, its benefits will have to be weighed against the required additional computational power (if available). As part of future work we plan to investigate the performance of double processing in the presence of clutter and using adaptive PNF notch widths for both the strong and weak-trip PNFs.

5. References

Doviak, R. J. and D. S. Zrnić, 1993: *Doppler radar and weather observations.* Academic Press, New York, 562p.

Ice, R. L., D. A. Warde, D. Sirmans, and D. Rachel, 2004: Open RDA – RVP8 Signal Processing. Part 1: Simulation Study, WSR-88D Radar Operations Center Report, 87 pp.

Sachidananda, M., and D.S. Zrnić, 2005: Ground clutter filtering dual-polarized staggered PRT sequences. Submitted to JTECH.

Sachidananda, M., D. Zrnić, and R. Doviak, 1999: Signal design and processing techniques for WSR-88D ambiguity resolution, Part 3, NOAA/NSSL Report, 81 pp.

Sachidananda, M., D. Zrnić, and R. Doviak, 2000: Signal design and processing techniques for WSR-88D ambiguity resolution, Part 4, NOAA/NSSL Report, 99 pp.

Sachidananda, M., D. Zrnić, and R. Doviak, 2001: Signal design and processing techniques for WSR-88D ambiguity resolution, Part 5, NOAA/NSSL Report, 75 pp.

Torres S., D. Zrnić, and Y. Dubel, 2003: Signal Design and Processing Techniques for WSR-88D Ambiguity Resolution, Part 7, NOAA/NSSL Report, 128 pp.

Torres S., M. Sachidananda, and D. Zrnić, 2004: Signal Design and Processing Techniques for WSR-88D Ambiguity Resolution, Part 8, NOAA/NSSL Report, 113 pp.

Zrnić, D., and P. Mahapatra, 1985: Two methods of ambiguity resolution in pulse Doppler weather radars. *IEEE Trans. Aerosp. Electron. Syst.*, **21**, 470-483.

LIST OF NSSL REPORTS FOCUSED ON POSSIBLE UPGRADES

TO THE WSR-88D RADARS

Zrnić, D.S., Melnikov, V.M., and J.K. Carter, 2005: Calibrating differential reflectivity on the WSR-88D. NOAA/NSSL Report, 34 pp.

Torres S., M. Sachidananda, and D. Zrnić, 2004: Signal Design and Processing Techniques for WSR-88D Ambiguity Resolution: Phase coding and staggered PRT: Data collection, implementation, and clutter filtering. NOAA/NSSL Report, Part 8, 113 pp.

Zrnić, D., S. Torres, J. Hubbert, M. Dixon, G. Meymaris, and S. Ellis, 2004: NEXRAD range-velocity ambiguity mitigation. SZ-2 algorithm recommendations. NCAR-NSSL Interim Report.

Melnikov, V, and D Zrnić, 2004: Simultaneous transmission mode for the polarimetric WSR-88D – statistical biases and standard deviations of polarimetric variables. NOAA/NSSL Report, 84 pp.

Bachman, S., 2004: Analysis of Doppler spectra obtained with WSR-88D radar from non-stormy environment. NOAA/NSSL Report, 86 pp.

Zrnić, D., S. Torres, Y. Dubel, J. Keeler, J. Hubbert, M. Dixon, G. Meymaris, and S. Ellis, 2003: NEXRAD range-velocity ambiguity mitigation. SZ(8/64) phase coding algorithm recommendations. NCAR-NSSL Interim Report.

Torres S., D. Zrnić, and Y. Dubel, 2003: Signal Design and Processing Techniques for WSR-88D Ambiguity Resolution: Phase coding and staggered PRT: Implementation, data collection, and processing. NOAA/NSSL Report, Part 7, 128 pp.

Schuur, T., P. Heinselman, and K. Scharfenberg, 2003: Overview of the Joint Polarization Experiment (JPOLE), NOAA/NSSL Report, 38 pp.

Ryzhkov, A, 2003: Rainfall Measurements with the Polarimetric WSR-88D Radar, NOAA/NSSL Report, 99 pp.

Schuur, T., A. Ryzhkov, and P. Heinselman, 2003: Observations and Classification of echoes with the Polarimetric WSR-88D radar, NOAA/NSSL Report, 45 pp.

Melnikov, V., D. Zrnić, R. J. Doviak, and J. K. Carter, 2003: Calibration and Performance Analysis of NSSL's Polarimetric WSR-88D, NOAA/NSSL Report, 77 pp.

NCAR-NSSL Interim Report, 2003: NEXRAD Range-Velocity Ambiguity Mitigation SZ(8/64) Phase Coding Algorithm Recommendations.

Sachidananda, M., 2002: Signal Design and Processing Techniques for WSR-88D Ambiguity Resolution, NOAA/NSSL Report, Part 6, 57 pp.

Doviak, R., J. Carter, V. Melnikov, and D. Zrnić, 2002: Modifications to the Research WSR-88D to obtain Polarimetric Data, NOAA/NSSL Report, 49 pp.

Fang, M., and R. Doviak, 2001: Spectrum width statistics of various weather phenomena, NOAA/NSSL Report, 62 pp.

Sachidananda, M., 2001**:** Signal Design and Processing Techniques for WSR-88D Ambiguity Resolution, NOAA/NSSL Report, Part 5, 75 pp.

Sachidananda, M., 2000**:** Signal Design and Processing Techniques for WSR-88D Ambiguity Resolution, NOAA/NSSL Report, Part 4, 99 pp.

Sachidananda, M., 1999**:** Signal Design and Processing Techniques for WSR-88D Ambiguity Resolution, NOAA/NSSL Report, Part 3, 81 pp.

Sachidananda, M., 1998**:** Signal Design and Processing Techniques for WSR-88D Ambiguity Resolution, NOAA/NSSL Report, Part 2, 105 pp.

Torres, S., 1998: Ground Clutter Canceling with a Regression Filter, NOAA/NSSL Report, 37 pp.

Doviak, R. and D. Zrnić, 1998**:** WSR-88D Radar for Research and Enhancement of Operations: Polarimetric Upgrades to Improve Rainfall Measurements, NOAA/NSSL Report, 110 pp.

Sachidananda, M., 1997**:** Signal Design and Processing Techniques for WSR-88D Ambiguity Resolution, NOAA/NSSL Report, Part 1, 100 pp.

Sirmans, D., D. Zrnić, and M. Sachidananda, 1986**:** Doppler radar dual polarization considerations for NEXRAD, NOAA/NSSL Report, Part I, 109 pp.

Sirmans, D., D. Zrnić, and N. Balakrishnan, 1986**:** Doppler radar dual polarization considerations for NEXRAD, NOAA/NSSL Report, Part II, 70 pp.

Appendix A. Staggered PRT GCF: Intuitive explanation

Herein we present a heuristic explanation of the ground clutter filtering procedure for the staggered PRT. It compliments the explanations given in section 3 and might help readers get a better grasp of the manipulations in the spectral domain.

Start with the definition:

- $e(nT_u)$ – is a uniform sequence with sample spacing T_u
- $v(nT_u)$ – is the observed part of the sequence through staggered sampling
- Code(nT_u) – is the staggered sample spacing, it starts at T_1

Then in the time domain the following holds:

$$v(nT_u) = \text{Code}(nT_u)\, e(nT_u) \tag{A.1}$$

$$\text{Code}(nT_u) = 101001010010100....$$

In the frequency domain the Fourier transforms (see Fig. A.1) are

$$\text{FT}(v) = \text{FT}(\text{Code}) * \text{FT}(e) \tag{A.2}$$

where $*$ is the convolution operator. In our case the staggered ratio is 2/3 and the code length is 160 = 5•32.

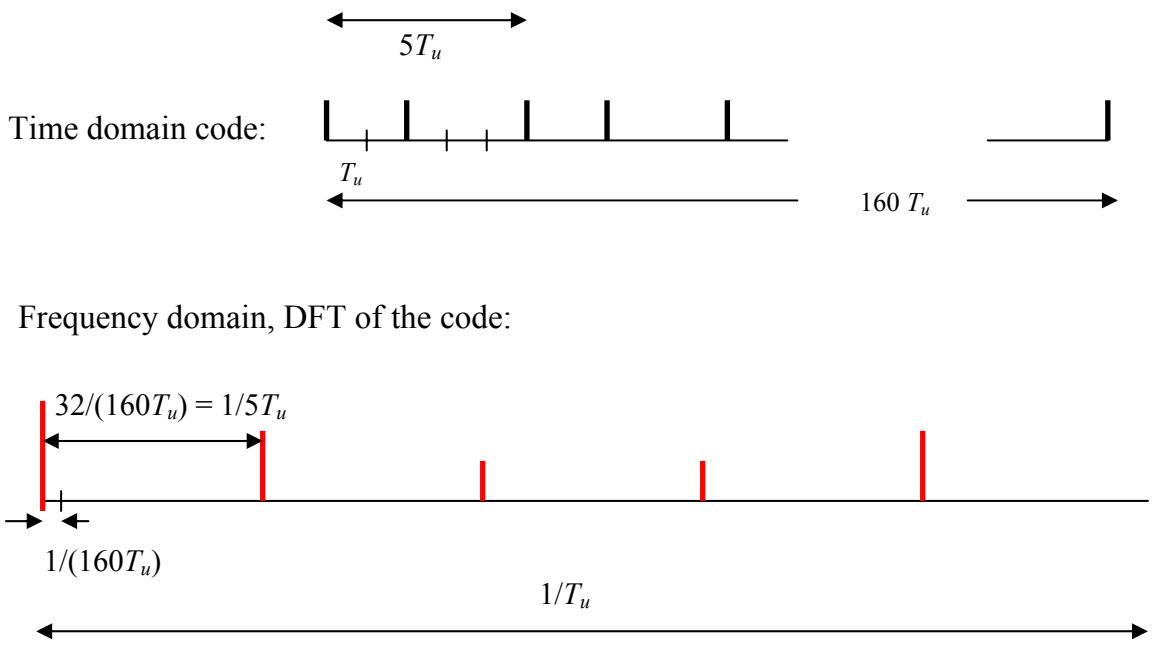

Fig. A.1 Time domain representation of the code and its discrete Fourier transform. The pulses in the time domain correspond to 1s and the basic time unit is T_u.

In Fig. A.1, is the code sequence of 1s and 0s over a time length of 160 T_u. The Fourier transform of the code at the bottom of the figure depicts five spectral lines. The total frequency span (Nyquist interval) equals the reciprocal of the basic time unit $1/T_u$. The spectral coefficients are spaced by $1/(160\ T_u)$ and most are zero. The basic staggered indicator 10100 of length five repeats periodically 32 times within the total code length of 160 T_u. Therefore, the code has strong spectral lines separated by $1/(5T_u)$ or 32 spectral coefficients. In the figure, magnitudes of the spectral lines are drawn (absolute values of voltages), and it is important to remember that the coefficients are complex and have associated phases.

It is obvious that the $v(nT_u)$ is the time representation of the code (A.1) if $e(nT_u)$ is a unit constant, and hence the Fourier transform of $v(nT_u)$ will be the transform of the code. If $e(nT_u)$ is an arbitrary constant; then, the transform of its coded rendition $v(nT_u)$ will be a scaled version of the code transform. Moreover, if $e(nT_u)$ is a pure sinusoid centered on one of the line frequencies; then, the transform of the coded version would have a line centered at the frequency of the sinusoid and four scaled replicas spaced by $1/(5T_u)$. That is, the spectrum would be the same as for the code (at DC) but shifted to the line frequency. Hence, relative phases and magnitudes of the spectral coefficients would be preserved! This allows separation of different sinusoids if they are offset from each other by $1/(5T_u)$ or 32 spectral coefficients.

In its essence, clutter filtering of staggered sequence can be broken into two regimes. One is if the weather and clutter signal overlap near zero frequency, the other is if the overlap is between the line frequency of the weather signal and a sideband of the clutter. To identify which case it is, one first filters the clutter and then computes the mean velocity from the residue. This velocity tells in which 1/5 of the spectrum the weather contribution is. Then, a correction is made to restore the weather signal in regions of overlap with the clutter sidebands.

We illustrate the process on a case of a single clutter component (at 0 frequency) and a weather component at $3/(5T_u)$. It is clear that the concept is applicable to several components; hence, extension to other than line spectrum is straightforward.

For illustration, let the weather component of a uniform sequence have a Fourier transform W (a complex number, or scaling factor that represents amplitude and phase of

the sinusoid) at frequency $3/(5T_u)$. Similarly the ground clutter component at zero frequency is G (complex). The known normalized spectrum of the code has 160 coefficients of which only five (spaced by 32 coefficients) differ from zero. Let's form a vector of these normalized coefficients

$$c_n = (c_0, c_1, c_2, c_3, c_4)^{\mathrm{T}}. \tag{A.3}$$

The spectrum of the coded clutter is then $G\, c_n$ (Fig. A.2). Similarly, the spectrum of the coded sinusoid is $W\, c_{n-3}$, where c_{n-3} is a cyclic shift of c_n by 3 units. The composite measured spectrum at values different from zero is

$$V = c_n\, G + c_{n-3}\, W. \tag{A.4}$$

In practice, $V = (V_0, V_1, V_2, V_3, V_4)^{\mathrm{T}}$ is measured (observed) and c_n is known. The cyclic shift and the complex scaling G and W are not known.

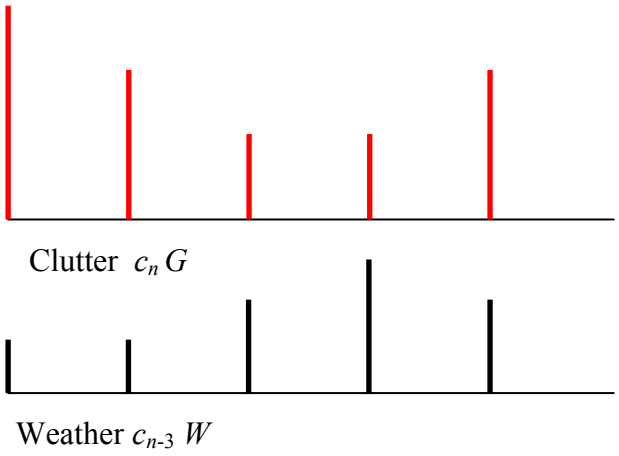

Fig. A.2 Doppler spectra of clutter (a DC component) and a sinusoidal weather component obtained from the staggered PRT sequence. Stagger ratio is 2/3 and the number of non zero samples is 64.

As explained in section 3 the filtered component is given by

$$V_f = V - c_n^{\mathrm{T}} * V c_n. \tag{A.5}$$

Substitution of (A.4) produces

$$V_f = (c_n G + c_{n-3} W) - c_n^{\mathrm{T}} * (c_n G + c_{n-3} W) c_n$$

$$= c_{n-3} W - c_n^{\mathrm{T}} * c_{n-3} c_n \mathrm{W}. \tag{A.6}$$

Recall that V_f is a five dimensional vector of which each component corresponds to one spectral coefficient. Clearly, after filtering the clutter the spectral lines have been removed from V and the remaining vector (five lines) are scaled versions of the signal W. The normalized code spectrum c_n is known, but the cyclic shift n-3 is not. To find it, one uses magnitude deconvolution and autocovariance processing. Knowing n-3 allows several ways to obtain W. For instance, a possible solution for G and W can be obtained from (A.3) as

$$V_0 = c_0 G + c_2 W$$

$$V_1 = c_1 G + c_3 W,$$

but that is not the recommended approach. Rather, (A.6) is used directly to give

$$V_{f3} = [c_2 - (c_0 c_2 + c_1 c_3 + c_2 c_4 + c_3 c_0 + c_4 c_1) c_0] W.$$

Next, a slight generalization to other staggered ratios is outlined. Consider a stager ratio m/n, where m and n are integers, and assume that $T_1 = mT_u$ and $T_2 = nT_u$. Then, let the two staggered pulses (the pair) repeat L times so that the total code length is $L(m+n)T_u$.

The discrete Fourier transform of the code spectrum will have $L(m+n)$ coefficients of which $(m+n)$ are non zero. That is, there are $(m+n)$ lines and the spacing between adjacent lines is L points. The Nyquist interval is $1/T_u$ and it increases if m and n increase but the number of spectral lines also increases. Suppose that $(T_1 + T_2)$ is kept constant and $(m+n)$ varies. Then the spacing of the non-zero lines would be constant and equal to $(T_1 + T_2)^{-1}$. That is, although there would be more non-zero spectral lines, the total Nyquist interval would proportionally increase so that the net separation of spectral lines would remain unchanged.

Appendix B. Staggered PRT Spectral GCF: Functional description

Assumptions:

(a) The switching sequence is [T_1, T_2, T_1, T_2, …].

(b) $T_1 < T_2$, (T_1 /T_2) = κ = 2/3, and (T_2 - T_1) = T_u .

(c) M is the number of staggered PRT samples.

(d) N = 5M /2, number of DFT coefficients.

(e) Ground clutter is present.

(f) No overlaid signal.

Inputs:

(a) complex time series, g_i, i = 1, 2, 3, ..., M.

(b) ground clutter filter map.

(c) M, T_1, T_2, radar frequency, radial, range, *p_noise* (receiver noise).

Pre-compute: the following are pre-computed and supplied to the algorithm. These need to be recomputed only if M changes.

(a) Window coefficients for N points, b_i , i = 1, 2, 3, ..., N.

(b) Window power loss correction factor,

$$win\_cor = 10.\log_{10}(\frac{1}{N}\sum_{1}^{N}|b_i|^2) \text{ (dB).}$$

{*win_cor* = 4.1924(dB) for vonHann, 5.2311(dB) for Blackman}

(b) Re-arranged (5x5) convolution matrix, $\mathbf{C_r}$.

(c) Magnitude de-convolution matrix, $\{abs(\mathbf{C_r})\}^{-1}$.

(d) Matrices $\mathbf{C_{f1}}$, and $\mathbf{C_{f2}}$.

(e) Matrix **Z**

$\mathbf{Z}$ = [1111...(M/4),ξ_2,ξ_2,ξ_2...(M/2),ξ_3,ξ_3,ξ_3,...(M) ,ξ_2,ξ_2,ξ_2...(M/2),111...(M/4)]

{the numbers in ( ) brackets indicate number of time to repeat the element.}

{...

How to compute $\mathbf{C_r}$, $\mathbf{C_{f1}}$, and $\mathbf{C_{f2}}$:

(1) form code sequence of length 5 only, [10100].

(2) take $\mathbf{x}$ = DFT([10100]), normalize power to unity (divide each element by the square root of the total power in the spectrum)

(3) form matrix $\mathbf{C_r}$ with these 5 coefficients as the first column, and form the second and subsequent columns by down shifting cyclically by one coefficient at a time.

(4) $\mathbf{C_{f1}}$, and $\mathbf{C_{f2}}$ are computed using 1st and 5th columns, $\mathbf{C_1}$, and $\mathbf{C_5}$ of $\mathbf{C_r}$.

$\mathbf{C_{f1}}$= $\mathbf{C_1}$ $\mathbf{C_1}^{t*}$ and $\mathbf{C_{f2}}$ = $\mathbf{C_5}$ $\mathbf{C_5}^{t*}$

...}

The clutter filter algorithm: {explanation/details is given in {} brackets.}

Input time series, radial, range:

if clutter is **not** present for the range gate {determine from the clutter filter map}

go to the pulse pair algorithm

{given in report 7, delete the clutter filtering part}.

elseif **overlaid** signal present

go to the pulse pair algorithm (report 7)

else {ground **clutter present** and **no overlay**} apply the algorithm below:

1. Form derived time series,

{insert zeros: $e = [g_1, 0, g_2, 0, 0, g_3, 0, g_4, 0, 0, ..., g_M, 0, 0]$ }

2. Apply window {multiply, $e.*b = e_i*b_i$; i=1,2,...N} - Blackman window

{if the *CNR* is known from the clutter map, one may select appropriate optimum window. It is also possible to estimate an approximate *CNR* as in step # 4 below and then select an optimum window. However, this involves DFT computation twice.}

3. Compute **V** = DFT($e.*b$). {**V** is a row vector}

4. Compute approximate *CNR*:

$$CNR\_aprox = [(|V_1|^2 + |V_2|^2 + |V_N|^2)\ (5/2)(5/2)] / (N \bullet p\_noise).$$

{The two 5/2 factors are to account for: (a) the inserted zeros, and (b) the spread of the clutter spectral power. The staggered PRT spectrum has 5 unequal replicas, with the main one having 2/5 of the power. The N in the denominator is needed because the DFT in Matlab does not normalize the spectra.}

5. Determine clutter filter width parameter, q.

{note: the following is obtained using Blackman window on different time series records (M=64) of the radar data of 4/6/03 on CD - the optimum q depends on the *CNR*, window function, and M}

$$CNR\_aprox < 50 \text{ dB}; \ q = 3,$$

$$50 \text{ dB} < CNR\_aprox < 70 \text{ dB}; \ q = 4,$$

$$70 \text{ dB} < CNR\_aprox < 90 \text{ dB}; \ q = 5,$$

$$CNR\_aprox > 90 \text{ dB}; \ q = 6.$$

{one may select an optimum combination of window and q - see section-2}

6. Compute clutter filter matrices, $\mathbf{I_{f1}}$, $\mathbf{I_{f2}}$, $\mathbf{I_1}$, $\mathbf{I_2}$. {all are row matrices}

$\mathbf{I_{f1}}$ = [1,1,... (q times),0,0, ...(M/2-q times)],

$\mathbf{I_{f2}}$ = [0,0,...(M/2-q+1 times),1,1,...(q-1 times)].

$\mathbf{I_2}$ = [($\mathbf{I_{f1}}$+ $\mathbf{I_{f2}}$),... repeat 5 times],

$\mathbf{I_1}$ = complement of $\mathbf{I_2}$, (interchange 0s and 1s).

{[$\mathbf{I_{f1}}$+$\mathbf{I_{f2}}$] has M/2 elements (first q and last q-1 elements are ones and the rest zeros), and $\mathbf{I_1}$ and $\mathbf{I_2}$ have N elements each.}

7. Row-wise re-arrange $\mathbf{V}$ into a (5x32) matrix $\mathbf{V_r}$. {see Eq. 3.15}

8. Filter the clutter: compute the spectrum, $\mathbf{V_f}$, after the clutter is filtered

$$\mathbf{V_f} = \mathbf{V_r} - \mathbf{C_{f1}}\,\mathbf{V_r}\,\mathbf{I_{f1}} - \mathbf{C_{f2}}\,\mathbf{V_r}\,\mathbf{I_{f2}}$$

9. Magnitude de-convolution

$$\mathbf{E_r} = abs(\,[abs\{\mathbf{C_r}\}]^{-1}\; abs\{\mathbf{V_f}\}).$$

10. Row-wise unfold $\mathbf{E_r}$ into a single row matrix, $\mathbf{E_s}$.

11. Compute the autocorrelation $R(T_u)$, and *initial* velocity

$$R(T_u) = \frac{1}{N}\sum_{1}^{N} |\,E_{sk}\,|^2\; e^{j2\pi(k-1)/N}$$

{E_{sk} are the elements of $\mathbf{E_s}$ }

$$v_{initial} = \frac{-v_a}{\pi}\arg[R(T_u)]; \qquad v_a = \frac{\lambda}{4T_u}.$$

12. Compute row matrix $\mathbf{I_v}$ { $M/2$ ones centered on $v_{initial}$ }

$$k_0 = round\left[\frac{-v_{initial}N}{2v_a}\right]; \quad \text{if } k_0 < 1 \text{ , } k_0 = k_0 + N,$$

$$k_1 = k_0 - M/4 + 1; \qquad \text{if } k_1 < 1 \text{ , } k_1 = k_1 + N,$$

$$k_2 = k_0 + M/4; \qquad \text{if } k_2 > N \text{ , } k_2 = k_2 - N,$$

{k_0 is the DFT index corresponding to $v_{initial}$, and k_1 to k_2 are M coefficients centered on mean velocity. The function *round* gives the nearest integer. If $k_1 > k_2$, the ones will span from k_1 to N, and 1 to k_2}

$\mathbf{I_v}$ = [0,0, ...,1,1,1,...,0,0,...]

{In the N element row matrix,

if $k_1 < k_2$, element # k_1 to k_2 are ones and the rest are zeros in $\mathbf{I_v}$.

if $k_2 < k_1$, element # (k_2+1) to (k_1 -1) are zeros and the rest are ones in $\mathbf{I_v}$.}

13. Interpolate the elements for the *velocity region*-1 in $\mathbf{E_s}$.

Let $s_1 = |E_s(q+1)|^2$, and $s_2 = |E_s(N-q+1)|^2$, the $(q+1)^{th}$, and $(N-q+1)^{th}$ element powers of $\mathbf{E_s}$. The elements in the *velocity_region*-(1) are replaced with interpolated values from s_1 and s_2.

$E_s(k) = [s_2 + (s_1 - s_2)\,(q + k - 1) / 2q]^{1/2}$, $\quad k = 1$ to q;

and $\quad E_s(k) = [s_2 + (s_1 - s_2)\,(q + k - 1 - N) / 2q]^{1/2}$, $\; k = N-q+2$ to N.

14. Compute the corrected spectrum, $\mathbf{E_c}$.

$$\mathbf{E_c} = \mathbf{E_s} \bullet \mathbf{I_1} + \mathbf{E_s} \bullet \mathbf{I_2} \bullet \mathbf{I_v} \bullet \mathbf{Z}$$

{all are row matrices, and the • represents the element by element multiplication (•* of MATLAB}

15. Re-compute the autocorrelation $R(T_u)$ using $\mathbf{E_c}$, and compute bias corrected mean velocity, v, from the phase of the autocorrelation. The mean power, p, is also computed from this spectrum. Add *win_cor* to p mean power to correct for the loss due to window. Compute reflectivity, z, in dBZ units. (need *syscal*, *noise*, *range*, and atmospheric attenuation)

16. Retain only M coefficients centered on the mean velocity, v, and delete the rest from $\mathbf{E_c}$.

$$k_0 = round\left[\frac{-vN}{2v_a}\right]; \quad \text{if } k_0 < 1 \text{ , } k_0 = k_0 + N,$$

$$k_1 = k_0 - M/2 + 1; \quad \text{if } k_1 < 1 \text{ , } k_1 = k_1 + N,$$

$$k_2 = k_0 + M/2; \quad \text{if } k_2 > N \text{ , } k_2 = k_2 - N.$$

if $k_1 < k_2$, set the elements of $\mathbf{E_c}$ from 1 to (k_1-1), and (k_2+1) to N, to zero to get $\mathbf{E_{cm}}$.

if $k_2 < k_1$, set the elements of $\mathbf{E_c}$ from (k_2+1) to (k_1-1) to zero to get $\mathbf{E_{cm}}$.

17. Compute spectrum width from $\mathbf{E_{cm}}$ (modified spectrum) using the width estimator (Eq. 6.37 of Doviak and Zrnić, 1993). Note that the $R(T_u)$ and the mean power, S, used in that expression has to be computed from $\mathbf{E_{cm}}$, and not from $\mathbf{E_c}$.

18. Output the spectral parameters, p (or compute reflectivity z), v, and w.

19. Go to the next data set.

Appendix C. SZ-2 Critical Enhancements and Errata: Functional description

- Page 5, table of censoring thresholds.

Add K_{CSR3} with a recommended value of 10 to 31.6228 (10 to 15 dB).
Add K_{IGN} with a recommended value of 10 to 100 (10 to 20 dB).
Disclaimer: these thresholds have not been thoroughly tested and may need refinement.
Remove K_1 and K_2.

- Page 6, step 1.

Add t as an output from this step.

- Page 7, step 1.

If $t_A = -1$ and $t_B = -1$, set $t_C = -1$ and the algorithm continues at step 6.

- Page 7, step 2.

Add P_L, C_L, and t as inputs to this step.

Replace step 2 with the following:
In the case of overlaid clutter, an additional check is made using the long PRT powers to prevent algorithm failure from incorrectly defined maps.

(Determine trips with clutter)
$n_C = 0$
For $0 \leq l < 4$
  If $n + lN < N_L$
    (Within the long-PRT range)
    If $B(n + lN) = FILTER$
      (There is clutter in the l-th trip; therefore, store clutter trip number and increment clutter trip count)
      $clutter\_trips(n_C) = l$
      $n_C = n_C + 1$
    End
  End
End
If $n_C > 1$
  (According to the Bypass map there is overlaid clutter; therefore, re-determine trips with clutter using both Bypass map and long-PRT powers)
  $n_C = 0$
  For $0 \leq l < 4$
    If $n + lN < N_L$
      (Within the long-PRT range)
      If $B(n + lN) = FILTER$ and $C_L(n + lN) > P_L(n + lN)\, K_{CSR3}$
        (There is clutter in the l-th trip)

```
                clutter_trips(n_C) = l
                n_C = n_C + 1
            End
        End
    End
End

(Handle clutter)
If n_C = 0
    (No clutter anywhere; therefore, clutter filter will not be applied)
    t_C = –1

ElseIf n_C = 1
    (Non-overlaid clutter)
    t_C = clutter_trips(0)
    If t_C ≠ t_A
        (The strong trip does not contain clutter)
        If t_C = t_B
            (The weak trip contains clutter)
            If P(0) > Q(1) K_IGN
                (Strong signal is K_IGN-times larger than the total signal in the trip with
                clutter; therefore, clutter can be ignored and the weak signal is not
                recoverable)
                t_B = –1
                t_C = –1
            End
        Else
            (One of the unrecoverable trips contain clutter)
            If P(0) > Q[r(t_C)] K_IGN
                (Strong signal is K_IGN-times larger than the total signal in the trip with
                clutter; therefore, clutter can be ignored)
                t_C = –1
            End
        End
    End

ElseIf n_C = 2
    (Overlaid clutter in two trips)
    CwS = FALSE      (clutter with strong signal)
    CwW = FALSE      (clutter with weak signal)
    CwU = FALSE      (clutter with unrecoverable signals)
    For 0 ≤ l < n_C
        If clutter_trips(l) = t_A
            (The trip with the strong signal contains clutter)
            CwS = TRUE
        ElseIf clutter_trips(l) = t_B
```

(The trip with the weak signal contains clutter)
CwW = TRUE
Else
(One of the trips with unrecoverable signals contains clutter)
CwU = TRUE
t_{CU} = *clutter_trips*(*l*)
End
End
If *CwS* and *CwW*
(Clutter is with the strong and weak trips, weak signal cannot be recovered)
$t_B = -1$
If $P(0) > Q(1)\ K_{IGN}$
(Trip with weak signal can be ignored)
$t_C = t_A$
Else
(None of the trips can be recovered, ignore clutter)
$t_A = -1$
$t_C = -1$
End
ElseIf *CwS* and *CwU*
(Clutter is with the strong and one of the unrecoverable trips)
If $P(0) > Q[r(t_{CU})]\ K_{IGN}$
(Trip with unrecoverable signal can be ignored)
$t_C = t_A$
Else
(None of the trips can be recovered, ignore clutter)
$t_A = -1$
$t_B = -1$
$t_C = -1$
End
ElseIf *CwW* and *CwU*
(Clutter is with the strong and one of the unrecoverable trips)
If $P(0) > \{Q(1) + Q[r(t_{CU})]\}\ K_{IGN}$
(All trips with clutter can be ignored and weak signal cannot be recovered)
$t_B = -1$
$t_C = -1$
ElseIf $P(0) > Q[r(t_{CU})]\ K_{IGN}$
(Trip with unrecoverable signal can be ignored)
$t_C = t_B$
ElseIf $P(0) > Q(1)\ K_{IGN}$
(Trip with weak signal can be ignored and weak signal cannot be recovered)
$t_B = -1$
$t_C = t_{CU}$
Else
(None of the trips can be recovered, ignore clutter)
$t_A = -1$

$t_B = -1$
$t_C = -1$
End
ElseIf *CwU*
(Clutter is with both of the unrecoverable trips)
If $P(0) > \{Q(2) + Q(3)\}\ K_{IGN}$
(All trips with clutter can be ignored)
$t_C = -1$
ElseIf $P(0) > Q(2)\ K_{IGN}$
(One of the trips with unrecoverable signals can be ignored)
$t_C = t(3)$
ElseIf $P(0) > Q(3)\ K_{IGN}$
(One of the trips with unrecoverable signals can be ignored)
$t_C = t(2)$
Else
(None of the trips can be recovered, ignore clutter)
$t_A = -1$
$t_B = -1$
$t_C = -1$
End
End

ElseIf $n_C = 3$
(Overlaid clutter in three trips)
CwS = FALSE
CwW = FALSE
CwU = FALSE
For $0 \leq l < n_C$
If *clutter_trips*$(l) = t_A$
(The trip with the strong signal contains clutter)
CwS = TRUE
ElseIf *clutter_trips*$(l) = t_B$
(The trip with the weak signal contains clutter)
CwW = TRUE
Else
(One of the trips with unrecoverable signals contains clutter)
CwU = TRUE
t_{CU} = *clutter_trips*(l)
End
End
If *CwS* and *CwW* and *CwU*
(Weak trip is unrecoverable)
$t_B = -1$
If $P(0) > \{Q(1) + Q[r(t_{CU})]\}\ K_{IGN}$
(Trips with weak and unrecoverable signals can be ignored)
$t_C = t_A$

Else
(None of the trips can be recovered, ignore clutter)
$t_A = -1$
$t_C = -1$
End
ElseIf *CwS* and *CwU*
If $P(0) > [Q(2) + Q(3)]\ K_{IGN}$
(Trips with unrecoverable signals can be ignored)
$t_C = t_A$
Else
(None of the trips can be recovered, ignore clutter)
$t_A = -1$
$t_B = -1$
$t_C = -1$
End
Else
If $P(0) > [Q(1) + Q(2) + Q(3)]\ K_{IGN}$
(All trips with clutter can be ignored and weak trip is unrecoverable)
$t_B = -1$
$t_C = -1$
ElseIf $P(0) > [Q(1) + Q(2)]\ K_{IGN}$
(Trips with weak and one unrecoverable signal can be ignored and weak trip is unrecoverable)
$t_B = -1$
$t_C = t(3)$
ElseIf $P(0) > [Q(1) + Q(3)]\ K_{IGN}$
(Trips with weak and one unrecoverable signal can be ignored and weak trip is unrecoverable)
$t_B = -1$
$t_C = t(2)$
ElseIf $P(0) < [Q(2) + Q(3)]\ K_{IGN}$
(Both trips with unrecoverable signals can be ignored)
$t_C = t_B$
Else
(None of the trips can be recovered, ignore clutter)
$t_A = -1$
$t_B = -1$
$t_C = -1$
End
End

Else ($n_C = 4$)
(Overlaid clutter in four trips)
(Weak trip is unrecoverable)
$t_B = -1$
If $P(0) > [Q(1) + Q(2) + Q(3)]\ K_{IGN}$

(Trips with weak and both unrecoverable signals can be ignored)
$t_C = t_A$
Else
(None of the trips can be recovered, ignore clutter)
$t_A = -1$
$t_C = -1$
End
End

- Page 9, step 3

We could use the Hanning (a.k.a. von Hann) window when $t_C = -1$. (Q: Is that how ORDA will operate?)
If $t_C = -1$, set $k_{GMAP} = 0$ and the algorithm continues at step 6.

- Page 17, step 21

Add t as an input to this step.

The following segment of code should be added at the beginning:

For $0 \leq l < 4$
If $t_C = t(l)$
$PQ(l) = P(l)$
Else
$PQ(l) = Q(l)$
End
End

The P's involved in SNR* censoring (pages 17 and 18) should be replaced with PQ.

- Page 18, step 21

The last 'If' (end of this page) should be: If $w_W/2v_{a,L} > w_{n,max}$